

**Dynamics of Rotationally Resolved Multiphoton
Ionization Processes in Molecules**

Thesis by

Henrik Rudolph

In Partial Fulfillment of the Requirements
for the Degree of
Doctor of Philosophy

California Institute of Technology
Pasadena, California

1989

(Submitted May 15, 1989)

ACKNOWLEDGMENTS

I would like to express my gratitude to my research advisor, professor Vincent McKoy, for his support, guidance and patience during the course of this work. I would also like to thank all past and present members of the McKoy group, including our friends from Brazil. I have a great number of people I am especially grateful to:

- The REMPI veterans: Diane L. Lynch and Sham N. Dixit for their help and friendship during my introduction to the world of REMPI.
- The REMPI experimentalists: Sarah Allendorf, Dave Leahy, Dick Zare, James Reilly, Pat and Joe Dehmer, and Stephen Pratt, who have always been willing to share their results with us.
- The professors and teaching assistants I worked with in CHEM 1. Their hard work and dedication made it fun to be part of CHEM 1.
- The friends we met through Caltech: Karen and Bob Donnelly, the whole Ruzek family, Andy Axup, Katia and Mark Lusek. Your friendship means a lot to us.
- Our family and friends in Denmark, who have been very supportive. 'Uden Jeres hjælp havde dette aldrig været muligt.'
- Carl Ballhausen for his friendship, help and support. Without you, this would not have been possible.
- The Fulbright Commission, the I.I.E., the Danish Natural Science Research Council, the NATO Science Fellowship Programme (Denmark), and the Carlsberg Foundation for their help and support.

Finally I wish to express my gratitude to Sonnie, without her love, friendship, support and understanding, especially in the first few years here, I would not have been able to finish this work.

ABSTRACT

This dissertation presents the results of studies of several rotationally-resolved resonance enhanced multiphoton ionization (REMPI) processes in some simple molecular systems. The objective of these studies is to quantitatively identify the underlying dynamics of this highly state-specific process which utilizes the narrow bandwidth radiation of a laser to ionize a molecule by first preparing an excited state via multiphoton absorption and subsequently ionizing that state before it can decay. Coupled with high-resolution photoelectron spectroscopy, REMPI is clearly an important probe of molecular excited states and their photoionization dynamics.

A key feature of our studies is that they are carried out using accurate Hartree-Fock orbitals to describe the photoelectron orbitals of the molecular ions. The use of such photoelectron orbitals is important in rotationally-resolved studies where the angular momentum coupling in the photoelectron orbital plays a significant role in the photoionization dynamics. In these studies the Hartree-Fock molecular photoelectron orbitals are obtained by numerical solution of a Lippmann-Schwinger integral equation.

Studies reported here include investigations of (i) ionic rotational branching ratios and their energy dependence for REMPI via the $A^2\Sigma^+(3s\sigma)$ and $D^2\Sigma^+(3p\sigma)$ states of NO, (ii) the influence of angular momentum constraints on branching ratios at low photoelectron energies for REMPI via low- J levels of the resonant intermediate state, (iii) the strong de-

pendence of photoelectron angular distributions on final ionic rotational state and on the alignment in REMPI of the $A^2\Sigma^+$ state of NO, (iv) vibrational state dependence of ionic rotational branching ratios arising from rapid orbital evolution in resonant states ($E'^2\Sigma^+(3p\sigma)$ of CH), (v) the influence of rovibronic interactions on the rotational branching ratios seen in REMPI via the $D^2\Sigma^+(3p\sigma)$ state of NO, and (vi) effects of laser intensity on the photoionization dynamics of REMPI.

TABLE OF CONTENTS

	Page
Acknowledgments	ii
Abstract	iii
Introduction and Overview	1
CHAPTER 1 (2+1) REMPI of NO via the $D^2\Sigma^+$ state: Rotational branching ratios [H. Rudolph, S.N. Dixit, V. McKoy, and W.M. Huo, Chem. Phys. Lett. 137, 521 (1987)]	31
CHAPTER 2 Ionic rotational branching ratios in resonant enhanced multiphoton ionization of NO via the $A^2\Sigma^+(3s\sigma)$ and $D^2\Sigma^+(3p\sigma)$ states [H. Rudolph, S.N. Dixit, V. McKoy, and W.M. Huo, J. Chem. Phys. 88, 637 (1988)]	35
CHAPTER 3 Rotational branching ratios at low photoelectron energies in resonant enhanced multiphoton ionization of NO [H. Rudolph, V. McKoy, and S.N. Dixit, J. Chem. Phys. 90, 2570 (1989)]	41
CHAPTER 4 Rotationally-resolved photoelectron angular distributions in resonance enhanced multiphoton ionization of NO [H. Rudolph and V. McKoy, submitted to J. Chem. Phys.]	47
CHAPTER 5 Dependence of NO rotational photoionization propensity rules on electron kinetic energy [Xinbei Song, Ellen Sekreta, James P. Reilly, H. Rudolph, and V. McKoy, submitted to J. Chem. Phys.]	66
CHAPTER 6 Vibrational state dependence of ionic rotational branching ratios in resonance enhanced multiphoton ionization of CH [H. Rudolph, J.A. Stephens, V. McKoy, and M.-T. Lee, submitted to J. Chem. Phys.]	102

CHAPTER 7 (2+1) resonant enhanced multiphoton ionization of H_2 via the $E,F^1\Sigma_g^+$ state [H. Rudolph, D.L. Lynch, S.N. Dixit, and V. McKoy, J. Chem. Phys. 86 , 1748 (1987)]	112
CHAPTER 8 Photoionization cross sections of rovibrational levels of the $B^1\Sigma_u^+$ state of H_2 [H. Rudolph, D.L. Lynch, S.N. Dixit, and V. McKoy, J. Chem. Phys. 84 , 6657 (1986)]	117
CHAPTER 9 (1+1) resonant enhanced multiphoton ionization via the $A^2\Sigma^+$ state of NO: Ionic rotational branching ratios and their intensity dependence [H. Rudolph, S.N. Dixit, V. McKoy, and W.M. Huo, J. Chem. Phys. 88 , 1516 (1988)]	123

INTRODUCTION and OVERVIEW

The technique of resonance enhanced multiphoton ionization (REMPI) combined with high resolution photoelectron spectroscopy (PES) has developed dramatically in the last decade.¹⁻³ REMPI is a highly state-selective process, in contrast to photoionization with conventional light sources, e.g., synchrotron radiation, where single-photon absorption ionizes a thermal distribution of molecules. In REMPI the narrow bandwidth of the laser allows the m-photon resonant excitation from a specific rovibrational level of the ground state to a specific rovibrational level of the intermediate state, followed by a n-photon ionization out of this state prior to decay. The REMPI process is therefore molecule-specific and state-selective with a resolution determined by the laser systems employed (typically $\approx 1\text{cm}^{-1}$).

The selectivity of the REMPI process, combined with its high sensitivity, has made REMPI an important technique used for the state-selective production of ions, the determination of state populations, and as a diagnostic for detecting and identifying short-lived radicals and reactive intermediates.¹⁻⁴ The selection rules for REMPI processes also makes REMPI important for excited-state spectroscopy since it is possible to populate states that are forbidden in single-photon spectroscopy, e.g., the (2+1) REMPI excitation via the $C^3\Pi_g$ state of O_2 .⁵ Most REMPI studies have emphasized spectroscopic aspects of molecular structure, in particular the determination of excitation energies of excited states and their rotational and vibrational constants. In REMPI studies which combine high-resolution photoelectron spectroscopy (REMPI-PES) consider-

able interest has focussed on the vibrational state distributions of the ions formed, and how these relate to differences between excited state and ion potential energy surfaces.² The REMPI-PES technique also makes it possible to resolve the rotational levels of the resulting ion. Recently, several experiments⁶⁻¹² have achieved rotational resolution in the photoelectron spectra, and have yielded significant insight into the photoionization dynamics of the REMPI process.

In this thesis we study the underlying dynamics of rotationally-resolved REMPI processes in diatomic molecules. We show that rotationally-resolved REMPI, combined with studies of photoelectron angular distributions, is a sensitive probe of the intermediate state's properties and alignment. We also demonstrate that the REMPI process makes it possible via selective excitation of the intermediate state to probe features of the electronic continuum, e.g., the energy dependence of the photoionization process. To illustrate the theoretical framework used in these rotationally-resolved REMPI studies, we will discuss the particular example of (2+1) REMPI via the $D^2\Sigma^+(3p\sigma)$ state of NO. This work is discussed in chapters one and two. These studies were motivated by the pioneering work of Reilly *et al.*,⁹ where conventional TOF-PES techniques were used to measure photoelectron branching ratios both parallel and perpendicular to the laser polarization direction, for (2+1) REMPI via the $D^2\Sigma^+(3p\sigma)$ state of NO.

We begin by describing a "typical" REMPI experiment, in order to appreciate the complexity and difficulty of these experiments. In Fig. 1 (p. 25) we show a one-laser REMPI setup. The laser often employed for

REMPI experiments is a pulsed Nd:YAG laser pumping a dye laser system. These often operate in a multi-mode state with a incompletely defined spatial and temporal profile. The repetition rate is ~ 5 -100 Hz with a ~ 5 ns pulse duration and an average fluence for the focused ionizing laser of 10^5 - 10^9 W/cm². As depicted in Fig. 1, the laser beam can be split, frequency doubled, Raman shifted etc., so as to obtain the appropriate wavelength for ionization. The light polarization is rotated to obtain photoelectron angular distribution measurements since the time-of-flight (TOF) photoelectron detector direction is fixed.³ The laser-molecule interaction region is kept at a pressure for "collision-free" conditions, which is typically about $\lesssim 10^{-5}$ Torr.¹² For most stable or long-lived radicals a standard molecular beam arrangement is used. Short-lived radicals may be created *in situ* by laser photodissociation, as in the case of CH.¹³ The expansion in the molecular beam is very effective at rotationally cooling the molecules, typically resulting in a Boltzman distribution with a rotational temperature $T_{\text{rot}} \sim 5$ K.

The emitted photoelectrons are usually detected with a high resolution photoelectron spectrometer. Ionic rotationally-resolved REMPI-PES spectra have been obtained only for H₂ and NO because few conventional time-of-flight (TOF) detection experiments can achieve the required resolution.⁶⁻¹² There are three general types of photoelectron energy analyzers: (i) The conventional TOF method with a spatial resolution of $\sim 6^\circ$ and an optimal resolution of ~ 3 meV ($1 \text{ meV} \approx 8 \text{ cm}^{-1}$).^{8,9} With a typical value for the rotational constant, $B_+ = 2 \text{ cm}^{-1} \approx 0.25 \text{ meV}$ (for NO⁺),¹⁴ the lowest N_+ value that can be fully resolved for this method is $N_+ \sim 10$. (ii) The magnetic bottle technique, which uses an inhomogeneous magnetic field to

collect photoelectrons in a 2π hemisphere. This method has an energy resolution of about 20 meV.² (iii) Zero-kinetic-energy photoelectron spectroscopy (ZEKE-PES), which makes use of the fact that photoelectrons with low kinetic energy do not move out of the interaction region.¹¹ The photoelectrons are extracted and detected with a delay sufficiently large to allow "all" non-zero energy electrons to diffuse out of the interaction region. No angular resolution is obtained with this method but the energy resolution is laser limited ($\approx 1 \text{ cm}^{-1}$).

(2+1) REMPI via the $D^2\Sigma^+(3p\sigma)$ state of NO

Nitric oxide is an ideal system for molecular REMPI. It has a low ionization potential (I.P. 9.26 eV)¹⁴ and only a few UV-photons are needed (2-3) to exceed the I.P. The rotational constant of the ion ($B_+ = 2 \text{ cm}^{-1}$) is sufficiently large to partially resolve its rotational levels for values of $N_+ \sim 10$. In Fig. 2 we list the spectroscopic constants for some of the excited states of NO, and also show their potential energy curves.¹⁴ The excited state spectrum of NO has been extensively studied.¹⁵⁻¹⁷ The ground state of NO ($X^2\Pi$) has the electronic configuration $1\sigma^2 2\sigma^2 3\sigma^2 4\sigma^2 5\sigma^2 1\pi^4 2\pi$.¹⁴ Excitation of the 2π electron results in a Rydberg state with an electron configuration $(1\sigma^2 2\sigma^2 3\sigma^2 4\sigma^2 5\sigma^2 1\pi^4)n\ell_0$, where n and ℓ_0 indicate the principal and angular momentum quantum numbers for the Rydberg orbital. The configuration of the ground state of NO^+ ($X^1\Sigma^+$) is $1\sigma^2 2\sigma^2 3\sigma^2 4\sigma^2 5\sigma^2 1\pi^4$, so that the Rydberg state consist of the ion core plus an excited electron. The Rydberg states therefore have rotational constants and equilibrium bond

distances similar to that of the ion.¹⁶ The near identity of the Rydberg and ionic state potential strongly influences the vibrational and rotational propensity rules expected for REMPI via these Rydberg states.

The first excited state of NO with overall Σ^+ symmetry is the $A^2\Sigma^+(3s\sigma)$ state ($T_e \sim 44,000 \text{ cm}^{-1}$), i.e., with $n=3$ and $\ell_0=0$.¹⁴ It has been the subject of numerous REMPI studies,^{8,9,11,12} most of which are of the $(1+1)$ or $(1+1')$ excitation scheme, where the prime indicates a different wavelength for the ionizing photon. These experiments have elucidated a number of important aspects of REMPI, which will be discussed further in chapters 2-5.

The second member of the Σ^+ Rydberg series is the $D^2\Sigma^+(3p\sigma)$ state, with $T_e=53085 \text{ cm}^{-1}$ and I.P.($v=0$)=2.66 eV. This state is the focus of the present discussion. Reilly *et al.*⁹ measured the rotationally-resolved $(2+1)$ one-color REMPI spectrum via the 0-0 band for the $S_{21}(11.5)$ and the mixed $S_{11}+R_{21}(15.5)$ branches of the $D^2\Sigma^+$ state. The photoelectrons have a kinetic energy of about 650 meV, and their intensity was measured parallel and perpendicular to the direction of the laser polarization. In Fig. 3 we show the possible rotational branches for one-photon excitation of NO. The spin of the unpaired electron can couple with or against the total electronic angular momentum in the ground state ($\Lambda=1$), forming a $^2\Pi_{1/2}$ and a $^2\Pi_{3/2}$ manifold designated F_1 and F_2 , respectively.¹⁶⁻¹⁷ Similarly for the Rydberg state the unpaired electron can couple with or against the angular momentum N_i of the molecular frame. This is indicated by a further subscript 1 or 2. The rotational branches are designated with ΔJ and two subscripts, where the first subscript in-

dicates the coupling of the spin in the upper state and the second the coupling in the ground state. These coupling schemes result from applying Hund's case (b) to the upper Rydberg state and the intermediate coupling (between Hund's case (a) and (b)) to the ground state.¹⁶ The $S_{21}(11.5)$ rotational line therefore implies $J_0=11.5$, $N_0=11$, and $J_1=13.5$, $N_1=14$. This branch has $\Delta N=3$ for a 2-photon excitation and would be forbidden in the absence of spin coupling. It is hence a weak transition, but it is rotationally clean meaning that only one rotational branch is accessed. Mixed branches occur because states with $J_1=N_1 \pm 1/2$ cannot be resolved experimentally, since this splitting is less than the laser bandwidth ($\sim 1\text{cm}^{-1}$). The two intermediate rotational levels are incoherently excited and are treated as independent photoionization channels.

In Figs. 4 and 5 we show the measured photoelectron spectra for the $S_{21}(11.5)$ and $S_{11}+R_{21}(15.5)$ branches, respectively.⁹ The odd- ΔN ($\Delta N \equiv N_+ - N_1$) signals are seen to be dominant but with a substantial $\Delta N=0$ signal for parallel detection. In an atomic-like picture of photoionization the photoelectron continuum should be dominated by the $\ell = \ell_0 \pm 1$ channels, where ℓ_0 is the angular momentum of the Rydberg electron and ℓ is a partial-wave component of the photoelectron orbital. It can further be shown that a strict $\Delta N + \ell = \text{odd}$ selection rule applies for a $\Sigma \rightarrow \Sigma$ transition in the photoionization step.¹⁸ Extensive *ab initio* studies of the $3p\sigma$ orbital of the $D^2\Sigma^+(3p\sigma)$ state by Viswanathan *et al.*⁹ found it to be more than 99% p-wave character ($\ell_0=1$). Based on an atomic picture we therefore expect photoionization into the even partial waves of the continuum ($\ell=0,2$) and hence should observe $\Delta N=\text{odd}$ peaks in the spectra. The

$\Delta N = \text{odd}$ signals are indeed seen to be dominant in the experimental spectra. The strong $\Delta N = 0$ signal in the parallel direction, however, cannot be explained by this atomic picture. This would require odd ($\ell = 1, 3, \dots$) partial waves in the photoelectron orbital, i.e., a $3p \rightarrow kp$ transition. In order to account for the presence of the $\Delta N = 0$ peak we will show that it is necessary to consider the non-isotropic character of the molecular molecular potential in the description of the photoionization dynamics into account.

The calculation of the photoionization step in REMPI requires the evaluation of the transition moment between the Rydberg state and the final state. In the frozen-core approximation, where the ionic core orbitals are constrained to be identical to the the orbitals of the Rydberg state, this devolves to a calculation of the transition matrix element r_{fi} between the Rydberg orbital and the photoelectron continuum orbital $\Psi_{\vec{k}}^{-}(\vec{r})$. In our work the continuum orbital is the solution to the one-electron Schrödinger equation

$$\left[-\frac{1}{2} \nabla^2 + V_{N-1}(\vec{r}) - \frac{k^2}{2} \right] \Psi_{\vec{k}}^{-}(\vec{r}) = 0, \quad (1)$$

where $\frac{k^2}{2}$ is the photoelectron kinetic energy, and V_{N-1} is the non-isotropic and non-local ion potential. Expansion of $\Psi_{\vec{k}}^{-}(\vec{r})$ in spherical harmonics about \hat{k} and \hat{r} gives the partial-wave expansion¹⁹ of $\Psi_{\vec{k}}^{-}$,

$$\Psi_{\mathbf{k}}^{\leftarrow}(\vec{r}) = \left(\frac{2}{\pi}\right)^{1/2} \sum_{\ell, \ell', m} i^{\ell} \Psi_{\ell \ell' m}(r) Y_{\ell' m}(\hat{r}) Y_{\ell m}^*(\hat{k}), \quad (2)$$

and the relevant partial-wave transition moment $r_{fi}^{\ell \lambda \mu}$ is

$$r_{fi}^{\ell \lambda \mu} = \sum_{\ell', \ell_0} \langle \Psi_{\ell \ell' \lambda}(r) Y_{\ell' \lambda}(\hat{r}) | r Y_{1 \mu}(\hat{r}) | \Phi_{i \ell_0}(r) Y_{\ell_0 \lambda - \mu}(\hat{r}) \rangle. \quad (3)$$

It is important to note that for a central potential, $\ell = \ell'$. The non-spherical nature of the molecular ion potential causes a mixing between different ℓ and ℓ' . The dipole selection rules imply $\ell' = \ell_0 \pm 1$ in Eq. (3). This does not, however, imply that $\ell = \ell_0 \pm 1$. If the potential is very non-spherical it can create a greater torque on the outgoing photoelectron, and the dominant ℓ can be very different from ℓ' . The one-electron Schrödinger equation for $\Psi_{\mathbf{k}}^{\leftarrow}$ is solved using the iterative Schwinger method, which is an *ab initio* method based on the integral form of Eq. (1).¹⁹ The intermediate state wave function is calculated using the improved virtual orbital method (IVO),²⁰ an *ab initio* method where the Rydberg orbital is optimally determined in the potential of the (N-1) electron ion core. Use of the IVO and Hartree-Fock continuum orbitals corresponds to a one-electron treatment of the photoionization dynamics, and has been shown to be a good description of the photoionization of NO.

The 3pσ orbital of D-state has an angular composition (ℓ_0 -expansion) of 0.55% s-, 99.20% p-, 0.11% d-, and 0.07% f-character, respectively. The Rydberg orbital is therefore very atomic-like, in agreement with the results of Reilly *et al.*⁹ Partial-wave mixing in the intermediate state

therefore cannot be responsible for the strong $\Delta N=0$ signal. The calculated transition moment between the D-state and the photoelectron continuum reveals, however, a significant contribution from the p-wave of the continuum. This is due to the non-isotropic (non-atomic) ionic potential which leads to a substantial continuum partial-wave mixing.¹⁹ It is essential to account for the effect of the non-isotropic ion potential on the photoelectron in order to correctly predict this strong ℓ -mixing in the continuum.

In order to determine the rotational branching ratios it is necessary to consider the excitation dynamics of the overall REMPI process. The (2+1) REMPI process can be viewed as a two-photon excitation from an initially unaligned ground state to an aligned resonant intermediate state (the D-state), followed by a one-photon ionization out of this aligned state,²¹



The total angular momentum (\vec{J}) and its projection (M_J) on the laboratory Z-axis (defined by the polarization direction of the laser) are good quantum numbers. The term alignment refers to the relative population of the different M_J -levels. For a molecule in field-free space there is no preferred direction and all M_J -levels are equally populated. Such molecules are said to be unaligned. The intermediate state's alignment in the perturbative limit and in the absence of M_J -mixing terms is proportional to a product of 3-j symbols and the line strength B ,²²

$$\rho_{ii} \propto \begin{pmatrix} J_i & 2 & J_0 \\ M_i & 0 & -M_i \end{pmatrix}^2 B \quad (5)$$

The line strength B is important for rotationally-mixed branches since it reflects the relative transition strength of the different rotational branches. The calculation of B requires a number of spectroscopic constants for the relevant states, and can be determined according to the guidelines of Halpern *et al.*²³ The ionic rotational branching ratios are then evaluated as a sum over the individual M_J -level's cross section, weighted by their relative population ρ_{ii} .

In Figs. 4 and 5 we compare the calculated and experimental⁹ branching ratios for (2+1) REMPI via the $S_{21}(11.5)$ and $S_{11}+R_{21}(15.5)$ branches of the $D^2\Sigma^+$ state of NO. The calculated branching ratios have been convoluted with a Lorentzian detector function with a FWHM=6meV. The agreement in the perpendicular direction is particularly good. The calculated magnitude of the $\Delta N=0$ signal for parallel detection is substantial, although not as strong as observed experimentally. The $\Delta N+\ell=\text{odd}$ selection rule implies that the strong $\Delta N=0$ signal is due to an odd-wave contribution to the continuum wave function. An explanation of the strong $\Delta N=0$ signal in the parallel direction (but weak signal in the perpendicular detection) is therefore due to a significant p-wave component in the continuum. Such a p-wave has a nodal plane in the perpendicular direction (imagine a p_x -orbital along the x-axis) and would not contribute to the perpendicular signal. These measurements by Reilly *et al.*⁹ of rotational branching ratios at two angles are the first example of the use of rotationally-resolved photoelectron angular distributions for identi-

fying the angular momentum composition of molecular photoelectron orbitals.

In Fig. 6 we show the rotational branching ratios for the $S_{21}(15.5)$ branch via the D-state and the $R_{22}(21.5)$ branch of the A-state of NO as a function of photoelectron kinetic energy. The branching ratios for the D-state are found to be very energy dependent whereas the A-state branching ratios are almost energy independent. The N-1 electron ionic core of the two Rydberg states are identical, so that the photoelectron wave functions calculated in the frozen-core approximation are essentially the same for these two states. The rotational branching ratios depend, however, on both the Rydberg state and the photoelectron continuum character since the transition moment between the two states determines the magnitude of the cross section. The difference between the energy dependence of the A- and D-state therefore reflects the differences in the way they couple to the photoelectron continuum.²² The almost pure s-character of the A-state (>98% s-character) predominantly probes the p-wave of the continuum wave function ($s \rightarrow kp$). The p-wave character of the photoelectron continuum for this system is found not to change dramatically over this limited energy range, whereas the higher partial waves (d,f,...) are more energy dependent. The strong p-character of the D-state provides a strong coupling to the d-component ($3p \rightarrow ks, kd$) of the continuum, and the rotational branching ratios for the D-state are therefore more energy dependent than those of the A-state. The symmetry and character of the intermediate state can hence be used to probe certain parts of the continuum and their energy dependence by rotationally-selective excitation.

This predicted energy dependence of the rotational branching ratios for the D-state later prompted Song *et al.*¹⁰ to do a (1+1') two-color REMPI experiment via the D-state. Chapter 5, where we reinvestigate the D-state results, discusses our collaboration with Reilly's group. The experimental energies are different from those previously calculated, but the observed branching ratios are found to depend strongly on photoelectron kinetic energy. The experimental $\Delta N=0$ signal is again seen to be stronger than theoretically predicted. We find that this is due to a non-adiabatic interaction between the A-state and the D-state. This causes the effective electronic wave function to have a 2% A-state character and 98% D-state character. This small contribution of the A-state is sufficient to account for the large $\Delta N=0$ signal in the parallel direction and its energy dependence. The calculated branching ratios do not change in the perpendicular direction because of this mixing since the A-state component contributes an almost exclusive p-character to the $\Delta N=0$ signal (see Figs. 4 and 5 of chapter 5). These results illustrate how studies of ionic rotational branching ratios have made it possible to identify non-adiabatic coupling in the intermediate state. This identification would not have been possible on the basis of rotationally-unresolved REMPI spectra.

Recently Sander *et al.*¹¹ measured the ionic rotational branching ratios for (1+1') REMPI via the $P_{11}(J_0=3/2-7/2)$ branch of the $A^2\Sigma^+(3s\sigma)$ state of NO using the ZEKE technique. This technique measures threshold photoelectrons with a resolution of $\sim 1\text{cm}^{-1}$, which is not obtainable with conventional TOF methods. The rotational branching ratios were found to

be very J -dependent. The ratio of $\Delta N=0$ to $\Delta N=2$ signals is observed to drop from about 0.5 for the $P_{11}(3/2)$ branch to about 0.25 for the $P_{11}(5/2)$ branch (see Fig. 1 of chapter 3). A change in J of one unit leads to the change in the branching ratios by a factor of 2! This decrease in the branching ratios does not continue when higher rotational levels are accessed. This is a surprising result since all previous studies at higher J values have shown the branching ratios to be almost J independent. It is of interest to understand what makes these low- J studies so unique for molecular REMPI. This result could arise from an energy dependence of the branching ratios. However, as shown above, we do not expect the branching ratios to be strongly energy dependent for the A-state. In chapter 3 we study the high resolution, low- J rotational branching ratios for $(1+1')$ REMPI via the P_{11} and R_{22} branches of the $A^2\Sigma^+$ state of NO. The calculated branching ratios for the P_{11} branch are in excellent agreement with the experimental results, and it is possible to explain the observed phenomena rigorously on the basis of angular momentum constraints, specifically the $\Delta N=0$ signal of the $P_{11}(3/2)$ branch is restricted to only having the p-wave of the continuum contributing to its signal. The measured photoelectron angular distribution would display the pure p-character. Calculated photoelectron angular distributions depend strongly on ΔN . The R_{22} branch for similarly low- J values does not have the same angular momentum constraints, and the calculated branching ratios do not show this dramatic dependence on J . This demonstrates how unique the low- J limit is for molecular REMPI and how it makes it possible to study photoionization dynamics in greater detail than in conventional PES.

In chapter 4 we study the high-J limit ($J \geq 10$) for rotationally resolved ($1+1'$) REMPI via the $A^2\Sigma^+(3s\sigma)$ state of NO. The preliminary results for these studies were presented at the American Physical Society's Spring Meeting in Baltimore in April of 1988.²⁴ These results showed: (i) strong ΔN dependence of the photoelectron angular distributions, (ii) that the ΔN and $-\Delta N$ distributions are identical, i.e., symmetric around $\Delta N=0$, and (iii) that the distributions are alignment dependent. Allendorf *et al.*²⁵ have also reported photoelectron angular distributions for the $\Delta N = -2, -1$, and 0 signals via the $R_{21}(20.5)$ branch of the $A^2\Sigma^+$ state of NO. The agreement with the calculated distributions was very encouraging. Allendorf *et al.*¹² have since measured rotational branching ratios and photoelectron angular distributions via other rotational branches of the A-state. The agreement between the experimental and calculated spectra is very good and confirm not only that the angular distributions depend on ΔN and are symmetric around $\Delta N=0$, but also that they are very dependent on the alignment of the intermediate state. The $\Delta N + \ell = \text{odd}$ selection rule means that only the even- ℓ can contribute to the odd- ΔN signals, and the dependence of the photoelectron angular distributions on ΔN hence reflect the relative importance of the different partial waves of the continuum, i.e., the partial-wave mixing. The rotationally unresolved photoelectron angular distributions, on the other hand, have contributions from all the partial waves and are dominated by the strong p-wave in the continuum of the $\Delta N=0$ signal. The rotationally-unresolved angular distributions are, therefore, not very branch or J-dependent. This is found to be the case experimentally and theoretically. This work demonstrates the fundamental role that rotational resolution provides for probing the alignment of the intermediate state from

the photoelectron signal. It also illustrates the symmetry around $\Delta N=0$ of the branching ratios and photoelectron angular distributions in the high-J limit (see Fig. 1 of chapter 4).

Chapter 5 presents results of our joint studies with the experimental group of Reilly *et al.*¹⁰ at Indiana University. Here we study the energy dependence of the rotational branching ratios for (1+1') REMPI via the D-state of NO. The strong $\Delta N=0$ signal was found to be due to a combination of strong ℓ -mixing in the continuum and non-adiabatic coupling to the A-state.¹⁷ The effective vibronic mixing of the states is relatively small but the character of the A-state results in a stronger $\Delta N=0$ signal due to this state's strong $\Delta N=0$ propensity, as discussed in chapters 3 and 4. The calculated branching ratios for this mixed state are in good agreement with the experimentally observed energy dependence.

We have shown that the character and symmetry of the $A^2\Sigma^+$ and $D^2\Sigma^+$ states have a profound influence on the rotational branching ratios and their energy dependence. If the Rydberg state itself changes character as a function of internuclear distance, it should also affect the measured ionic rotational branching ratios. In chapter 6 we discuss such an example where we study the rotationally resolved (2+1') REMPI via the $E'^2\Sigma^+(3p\sigma)$ state of CH. The electronic wave function for this state changes character from $[1\sigma^2 2\sigma^2 3\sigma^2]3p\sigma$ (predominantly p-character) around the equilibrium internuclear distance ($R_e=2.25 a_0$) to $[1\sigma^2 2\sigma^2 3\sigma^2]3s\sigma$ (predominantly s-character) at larger R. This orbital evolution, the origin of which is not completely clear to us at present, creates a strong dependence of the photoionization matrix element on internuclear dis-

tance and therefore leads to strong non-Franck-Condon vibrational branching ratios in REMPI.²⁶ The lower vibrational levels of the E' -state have classical turning points close to R_e and are "dominated" by the p-character of the state.¹⁶ On the other hand, the higher vibrational levels probe the larger R region of the potential well and hence sample substantially greater s-wave character of the Rydberg orbital. Based on the $\Delta N + \ell = \text{odd}$ selection rule,¹⁸ and the atomic photoionization picture, we expect a $\Delta N = \text{odd}$ ($3p \rightarrow ks, kd$) rotational propensity rule for the lower vibrational levels of the E' -state due to the dominant p-character. The calculated branching ratios for $(2+1')$ REMPI via the $v=0$ level of the E' -state confirm this. However, the propensity rule changes to $\Delta N = \text{even}$ for photoionization via the higher vibrational levels of the E' -state, due to the change from p- to s-wave in the Rydberg orbital. This change in rotational distributions, resulting from rapid orbital evolution with internuclear distance in the intermediate state, has not yet been observed. It is quite general and should be most readily observable in other diatomic hydrides.

We have in all the above studies used the Hartree-Fock description for determining the Rydberg orbital, which is adequate for describing the orbital evolution in the E' -state of CH, since it is an interaction between two states that differ by one orbital. If, however, the interaction between the states involve more than one orbital, it is necessary to use a configuration interaction (CI) description for the interaction. These interactions are often referred to as avoided crossings or Rydberg-valence mixings. In chapter 7 we study $(2+1)$ REMPI via the double-well $E, F^1\Sigma_g^+$ state of H_2 . This state is formed by an avoided crossing

between the inner-well Rydberg E-state with a dominant $1\sigma_g 2\sigma_g$ configuration, and the outer-well valence F-state with a $1\sigma_u^2$ dominant configuration. In a one-electron picture only the E-state has a transition moment to the ground state of H_2^+ ($1\sigma_g$). The calculated vibrationally resolved photoionization spectra are found to be only slightly non-Franck-Condon. Experimentally the vibrational branching ratios show a stronger non-Franck-Condon behavior,²⁷ but recent theoretical calculations (by other groups) have confirmed our results.²⁸⁻²⁹ Autoionization is probably the cause of this discrepancy, although recent theoretical calculations suggest²⁹ laser intensity effects to result in apparent non-Franck-Condon effects.

It is very difficult to measure the absolute cross section of a REMPI photoionization process. The experimental uncertainties with respect to laser intensity, interaction volume, and the number density of molecules in this interaction volume make it difficult to accurately determine the absolute photoionization cross section. Recently, Meier *et al.*³⁰ suggested a method based on ionization measurements with saturation of the intermediate state to determine these cross sections for specific rovibronic levels of the $B^1\Sigma_u^+$ state of H_2 . In chapter 8 we calculate the corresponding theoretical cross sections and find them to be very different from the experimental ones by nearly an order of magnitude. Here the REMPI dynamics can no longer be treated in the perturbative limit and a density matrix approach is used. The set of coupled differential equations is solved in time and space to account for the spatial and temporal variations of the laser intensity. The photoionization efficiency is seen to be profoundly influenced by these

factors which may have caused the discrepancy between the experimentally deduced and the calculated cross sections. Another possible cause for the discrepancy is autoionization. The influence of this process could be probed experimentally by changing the wavelength of the second photon so as to detune away from the autoionizing feature.

Finally in chapter 9, we investigate the branch dependence and laser intensity effects on (1+1) rotationally resolved REMPI via the $A^2\Sigma^+(3s\sigma)$ state of NO. The experiments of Reilly *et al.*^{8,9} did not fully assign the rotational branch accessed in excitation of the resonant state. The calculated ion rotational distributions are found to be branch-dependent. Furthermore, the branching ratios and photoelectron angular distributions also depend strongly on laser intensity. Discrepancies still remain, however, between the calculated and measured branching ratios for detection of photoelectrons perpendicular to the laser polarization. The most likely cause for the discrepancy is a small contamination of the laser polarization. Since the photoelectron signal perpendicular to the laser polarization is only about 2% of the intensity for parallel detection, a small contamination (i.e., a linear polarization of less than 99%) is sufficient to account for the observed perpendicular signal.

In conclusion we have shown that rotationally-resolved REMPI is an important probe of the molecular excited states at a quantum state specific level. The analysis of such REMPI spectra provides valuable insight into the influence of the resonant intermediate state and photoelectron continua on the underlying dynamics of these processes. We have demonstrated for particular molecules how perturbations in the interme-

mediate state, orbital evolution, configuration interaction, and non-adiabatic interactions can have a profound impact on the observed REMPI spectra. We have also seen that the state specificity of the REMPI process combined with rovibrational propensity rules can be used for creating ions in a selected rovibrational level. The theoretical framework presented here makes it possible to address the influence of the different contributions to the overall REMPI spectrum and to qualitatively assess their relative importance. Autoionization and other competing processes, e.g., dissociation, have not been included in these studies and would have to be incorporated for a more complete description of the photoionization dynamics.

REFERENCES

- 1 K. Kimura, Adv. Chem. Phys. **60**, 161 (1985).
- 2 R.N. Compton and J.C. Miller, *Multiphoton Ionization Photoelectron Spectroscopy: MPI-PES* (Oak Ridge National Laboratory, 1987).
- 3 S.T. Pratt, P.M. Dehmer, and J.L. Dehmer, in *Advances in Multiphoton Processes and Spectroscopy, Vol. IV*, ed. S.H. Lin (World Scientific Press, Singapore, 1988) p. 69-169.
- 4 J.W. Hudgens, in *Advances in Multiphoton Processes and Spectroscopy, Vol. IV*, ed. S.H. Lin (World Scientific Press, Singapore, 1988) p. 171-296.
- 5 S. Katsumata, K. Sato, Y. Achiba, and K. Kimura, J. Electr. Spectr. Rel. Phen. **41**, 325 (1986).
- 6 J.E. Pollard, D.J. Trevor, J.E. Reutt, Y.T. Lee, and D.A. Shirley, J. Chem. Phys. **77**, 34 (1982).
- 7 S.T. Pratt, P.M. Dehmer, J.L. Dehmer, J. Chem. Phys. **78**, 4315 (1983).
- 8 W.G. Wilson, K.S. Viswanathan, E. Sekreta, and J. P. Reilly, J. Phys. Chem. **88**, 672 (1984).

- 9 K.S. Viswanathan, E. Sekreta, E.R. Davidson, and J.P. Reilly, J. Phys. Chem. **90**, 5078 (1986).
- 10 Xinbei Song, Ellen Sekreta, James P. Reilly, H. Rudolph, and V. McKoy, submitted to J. Chem. Phys. (Chapter 5 of this thesis).
- 11 M. Sander, L.A. Chewter, K. Müller-Dethlefs, and E.W. Schlag, Phys. Rev. A **36**, 4543 (1987).
- 12 S.W. Allendorf, D.J. Leahy, D.C. Jacobs, and R.N. Zare, accepted for publication in J. Chem. Phys.
- 13 P. Chen, J.B. Pallix, W.A. Chupka, and S.D. Colson, J. Chem. Phys. **86**, 516 (1987).
- 14 K.P. Huber and G. Herzberg, *Constants of Diatomic Molecules* (Van Nostrand Reinhold, New York, 1979).
- 15 R. Engleman, Jr., P.E. Rouse, H.M. Peek, V.D. Baiamonte, *Beta and Gamma Band Systems of Nitric Oxide* (Los Alamos National Laboratory, 1970).
- 16 G. Herzberg, *Spectra of Diatomic Molecules* (Van Nostrand Reinhold, New York, 1950).
- 17 H. Lefebvre-Brion and R.W. Field, *Perturbations in the Spectra of Diatomic Molecules* (Academic Press, Orlando, 1986).

- 18 S.N. Dixit and V. McKoy, Chem. Phys. Lett. **128**, 49 (1986).
- 19 R.R. Lucchese, G. Raseev, and V. McKoy, Phys. Rev. A **25**, 2572 (1982).
- 20 W.J. Hunt and W.A. Goddard III, Chem. Phys. Lett. **24**, 464 (1974).
- 21 S.N. Dixit and V. McKoy, J. Chem. Phys. **82**, 3546 (1985).
- 22 H. Rudolph, S.N. Dixit, V. McKoy, and W.M. Huo, J. Chem. Phys. **88**, 637 (1988).
- 23 J.P. Halpern, H. Zacharias, and R. Wallenstein, J. Mol. Spectrosc. **79**, 1 (1980).
- 24 V. McKoy *et al.*, Bull. of Am. Phys. Soc. **33** (4), 920 (1988).
- 25 S.W. Allendorf *et al.*, Bull. of Am. Phys. Soc. **33** (4), 919 (1988).
- 26 J. A. Stephens and V. McKoy, Phys. Rev. Lett. **62**, 889 (1989).
- 27 S.L. Anderson, G.K. Kubiak, and R.N. Zare, Chem. Phys. Lett. **105**, 22 (1984).
- 28 C. Cornaggia, A. Guisti-Suzorm and Ch. Jungen, J. Chem. Phys. **87**, 3934 (1987).

- 29 N. Sen, K.R. Dastidar, T.K.R. Dastidar, Phys. Rev. A **38**, 841 (1988).
- 30 W. Meier, H. Rotke, H. Zacharias, and K.H. Welge, J. Chem. Phys. **83**, 4360 (1985).

FIGURE CAPTIONS

- Figure 1 Schematic apparatus for molecular REMPI. From "ZARELAB" at Stanford University. From Ref. 12.
- Figure 2 List of the spectroscopic constants for the excited states of NO and their potential energy curves. Adapted from Refs. 16 and 17.
- Figure 3 The possible one-photon rotational transitions from the $X^2\Pi$ ground state of NO to a $^2\Sigma^+$ Rydberg state. The $P_{21}+Q_{11}$, $Q_{21}+R_{11}$, $P_{22}+Q_{12}$, and $Q_{22}+R_{12}$ branches are mixed branches.
- Figure 4 Experimental (Ref. 9), left, and calculated (Ref. 20) photoelectron spectra for (2+1) REMPI via the $S_{21}(11.5)$ line of the $D^2\Sigma^+$ state of NO, for (a) laser light polarized parallel (\parallel) to detection; (b) laser light polarized perpendicular (\perp) to detection.
- Figure 5 Same as Fig. 4, but for the mixed $R_{21}+S_{11}(15.5)$ branch.
- Figure 6 Ionic rotational branching ratios as a function of photoelectron kinetic energy, for the $S_{21}(11.5)$ branch via the $D^2\Sigma^+$ state of NO, and for the $R_{22}(21.5)$ branch via the $A^2\Sigma^+$ state. Total length of the abscissa corresponds to 100 meV.

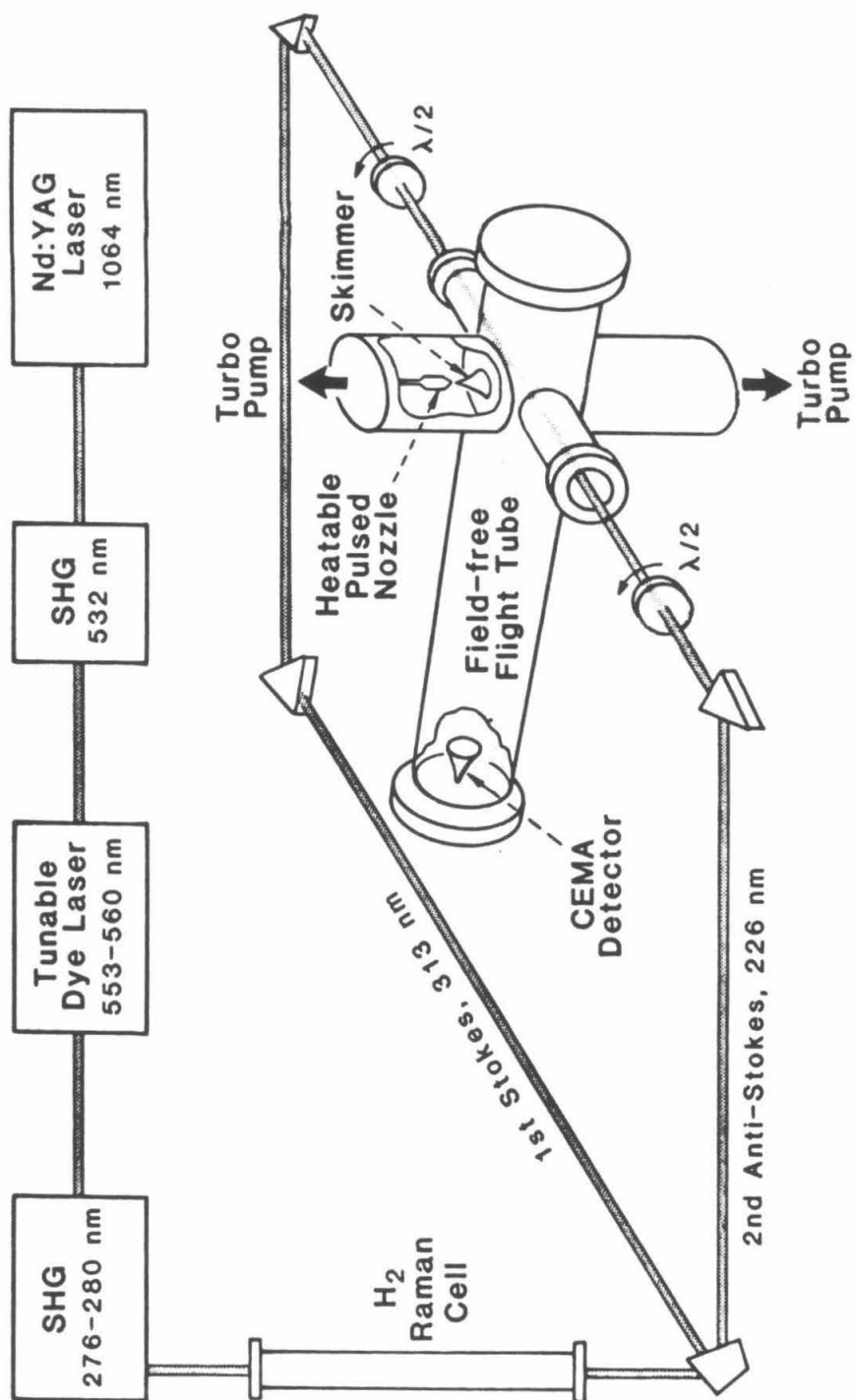


FIGURE 1

State	T_e	E_e	$E_e X_e$	B_e	r_e (Å)
$^{14}\text{N}^{16}\text{O}^+$		$D_0^0 = 10.850_6 \text{ eV}$ I.P. = 30.3 eV			
X $1\Sigma^+$	0	2376.42	16.262	1.99727	1.06322
$^{14}\text{N}^{16}\text{O}$		$\mu = 7.46643323$ $D_0^0 = 6.496_8 \text{ eV}$ I.P. = 9.26436 eV			
M $2\Sigma^+ 3d$	62473.4	[2339.4]		2.003	1.061 ₇
E $2\Sigma^+ 4s$	60628.8	2375.3	16.4 ₃	1.9863	
D $2\Sigma^+ 3p$	53084.7	2323.90	22.885	2.0026	1.061 ₈
C $2\Sigma^+ 3p$	52126	2395	15	2.000	1.062
B $2\Sigma^+$	45942.6 45913.6	1039.8 1037.2	8.3 7.7 ₀	1.152 1.092	1.416 ₇
A $2\Sigma^+ 3s$	43965.7	2374.31	16.106	1.9965	1.063 ₄
X $2\Sigma^+$	119.82 0	1904.04 ₀ 1904.20 ₆	14.100 14.075	[1.72016] [1.67195]	1.15077

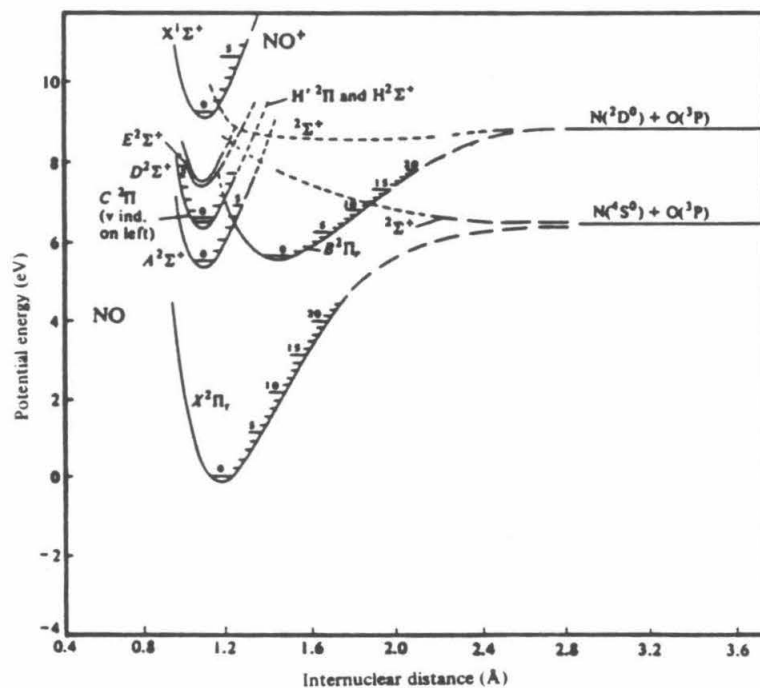


FIGURE 2

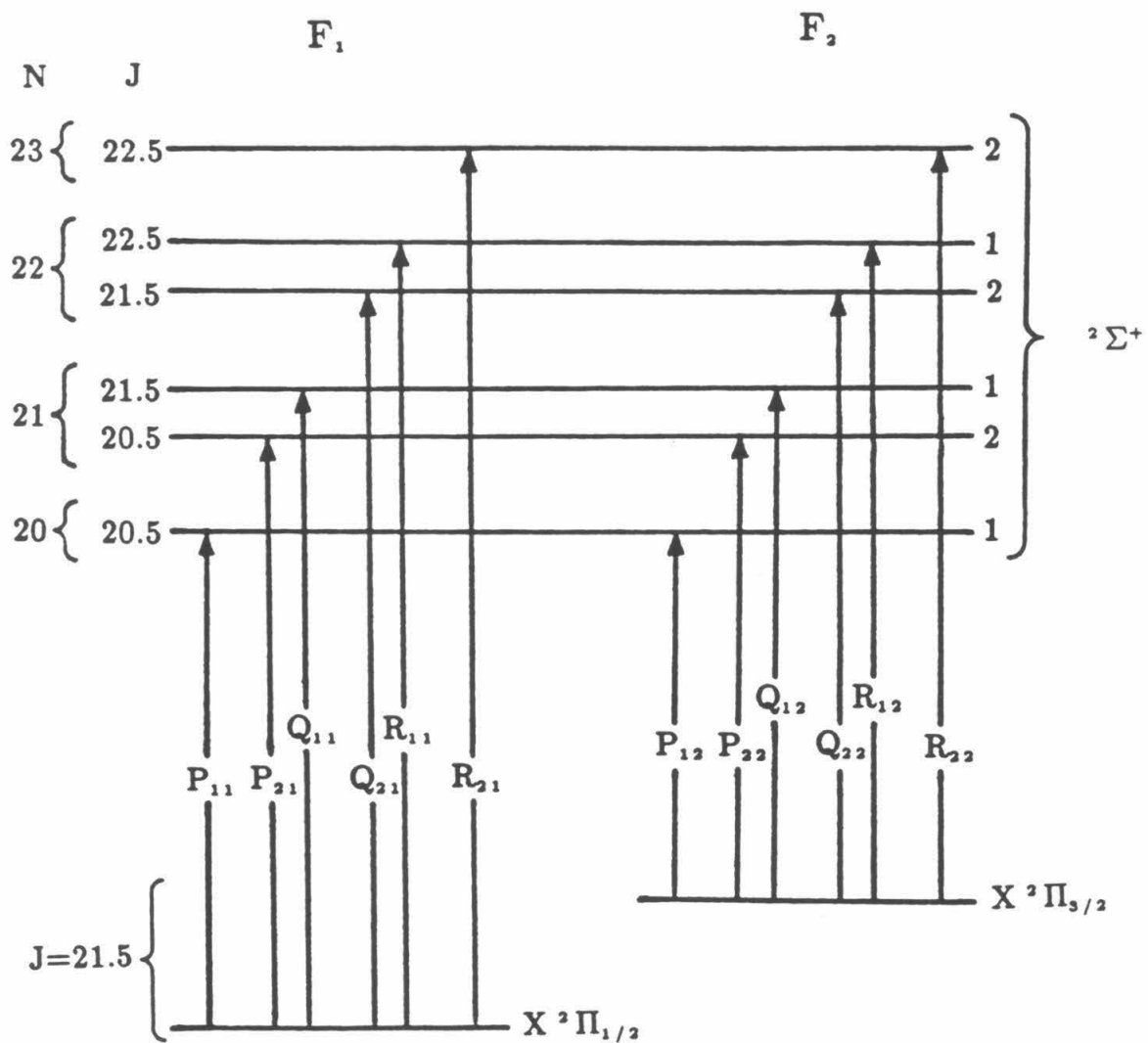


FIGURE 3

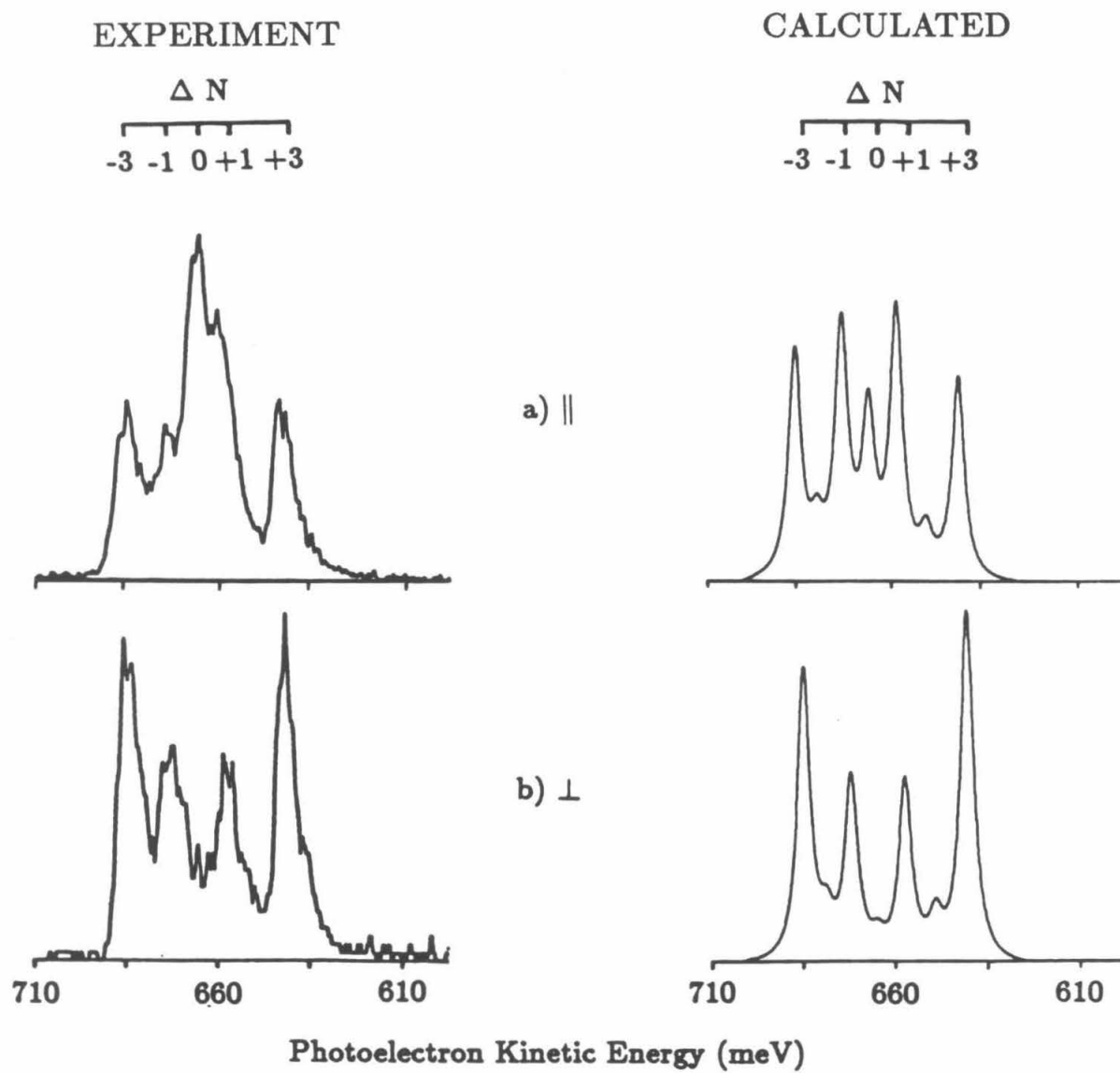


FIGURE 4

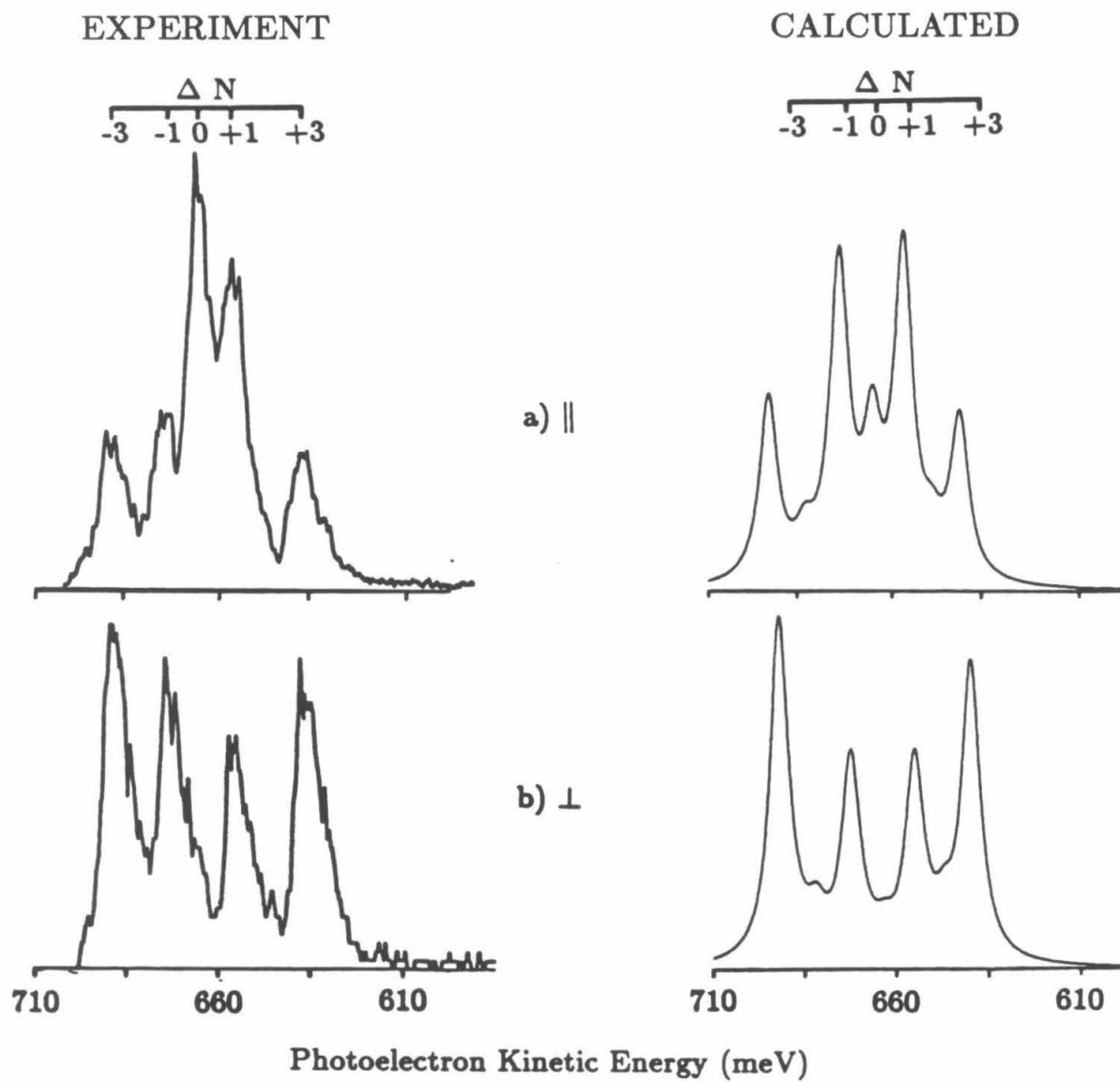


FIGURE 5

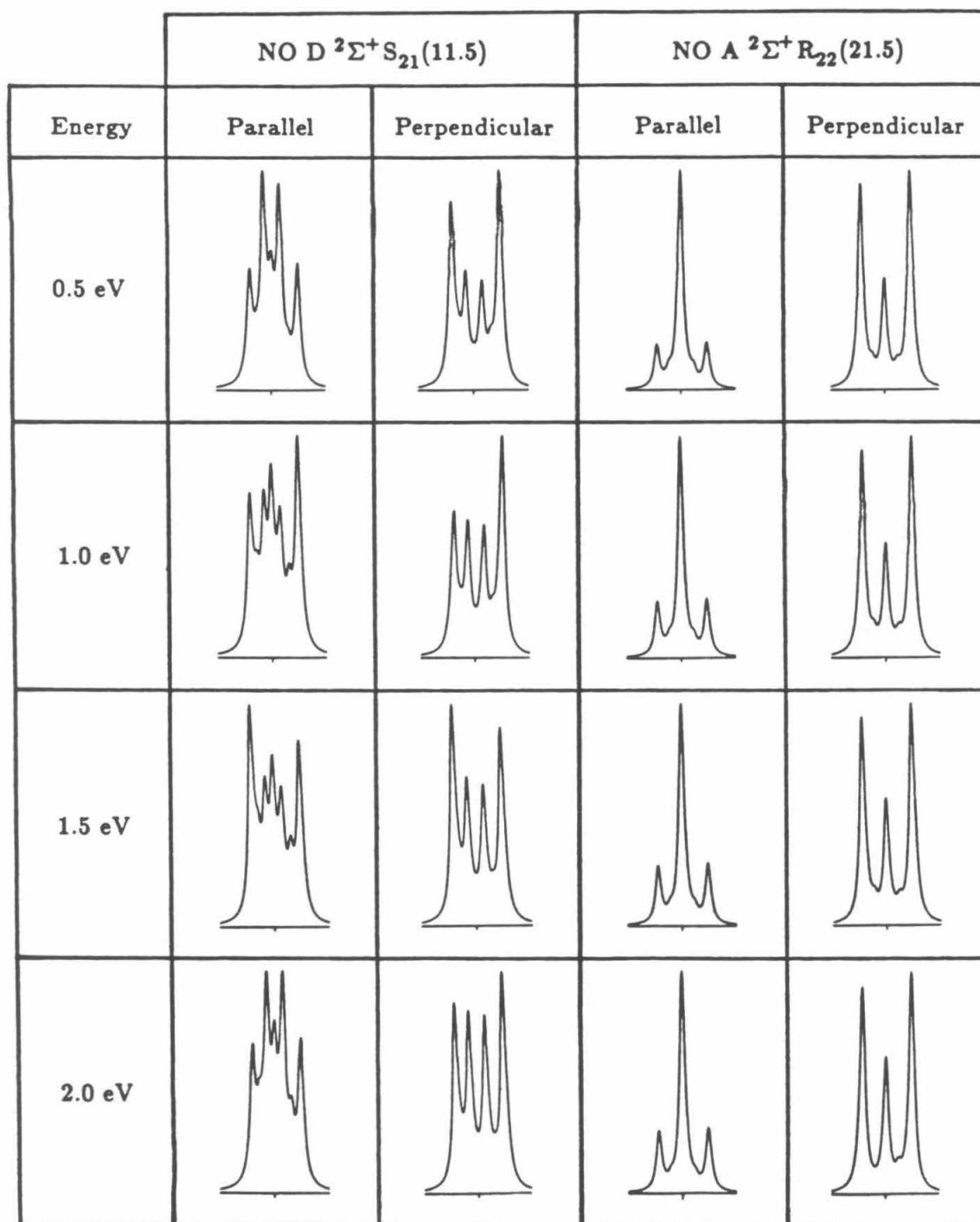


FIGURE 6

**Chapter 1: (2+1) REMPI of NO via the $D^2\Sigma^+$ state: Rotational
branching ratios**

[The text of this chapter appeared in: H. Rudolph, S.N. Dixit, V. McKoy,
and W.M. Huo, Chem. Phys. Lett. 137, 521 (1987)]

(2+1) REMPI OF NO VIA THE D²Σ⁺ STATE: ROTATIONAL BRANCHING RATIOS

H. RUDOLPH, S.N. DIXIT¹, V. MCKOY

Arthur Amos Noyes Laboratory of Chemical Physics², California Institute of Technology, Pasadena, CA 91125, USA

and

Winifred M. HUO

NASA-Ames Research Center MS230-3, Moffett Field, CA 94035, USA

Received 9 March 1987

Recent photoelectron spectroscopic studies in a (2+1) REMPI of NO via the Rydberg D²Σ⁺ state have revealed anomalous ionic rotational branching ratios. We have performed ab initio calculations of these branching ratios and find that the *molecular nature* of the ionization continuum plays an essential role in the dynamics. Even though the bound orbital is very atomic-like (> 98% p-like), the photoelectron continuum wavefunction is quite sensitive to the non-spherical nature of the molecular ionic potential and causes a strong persistence of the p-partial wave which, in turn, leads to a large Δ*N*=0 peak.

High resolution studies of photoelectron spectra (PES) produced by resonant-enhanced multiphoton ionization (REMPI) of individual ro-vibronic states are an important probe of the dynamics of such photoionization processes. Whereas ionic rotational states have been resolved in the photoelectron spectrum of H₂ with relative ease [1,2], the resolution of ionic states in heavier molecules has been very difficult because of the smaller rotational constants. Such studies have only been recently performed in NO [3-5]. The (1+1) REMPI PES of NO by Wilson et al. [4] revealed a number of peaks corresponding to various values of the difference (Δ*N*) in the angular momentum quantum numbers for the excited state (*N_i*) and the ion (*N₊*) (Δ*N*≡*N₊* - *N_i*). Ab initio calculations [6] of ionic rotational branching ratios helped to clarify some features of these spectra such as the dominance of the Δ*N*=0 peak and the suppression of the Δ*N*=±1 peaks. The recent (2+1) REMPI PES via the D²Σ⁺ (3pσ) state of NO by Viswanathan et al. [5] shows a strong Δ*N*=0 peak.

Due to the selection rule [6,7] Δ*N*+*l*=odd, valid for ionization of a Σ state leaving the ion in a Σ state, a Δ*N*=0 peak, of significant intensity implies that the photoelectron orbital must have substantial odd-wave (p, f, ...) character. This, combined with the "pure" Rydberg p nature of the 7σ orbital in the D state, led the authors of ref. [5] to suggest that there may be a strong *l*-mixing in the ionization continuum. In this communication, we present results of ab initio calculations of these ionic rotational spectra and compare them with the data of ref. [5]. Indeed, we find the p wave to be quite significant in the composition of the photoelectron orbital, hence accounting for the strong Δ*N*=0 peak. More importantly, these results illustrate the need for an adequate description of electronic continuum states in quantitative studies of low-energy photoionization dynamics.

Our calculations were done using the theoretical framework described earlier [8]. The photoelectron wavefunction is calculated in the frozen-core Hartree-Fock approximation using the iterative Schwinger variational technique for an internuclear separation of 2.008 *a*₀. This is the equilibrium internuclear distance for the NO⁺ ion and most of the

¹ Present address: Lawrence Livermore National Laboratory, L-421, P.O. Box 808, Livermore, CA 94550, USA.

² Contribution No. 7538.

Rydberg states of NO. We use a Gaussian basis set of (10s6p1d) on each atom contracted to [6s4p1d], supplemented with a (7s7p) uncontracted Gaussian basis at the center of mass (c.m.) of the molecule. This large and diffuse basis set on the origin assures the proper diffuseness of the Rydberg states. The electronic wavefunction of the 7σ orbital of the $D^2\Sigma^+$ state is calculated in the improved virtual orbital (IVO) scheme [9], using the NO^+ core ($E(NO^+) = -128.94691$ au). The total energy of the $D^2\Sigma^+$ state in this approximation is -129.03866 au. The use of the NO^+ core is based on the large relaxation of the NO core in the D state, compared to the ground state. Further details will be given elsewhere [10].

The 7σ IVO orbital calculated using the NO^+ core has 0.5% s, 99.2% p, and 0.1% d character, in a single center expansion about the c.m., in agreement with literature values [5,11]. For a photoelectron kinetic energy of ≈ 0.66 eV [5] the relative transition moments which are proportional to $|r_{if}^{\lambda\mu}|^2$, as defined by eq. (13) of ref. [6], are 0.0498 ($l=0$), 0.0566 ($l=1$), 0.0424 ($l=2$), 0.0047 ($l=3$), and 0.0002 ($l=4$) in the $k\sigma$ channel, and 0.0141 ($l=1$), 0.2093 ($l=2$), 0.0134 ($l=3$), and 0.0019 ($l=4$) in the $k\pi$ channel. These results support the conclusions of Viswanathan et al. [5], that the $l=1$ (p wave) is indeed present and very strong in the continuum. Note that an "atomic" like analysis would have predicted ionization into s and d waves only. The unusually large strength of the p wave is a consequence of the l -mixing in the photoelectron continuum, caused by the non-spherical potential of the molecular ion. The core potential for higher Rydberg states approaches the potential of the ion, and this is expected to cause similar anomalous features in photoionization out of higher Rydberg states.

In fig. 1 we compare the calculated photoelectron spectrum with the experimentally measured ones for two-photon resonant excitation via the S_{21} (11.5) line. This transition was chosen as it is unmixed and the calculation of relative M_j populations in the excited state is simple. Our calculated rotational branching ratios are convoluted with a Lorentzian detection function having a fwhm of about 6 meV. The agreement of the theoretical and experimental PES is quite good for detection parallel and excellent for detection perpendicular to the laser polarization.

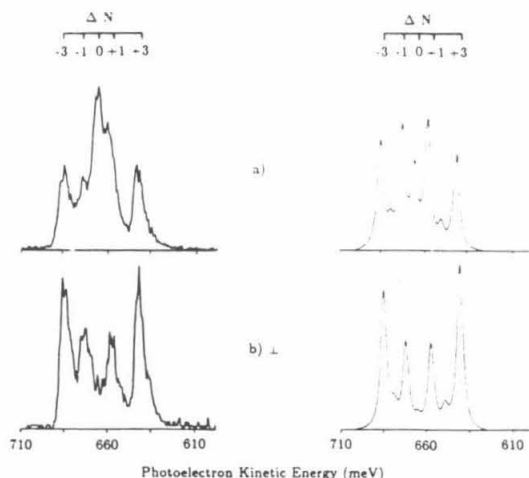


Fig. 1. Experimental [5] (left) and calculated (right) photoelectron spectra with the laser tuned to the S_{21} (11.5) line of the $X^2\Pi \rightarrow D^2\Sigma^+$ transition of NO, for (a) laser light polarized parallel (\parallel) to detection, (b) laser light polarized perpendicular (\perp) to detection.

The $\Delta N=0$ peak is quite significant in the parallel detection and is small, as observed experimentally as well, in the perpendicular detection. Combined with the selection rule $\Delta N + l = \text{odd}$, these results point to significant odd- l partial waves. More importantly, the good qualitative agreement between the theory and experiment illustrates the ability of ab initio calculations to unravel subtle features in the photoionization dynamics.

This material is based on research supported by the National Science Foundation under grant No. CHE-8521391 and AFOSR grant No. 87-0039. One of us (HR) gratefully acknowledges the support from the Danish Natural Science Research Council.

References

- [1] J.E. Pollard, D.J. Trevor, J.E. Reutt, Y.T. Lee and D.A. Shirley, *J. Chem. Phys.* 77 (1982) 34.
- [2] S.T. Pratt, P.M. Dehmer and J.L. Dehmer, *J. Chem. Phys.* 78 (1983) 4315.
- [3] K. Müller-Detlefs, M. Sander and E.W. Schlag, *Chem. Phys. Letters* 112 (1984) 291.

- [4] W.G. Wilson, K.S. Viswanathan, E. Sekreta and J.P. Reilly, J. Phys. Chem. 88 (1984) 672.
- [5] K.S. Viswanathan, E. Sekreta, E.R. Davidson and J.P. Reilly, J. Phys. Chem. 90 (1986) 5078.
- [6] S.N. Dixit, D.L. Lynch, V. McKoy and W.M. Huo, Phys. Rev. A32 (1984) 1267.
- [7] S.N. Dixit and V. McKoy, Chem. Phys. Letters 128 (1986) 49.
- [8] R.R. Lucchese, G. Raseev and V. McKoy, Phys. Rev. A25 (1982) 2572.
- [9] W.J. Hunt and W.A. Goddard III, Chem. Phys. Letters 24 (1974) 464.
- [10] H. Rudolph, S.N. Dixit and V. McKoy, J. Chem. Phys., to be published.
- [11] K. Kaufmann, C. Nager and M. Jungen, Chem. Phys. 95 (1985) 385.

**Chapter 2: Ionic rotational branching ratios in resonant
enhanced multiphoton ionization of NO via the
 $A^2\Sigma^+(3s\sigma)$ and $D^2\Sigma^+(3p\sigma)$ states**

[The text of this chapter appeared in: H. Rudolph, S.N. Dixit, V. McKoy,
and W.M. Huo, J. Chem. Phys. **88**, 637 (1988)]

Ionic rotational branching ratios in resonant enhanced multiphoton ionization of NO via the $A^2\Sigma^+(3s\sigma)$ and $D^2\Sigma^+(3p\sigma)$ states

H. Rudolph

Arthur Amos Noyes Laboratory of Chemical Physics, California Institute of Technology, Pasadena, California 91125

S. N. Dixit

Lawrence Livermore National Laboratory, L-401, P. O. Box 808, Livermore, California 94550

V. McKoy

Arthur Amos Noyes Laboratory of Chemical Physics, California Institute of Technology, Pasadena, California 91125

W. M. Huo

NASA-Ames Research Center MS230-3, Moffett Field, California 94035

(Received 21 August 1987; accepted 29 September 1987)

We present the results of *ab initio* calculations of the ionic rotational branching ratios in NO for a (1 + 1) REMPI (resonant enhanced multiphoton ionization) via the $A^2\Sigma^+(3s\sigma)$ state and a (2 + 1) REMPI via the $D^2\Sigma^+(3p\sigma)$ state. Despite the atomic-like character of the bound $3s\sigma$ and $3p\sigma$ orbitals in these resonant states, the photoelectron continuum exhibits strong l mixing. The selection rule $\Delta N + l = \text{odd}$ ($\Delta N \equiv N_+ - N_-$) implies that the peaks in the photoelectron spectrum corresponding to $\Delta N = \text{odd}$ ($\pm 1, \pm 3$) are sensitive to even partial waves while those corresponding to even ΔN probe the odd partial waves in the photoelectron continuum. Recent experimental high resolution photoelectron studies have shown a strong $\Delta N = 0$ peak for ionization via the $A^2\Sigma^+$ and the $D^2\Sigma^+$ states, indicating a dominance of odd- l partial waves. While this seems natural for ionization out of the $3s\sigma$ orbital, it is quite anomalous for $3p\sigma$ ionization. Based on extensive bound calculations, Viswanathan *et al.* [J. Phys. Chem. **90**, 5078 (1986)] attribute this anomaly to a strong l mixing in the electronic continuum caused by the nonspherical molecular potential. We have performed *ab initio* calculations of the rotational branching ratios and compared them with the experimental results. The electronic continuum shows a significant p -wave component which leads to the large $\Delta N = 0$ peak in both cases. Calculations are performed for both rotationally "clean" and "mixed" branches. The relative heights of the peaks are very sensitive to the photoelectron kinetic energy for the $D^2\Sigma^+$ state and less so for the $A^2\Sigma^+$ state. This is a direct consequence of the l mixing in the continuum.

I. INTRODUCTION

The technique of resonant enhanced multiphoton ionization (REMPI) combined with high resolution photoelectron spectroscopy (PES) has in recent years proven useful in elucidating the finer dynamical details of the photoionization of smaller molecules.¹⁻⁵ The rotationally resolved photoelectron spectra display highly detailed information concerning both the intermediate resonant state and the photoionization dynamics. The limitations on the resolution of the photoelectron energy detection (≈ 5 meV) have restricted rotationally resolved PES studies to H_2 ,⁶⁻⁹ and with some difficulty to NO.¹⁰⁻¹⁶ New techniques involving threshold photoelectron detection have achieved rotational resolution for relatively low rotational quantum numbers.¹⁷ In a series of recent papers¹⁴⁻¹⁶ Reilly and co-workers have demonstrated very detailed rotationally resolved photoelectron spectra via the $A^2\Sigma^+$, $D^2\Sigma^+$, and the $C^2\Pi$ state of NO. Their spectral resolution (3 meV at best) permits a separation of the rotational structure for medium to high values of J due to the relatively large rotational constant of the NO⁺

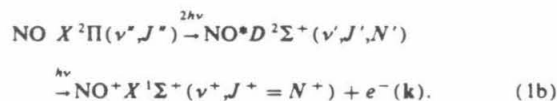
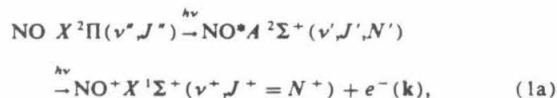
ion ($B_e \approx 2 \text{ cm}^{-1}$). The (1 + 1) REMPI via the $A^2\Sigma^+$ state shows a pronounced $\Delta N = 0$ peak with smaller, but significant, $\Delta N = \pm 2$ peaks. The (2 + 1) REMPI via the $D^2\Sigma^+$ state shows a significant $\Delta N = 0$ signal in addition to the expected $\Delta N = \pm 1, \pm 3$ peaks. While the observed rotational branching ratios for the $A^2\Sigma^+$ state¹⁴ could be rationalized on the basis of an atomic-like model, the $\Delta N = 0$ peak in the $D^2\Sigma^+(3p\sigma)$ photoelectron spectra is not consistent with such a model. The almost pure p character (98%)^{15,18} of the $D^2\Sigma^+$ state would predict a predominant s - or d -wave character of the continuum, giving rise to a dominant $\Delta N = \pm 1$ or ± 3 signal.¹⁹ On the basis of very extensive bound state calculations Viswanathan *et al.*¹⁵ suggested, that the $\Delta N = 0$ peak must be due to odd partial wave character in the electronic continuum arising from the nonspherical nature of the molecular potential.

Recently, we reported calculated rotationally resolved PES for (1 + 1) REMPI via the $A^2\Sigma^+$ state²⁰ as well as for the (2 + 1) REMPI via the $D^2\Sigma^+$ state.²¹ The results agreed quite well with experimental data.¹⁵ Our results for the $D^2\Sigma^+$ state show significant intensity in the $\Delta N = 0$

peak, thus confirming the suggestion of Viswanathan *et al.*¹⁵ that the $\Delta N = 0$ peaks were due to final state interactions. Due to their Rydberg character, the ion cores of the A and D states should be very similar. The photoelectron continuum of these ion cores, should also be similar in these two cases. This suggests that differences in the PES for REMPI via these two states are a consequence of the probing of different angular momentum components of the continuum through the photoelectron matrix element in these two cases. To analyze this feature, we have performed additional PES calculations for rotationally clean and mixed branches and for a range of photoelectron kinetic energies. The results presented in Sec. III demonstrate the importance of the molecular nature of the continuum and stress the necessity for a proper treatment of it.

II. THEORY

The general theory of molecular REMPI processes has been described previously²² and only details pertaining to this particular application will be given here. The $(n + m)$ REMPI process can be thought of conceptually as an n -photon absorption from an initially unaligned (all M_J levels equally populated) ground state, to a resonant intermediate state, followed by an m -photon ionization out of this aligned intermediate state,



REMPI out of each M_J level of the initial state can be treated as an independent channel in the case of linearly polarized photons and in the absence of M_J mixing terms (collisions, etc.). For weak field excitations, the population ρ_{ii} of the intermediate state can be calculated using lowest-order perturbation theory. For the single photon Π - Σ excitation of the A state, ρ_{ii} is given by

$$\rho_{ii} \propto \begin{pmatrix} J' & 1 & J'' \\ -M_J & 0 & M_J \end{pmatrix}^2 A \quad (2a)$$

and for the two-photon Π - Σ excitation of the D state

$$\rho_{ii} \propto \begin{pmatrix} J' & 2 & J'' \\ -M_J & 0 & M_J \end{pmatrix}^2 B, \quad (2b)$$

where J' and J'' are defined in Eq. (1). For a Π - Σ transition the constants A and B can be taken to be independent of the electronic transition moments.²³ For relative ρ_{ii} in pure branches (only one J' state) A and B can be disregarded as well. However, for mixed branches (two J' states corresponding to $N' \pm 1/2$) the relative weights A and B can be calculated using the description of Earls²⁴ and of Halpern,²³ respectively. The photoelectron angular distribution $P(\theta)$, where θ is the angle with respect to the polarization vector of the radiation, can then be written as

$$\frac{dP(\theta)}{d\Omega} \propto \sum_{\text{branches}} \sum_i \Gamma_i(\theta) \cdot \rho_{ii}. \quad (3)$$

Γ_i is the ionization width for the particular M_J level of the intermediate state and involves sums of the square of the transition matrix elements, i.e.,

$$r_{fi}^{\mu\mu} = \sum_{l, l_0} \langle \Psi_{kl\mu}(r) Y_{l, \lambda}(\hat{r}) | r Y_{l_0 \mu}(\hat{r}) | \Phi_{il_0}(r) Y_{l_0, 0}(\hat{r}) \rangle \quad (4)$$

as given by Eq. (13) of Ref. 20. The $r_{fi}^{\mu\mu}$ matrix elements are evaluated using photoelectron continuum orbitals obtained by the variational Schwinger method and the single-center expansion technique.²⁵ The photoelectron Hartree-Fock continuum wave function is determined in the frozen-core approximation using the intermediate state's $(N - 1)$ electron core for the A state and the fully-relaxed ion core for the D state. As shown later, the core of the A state is nearly identical to the fully relaxed ion core due to the diffuse nature of the Rydberg 6σ orbital. For similar reasons the calculations are done for an internuclear distance of $R_e = 1.062$ Å, corresponding to the equilibrium distance of the $^2\Sigma^+$ Rydberg states and the NO^+ ion.²⁶

It is important to note that the partial wave index l need not be equal to the single center expansion index l' in the case of molecular photoionization. For a central potential, $l = l'$. The nonspherical nature of the molecular ion potential causes a mixing between different l and l' . The dipole selection rules imply $l' = l_0 \pm 1$. This does not, however, imply that $l = l_0 \pm 1$. Which partial waves l are dominant depends on how l' and l are coupled via the molecular potential. For example, the 6σ orbital has predominantly $l_0 = 0$, and the 7σ $l_0 = 1$. Thus, for 6σ ionization we have $l' = 1$ while for 7σ ionization $l' = 0, 2$. In spite of this difference, the odd- l partial waves are seen to be dominant in both cases. The strong $\Delta N = 0$ peak corroborates this as well. Thus, even though the bound state may have a strong atomic character, the low-energy photoelectron continuum can be, and often is, quite nonatomic.

The 7σ orbital is determined in the improved virtual orbital (IVO) approximation²⁷ using the fully relaxed core of the ion. The basis set used is given in Table I. The use of the fully relaxed ion core is justified by analyzing the relaxation effects for the $A^2\Sigma^+$ state. The direct SCF energy for the $A^2\Sigma^+$ state is $-129.076\,576$ a.u. IVO calculations with the $X^2\Pi$ ground state core and with the SCF $X^1\Sigma^+$ NO^+ ion core give $-129.038\,179$ and $-129.076\,419$ a.u., respectively. These results show that the ion core of the $A^2\Sigma^+$ state is nearly identical to the $X^1\Sigma^+$ NO^+ state. We have hence performed the IVO and photoelectron continuum calculations using the fully relaxed NO^+ as the frozen core. The calculated energy for the $D^2\Sigma^+$ state is $-129.038\,658$ a.u., corresponding to an excitation energy of 6.186 eV, compared with the experimental value of 6.582 eV.

III. RESULTS

In this section we will first address the $(2 + 1)$ one-color experiments of Ref. 15 via the $D^2\Sigma^+$ state of NO , and then the dependence of the rotational branching ratios on

TABLE I. Gaussian basis set used for the $A^2\Sigma^+$ and $D^2\Sigma^+$ Rydberg states: (10s6p1d) contracted to [6s4p1d] on nitrogen and oxygen, with an additional (7s7p) uncontracted basis set at the center of mass.

Center	Type	Exponent	Coefficient
N	s	5909.44	0.006 24
N	s	887.451	0.047 669
N	s	204.749	0.231 317
N	s	59.8376	0.788 869
N	s	19.9981	0.792 912
N	s	2.6868	0.323 609
N	s	0.7000	1.0
N	s	0.2133	1.0
N	s	0.1000	1.0
N	p	26.7860	0.038 244
N	p	5.9564	0.243 846
N	p	1.7074	0.817 193
N	p	0.5314	1.0
N	p	0.1654	1.0
N	p	0.0800	1.0
N	d	0.8000	1.0
O	s	7816.54	0.006 436
O	s	1175.82	0.048 924
O	s	273.188	0.233 819
O	s	81.1696	0.784 798
O	s	27.1836	0.803 381
O	s	3.4136	0.316 72
O	s	9.5322	1.0
O	s	0.9398	1.0
O	s	0.2846	1.0
O	s	0.1000	1.0
O	p	35.1832	0.040 023
O	p	7.9040	0.253 849
O	p	2.3051	0.806 842
O	p	0.7171	1.0
O	p	0.2137	1.0
O	p	0.0800	1.0
O	d	0.8000	1.0
CM	s	0.4000	1.0
CM	s	0.2000	1.0
CM	s	0.1300	1.0
CM	s	0.0500	1.0
CM	s	0.0250	1.0
CM	s	0.0100	1.0
CM	s	0.0050	1.0
CM	p	0.4000	1.0
CM	p	0.2000	1.0
CM	p	0.1300	1.0
CM	p	0.0500	1.0
CM	p	0.0250	1.0
CM	p	0.0100	1.0
CM	p	0.0050	1.0

the photoelectron kinetic energy for the $(2+1')$ REMPI via the $D^2\Sigma^+$ state and the $(1+1')$ REMPI via the $A^2\Sigma^+$ state.

The $(2+1)$ REMPI experiments of Ref. 15 are one-color experiments via the 0-0 band of the $D-X$ transition, rotationally resolved in the final ion state and rotationally assigned on the basis of data from Huber and Herzberg.²⁶ Photoelectron spectra are measured for the rotationally clean (only one J' contributing) $S_{21}(11.5)$ branch and the mixed $S_{11} + R_{21}(15.5)$ branch, with electron collection parallel and perpendicular to the polarization vector of the radiation. The photoelectron spectra show in both cases a pronounced $\Delta N = 0$ peak, reflecting a large odd partial wave character in the electronic continuum. The 7σ orbital

has an angular decomposition of, 0.55% s , 99.20% p , 0.11% d , and 0.07% f character, in agreement with the results of Ref. 19. The bound-free dipole matrix elements, proportional to the $|r_{if}^{j\mu}|^2$ of Eq. (4), are 0.0498, 0.0566, 0.0424, 0.0047, and 0.0002 for $l = 0-4$, respectively, in the $k\sigma$ channel and 0.0141, 0.2093, 0.0134, and 0.0019 for $l = 1-4$, respectively, in the $k\pi$ channel. This confirms the suggestion of Viswanathan *et al.*,¹⁵ that the p wave is indeed present and strong, but also shows that the strongest ionization channel is the d wave of the $k\pi$ continuum. The total photoionization cross section is therefore dominated by the $k\pi$ channel. The rotationally unresolved, fixed nuclei, cross sections are 0.166 and 0.487 Mb for the $k\sigma$ and the $k\pi$ channel, respectively, in reasonable agreement with the earlier approximate calculations of Ref. 28. These calculated cross sections of the D state are about 50% of those obtained for the A state (see later). This trend is the exact opposite to that seen experimentally by Rottke and Zacharias,¹² who measured cross sections for the $A^2\Sigma^+$ state and the $D^2\Sigma^+$ state of 0.70 ± 0.09 and 6 ± 1 Mb, respectively (for specific rotational levels). We are at present unable to understand this discrepancy.

In Fig. 1, we compare the calculated photoelectron spectrum with the experimental spectrum¹⁵ for the $(2+1)$ REMPI via the rotationally clean $S_{21}(11.5)$ line of the 0-0 band of the $D-X$ transition. The calculated results are convoluted with a Lorentzian detector function having a FWHM of 6 meV, a value chosen as representative of the actual experimental resolution. The calculated rotational branching ratios relative to the $\Delta N = -1$ signal are listed in Table II. The total calculated intensity for perpendicular detection for $\Delta N = -1$ is 7.1% of the corresponding parallel signal. The agreement between the theoretical and the experimental photoelectron spectra is quite good for parallel detection and excellent for perpendicular. The $\Delta N = 0$ signal is, as observed experimentally, significant in the parallel direction,

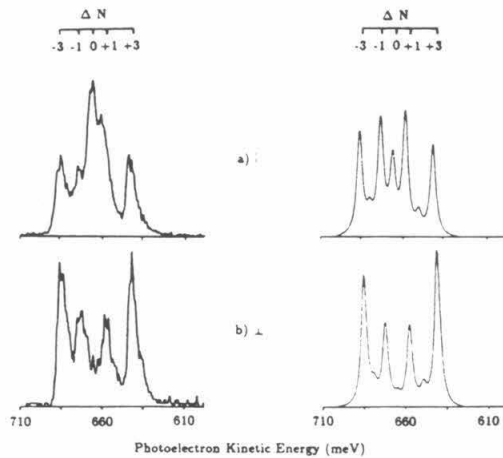


FIG. 1. Experimental (Ref. 15) (left-hand side) and calculated (right-hand side) photoelectron spectra with the laser tuned to the $S_{21}(11.5)$ line of the $D^2\Sigma^+ - X^2\Pi$ transition of NO, for (a) laser light polarized parallel (\parallel) to detection; (b) laser light polarized perpendicular (\perp) to detection.

TABLE II (2 + 1) REMPI via the $D^2\Sigma^+$ state. Calculated rotational branching ratios for the $S_{21}(11.5)$ branch and the $S_{11}(15.5) + R_{21}(15.5)$ branch.

ΔN	Parallel (\parallel)		Perpendicular (\perp)	
	$S_{21}(11.5)$	$S_{11} + R_{21}(15.5)$	$S_{21}(11.5)$	$S_{11} + R_{21}(15.5)$
-3	0.763	0.489	1.974	1.516
-2	0.150	0.101	0.209	0.168
-1	1.000*	1.000*	1.000*	1.000*
0	0.590	0.401	0.093	0.096
+1	0.936	0.965	1.009	1.016
+2	0.158	0.110	0.186	0.185
+3	0.857	0.560	1.643	1.765

* Normalized to this line.

but very small (nonobservable) in the perpendicular direction, demonstrating the sharpness around $\theta = 0^\circ$ of the angular distribution for the $\Delta N = 0$ peak. The $P(\theta)$ of Eq. (3), the angular distribution of the photoelectrons, can be expanded in Legendre polynomials $P_L[\cos(\theta)]$ as

$$P(\theta) = \sum_{L=0,2,\dots}^{L_{\max}} \beta_L \cdot P_L[\cos(\theta)], \quad (5)$$

where L_{\max} in these weak intensity studies is determined by the order of the process. For the $\Delta N = 0$ signal the normalized β parameters are $\beta_0 \equiv 1.000$, $\beta_2 = 1.899$, $\beta_4 = 0.104$, and $\beta_6 = 0.003$.

Mixed branches, such as the $S_{11}(15.5) + R_{21}(15.5)$ branch, can be treated as individual ionization channels, although indistinguishable in the photoelectron spectrum. They can be incoherently added with the proper weighting, as determined by Eq. (2). The relative weights [the B factor of Eq. (2)] are 0.012 20 and 0.004 92, as determined by Halpern,²³ for the $S_{11}(15.5)$ and the $R_{21}(15.5)$ branches, respectively. The two individual branches are calculated as outlined above. In Fig. 2, we compare the experimental and the calculated photoelectron spectra for the mixed $S_{11} + R_{21}(15.5)$ branch. The calculated intensities are again convoluted with a Lorentzian detection function with a FWHM of 6 meV, and the relative branching ratios are listed in Table II. The $\Delta N = 0$ signal is found to be strong in the parallel direction, although less pronounced in the calculated spectrum than in the experimental spectrum. The agreement is seemingly far better in the perpendicular direction. The calculated $\Delta N = 0$ signal is very small, consistent with the experimental observation. The normalized β parameters for the angular distribution of the $\Delta N = 0$ signal are $\beta_0 \equiv 1.000$, $\beta_2 = 1.796$, $\beta_4 = 0.099$, and $\beta_6 = -0.001$. The total strength of the perpendicular $\Delta N = -1$ signal is calculated to be about 18.3% of the corresponding parallel signal.

An important dynamical aspect of the photoionization is the energy dependence of the $\mu_{\alpha\mu}^{\mu\mu}$ matrix elements of Eq. (4). In the one-color experiments of Ref. 15 the final photoelectron kinetic energies span a range of about 1.0 eV for the REMPI via the different Rydberg states, i.e., from ~ 1.7 eV for (1 + 1) REMPI via the $A^2\Sigma^+$ state to ~ 0.7 eV for the (2 + 1) REMPI via the $D^2\Sigma^+$ state. The anomalous

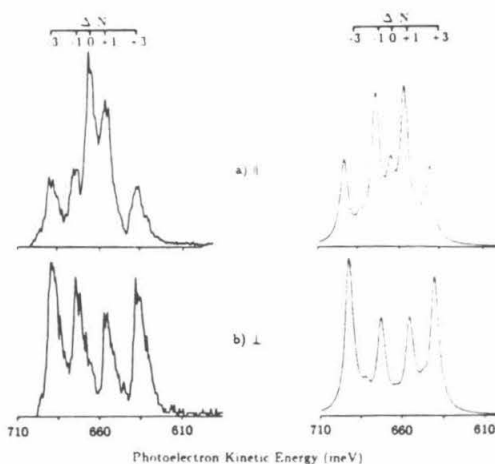


FIG. 2. Same as Fig. 1, but for the mixed $R_{21}(15.5) + S_{11}(15.5)$ branch.

$\Delta N = 0$ peaks, observed in the $D^2\Sigma^+$ REMPI experiments, can therefore be a possible consequence of this energy dependence. To investigate this, we have calculated the rotational branching ratios for a range of photoelectron kinetic energies (0.5, 1.0, 1.5, and 2.0 eV). In Fig. 3, we show the rotational branching ratios for the (2 + 1') REMPI via the $D^2\Sigma^+ S_{21}(11.5)$ branch and of the (1 + 1') REMPI via the $A^2\Sigma^+ R_{22}(21.5)$ branch as a function of the photoelectron kinetic energy. The branching ratios for the D state show a

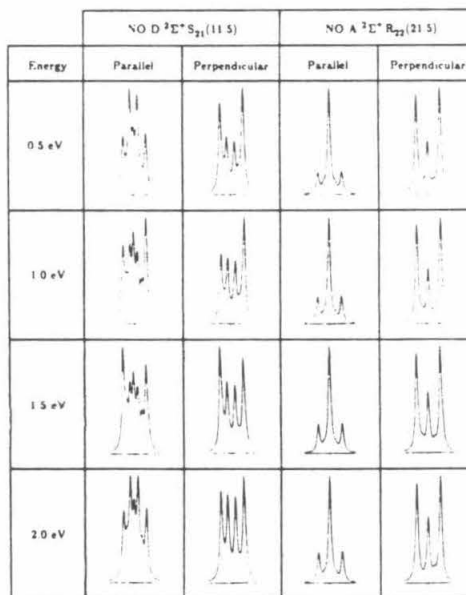


FIG. 3. Photoelectron spectra as a function of photoelectron kinetic energy, for the $S_{21}(11.5)$ branch of the $D^2\Sigma^+$ state, and for the $R_{22}(21.5)$ branch of the $A^2\Sigma^+$ state. Total length of the abscissa corresponds to 100 meV.

pronounced energy dependence for both directions of detection, whereas the branching ratios for the A state are rather insensitive to photoelectron kinetic energy. This may result from the fact that the A state ionization into the $l = 1$ partial wave does not require a nonspherical potential whereas for the D state this channel is a direct consequence of angular momentum coupling in the continuum, i.e., $l' \neq l$ mixing. This behavior in the D state photoionization is expected to be strongly energy dependent. The total cross sections (rotationally unresolved, fixed nuclei) show a similar dependence on the photoelectron kinetic energy, i.e., the D state cross sections are 0.806 (0.5 eV), 0.450 (1.0 eV), 0.320 (1.5 eV), and 0.273 Mb (2.0 eV), whereas the A state cross sections are, 1.188 (0.5 eV), 1.199 (1.0 eV), 1.172 (1.5 eV), and 1.122 Mb (2.0 eV).

IV. CONCLUSIONS

We have presented results for the rotationally resolved photoelectron spectra resulting from a $(2 + 1)$ one-color REMPI of NO via the rotationally clean S_{21} (11.5) and mixed S_{11} (15.5) + R_{21} (15.5) branches of the 0-0 transition in the $D-X$ band. The calculations were done in the fixed-nuclei frozen core approximation, where the frozen core of the $D^2\Sigma^+ \text{ Rydberg}$ state is taken to be the $X^1\Sigma^+ \text{ ground state of NO}^+$. The resulting photoelectron spectra, convoluted with a Lorentzian detection function, agree qualitatively with the experimental results of Viswanathan *et al.*,¹⁵ and support their conclusion, that the nonspherical nature of the molecular potential creates a substantial l mixing in the continuum, which in turn leads to the intense $\Delta N = 0$ peak. We have furthermore investigated the rather strong photoelectron energy dependence of the rotational branching ratios of the $D^2\Sigma^+ S_{21}$ (11.5) line, and compared this to the weak energy dependence of the $A^2\Sigma^+ R_{22}$ (21.5) line. We attribute this behavior to differences in the bound states and the different parts of the electronic continuum probed. This work illustrates the ability of *ab initio* calculations to unravel the subtle features in the photoionization dynamics for rotationally clean and mixed branches. The present work does not include effects of autoionization, high intensities, nor the possible alignment deteriorating effects.

ACKNOWLEDGMENTS

This material is based on research supported by the National Science Foundation under Grant NO. CHE-8521391,

AFOSR under Grant NO. 87-0039, and the Office of Health and Environmental Research of DOE (DE-FG03-87-ER60513), and by NASA-Ames Cooperative Agreement NO. NCC2-319. Work done by S.N.D. was performed under the auspices of the U. S. Department of Energy by Lawrence Livermore National Laboratory under Contract No. W-7405-Eng-48. H.R. gratefully acknowledges the support from the Danish Natural Science Research Council.

- ¹P. Chen, J. B. Pallix, W. A. Chupka, and S. D. Colson, *J. Chem. Phys.* **86**, 516 (1987).
- ²A. Sur, C. V. Ramana, W. A. Chupka, and S. D. Colson, *J. Chem. Phys.* **84**, 69 (1986).
- ³D. Normand, C. Cornaggia, and J. Morellec, *J. Phys. B* **19**, 2881 (1986).
- ⁴T. M. Orlando, L. Li, S. L. Anderson, and M. G. White, *Chem. Phys. Lett.* **129**, 31 (1986).
- ⁵S. L. Anderson, G. D. Kubiak, and R. N. Zare, *Chem. Phys. Lett.* **105**, 22 (1984).
- ⁶S. T. Pratt, P. M. Dehmer, and J. L. Dehmer, *J. Chem. Phys.* **78**, 4315 (1983).
- ⁷S. T. Pratt, P. M. Dehmer, and J. L. Dehmer, *J. Chem. Phys. Lett.* **105**, 28 (1984).
- ⁸W. Meier, H. Rottke, H. Zacharias, and K. W. Welge, *J. Chem. Phys.* **83**, 4360 (1985).
- ⁹J. E. Pollard, D. J. Trevor, J. E. Reutt, Y. T. Lee, and D. A. Shirley, *J. Chem. Phys.* **77**, 34 (1982).
- ¹⁰H. Zacharias, R. Schmeidl, and K. H. Welge, *Appl. Phys.* **21**, 127 (1980).
- ¹¹J. P. Booth, S. L. Bragg, and G. Hancock, *Chem. Phys. Lett.* **113**, 509 (1985).
- ¹²H. Rottke and H. Zacharias, *J. Chem. Phys.* **83**, 4831 (1985).
- ¹³J. C. Miller and R. N. Compton, *J. Chem. Phys.* **84**, 675 (1986).
- ¹⁴W. G. Wilson, K. S. Viswanathan, E. Sekreta, and J. P. Reilly, *J. Phys. Chem.* **88**, 672 (1984).
- ¹⁵K. S. Viswanathan, E. Sekreta, E. R. Davidson, and J. P. Reilly, *J. Phys. Chem.* **90**, 5078 (1986).
- ¹⁶K. S. Viswanathan, E. Sekreta, and J. P. Reilly, *J. Phys. Chem.* **90**, 5658 (1986).
- ¹⁷See, for example, K. Müller-Dethlefs, M. Sander, and E. W. Schlag, *Chem. Phys. Lett.* **112**, 291 (1984).
- ¹⁸S. N. Dixit and V. McKoy, *Chem. Phys. Lett.* **128**, 49 (1986).
- ¹⁹K. Kaufmann, C. Nager, and M. Jungen, *Chem. Phys.* **95**, 385 (1985).
- ²⁰S. N. Dixit, D. L. Lynch, V. McKoy, and W. M. Huo, *Phys. Rev. A* **32**, 1267 (1984).
- ²¹H. Rudolph, S. N. Dixit, V. McKoy, and W. M. Huo, *Chem. Phys. Lett.* **137**, 521 (1987).
- ²²S. N. Dixit and V. McKoy, *J. Chem. Phys.* **82**, 3546 (1985).
- ²³J. B. Halpern, H. Zacharias, and R. Wallenstein, *J. Mol. Spectrosc.* **79**, 1 (1980).
- ²⁴L. T. Earls, *Phys. Rev.* **48**, 423 (1935).
- ²⁵R. R. Lucchese, G. Raseev, and V. McKoy, *Phys. Rev. A* **25**, 2572 (1982).
- ²⁶K. P. Huber and G. Herzberg, *Constants of Diatomic Molecules* (Van Nostrand Reinhold, New York, 1979).
- ²⁷W. J. Hunt and W. A. Goddard III, *Chem. Phys. Lett.* **24**, 464 (1974).
- ²⁸P. Cremaschi, *Chem. Phys. Lett.* **83**, 106 (1981).

**Chapter 3: Rotational branching ratios at low photoelectron
energies in resonant enhanced multiphoton ionization
of NO**

[The text of this chapter appeared in: H. Rudolph, V. McKoy, and S.N.
Dixit, J. Chem. Phys. **90**, 2570 (1989)]

Rotational branching ratios at low photoelectron energies in resonant enhanced multiphoton ionization of NO

H. Rudolph and V. McKoy

Arihur Amos Noyes Laboratory of Chemical Physics, California Institute of Technology, Pasadena, California 91125

S. N. Dixit

Lawrence Livermore National Laboratory, L-401, P.O. Box 808, Livermore, California 94550

(Received 13 July 1988; accepted 18 November 1988)

We report calculated rotational branching ratios for very low energy (50 meV) photoelectrons resulting from $(1 + 1')$ resonant enhanced multiphoton ionization (REMPI) via the $J_i = 1/2, 3/2, 5/2$, and $7/2$ levels of the P_{11} branch of the $A^2\Sigma^+(3s\sigma)$ state of NO. Even angular momentum transfer ($\Delta N \equiv N_+ - N_i$) peaks are dominant in these rotational distributions, in agreement with the selection rule $\Delta N + l = \text{odd}$. Angular momentum coupling in the photoelectron wave function arising from the molecular ion potential leads to smaller but appreciable $\Delta N = \text{odd}$ peaks. The calculated $\Delta N = 0$ to $\Delta N = +2$ peak ratios show the same strong decrease when J_i increases from $1/2$ to $3/2$ as seen in the experimental zero-kinetic-energy (ZEKE) photoelectron spectra [Sander *et al.*, Phys. Rev. A **36**, 4543 (1987)], but do not show the rapid die-off of the $\Delta N \neq 0$ peaks for higher J_i observed experimentally. The calculated trend in the $\Delta N = +2$ vs $\Delta N = 0$ peaks could be understood on the basis of simple angular momentum transfer arguments. These same arguments indicate that this trend in the $\Delta N = 0$ and $+2$ peaks with increasing angular momentum is not generally expected in other branches. Spectra via the $R_{21}(J)$ branch are presented to support this assertion. We also present photoelectron angular distributions which show a strong dependence on ΔN reflecting the changing composition of the photoelectron wave function.

1. INTRODUCTION

In recent years resonant enhanced multiphoton ionization (REMPI)-photoelectron spectroscopy (PES) has seen a substantial improvement in photoelectron kinetic energy resolution. Conventional time-of-flight (TOF) methods for PES have been sufficiently refined to provide rotationally resolved spectra for small molecules.¹⁻⁵ Due to the small rotational constants, studies in heavier molecules such as NO have focused on high- J levels of the ion. Recently, Müller-Dethlefs *et al.* have developed a novel method of zero-kinetic-energy (ZEKE) photoelectron spectroscopy.^{6,7} This method employs photoionization under field-free conditions and application of a delayed pulse extraction field.^{6,7} The technique, facilitated by steradiancy, yields a resolution of $1-2 \text{ cm}^{-1}$ in threshold PES. In contrast, the TOF-PES studies at low energies by Allendorf *et al.*⁵ achieve a resolution of $3-4 \text{ meV}$ around an energy of 180 meV . Using this latter technique, Allendorf *et al.*⁵ have recently reported photoelectron angular distributions for rotationally resolved PES of NO, a significant step towards the "complete" characterization of the photoionization process.

A common feature in these rotationally resolved REMPI-PES studies of NO has been the deviations of the branching ratios from values expected on the basis of an atomic-like model.^{2,4,7} For example, ionization out of the $A^2\Sigma^+(3s\sigma)$ state showed a $\Delta N = 1$ peak^{5,7} ($\Delta N \equiv N_+ - N_i$, where N_+ and N_i denote the angular momentum quantum numbers, exclusive of spin, of the ion and

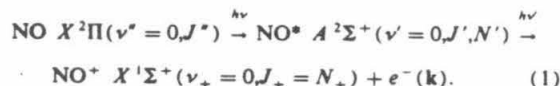
resonant intermediate state, respectively). On the basis of the selection rule $\Delta N + l = \text{odd}$,^{8,9} the presence of this peak implies photoelectron ejection into the even l 's of the continuum, i.e., $3s\sigma \rightarrow ks, kd$, etc.. This is inconsistent with an atomic-like view of the process which would predict ionization primarily into the p continuum. Explicit calculations of these rotational distributions for ionization out of both the $A^2\Sigma^+(3s\sigma)$ and the $D^2\Sigma^+(3p\sigma)$ states^{9,16} quantitatively confirm this non-atomic-like behavior observed for high J values. The ZEKE-PES experiments of Sander *et al.*,^{6,7} carried out through low N_i levels of the $A^2\Sigma^+$ state of NO, also display these non-atomic-like rotational branching ratios. For the $P_{11}(J)$ ($J = 3/2-7/2$) branch the $\Delta N = 0$ peak is, as expected, dominant. For $\Delta N \neq 0$, the even ΔN peaks are stronger than those for ΔN odd, in agreement with the $\Delta N = \text{even}$ propensity rule. However, the $\Delta N \neq 0$ peaks die off rapidly with increasing J of the resonant $A^2\Sigma^+$ state. This dynamically interesting behavior is in contrast to the observed branching ratios for ionization via the high J levels.^{2,4,5}

In the present paper we report calculated rotational branching ratios for very low energy (50 meV) photoelectrons resulting from $(1 + 1')$ REMPI via these same low J levels of the P_{11} branch of the $A^2\Sigma^+$ state of NO. The main objective of these studies is to provide insight into the underlying reasons for the difference in the observed branching ratios for the high and low J levels. Although these calculated rotational branching ratios agree well with the observed

ZEKE values for $N_i = 0$ and 1, they do not show the rapid die off of the $\Delta N \neq 0$ peaks for higher N_i , seen experimentally. It is, in principle, possible that non-Born-Oppenheimer behavior could influence these ZEKE spectra. However, the agreement between the calculated and measured ZEKE spectra for $N_i = 0$ and 1, suggests that these low-energy studies reproduce some of the essential dynamics of the ZEKE experiments. Furthermore, the calculated trends in $\Delta N = 2$ vs the $\Delta N = 0$ peaks could be understood on the basis of simple angular momentum transfer considerations. The validity of these arguments is further supported by the behavior of the branching ratios for REMPI via the $R_{21}(J)$ branch. To provide additional insight into the dynamics of the state-specific processes and for possible comparison with measurements we also present photoelectron angular distributions for ionization via the $P_{11}(J)$ branch.

II. THEORY

The framework for our analysis of REMPI processes has been described in detail elsewhere.¹¹ The $(1+1')$ REMPI process can be thought of as a one-photon excitation from an initially unaligned (all M_J levels equally populated) ground state ($X^2\Pi$) to an aligned resonant intermediate state ($A^2\Sigma^+$) followed by a one-photon ionization out of this state:



Each M_J level is treated as an independent ionization channel, in the absence of M_J mixing terms (collision-free conditions, etc.). The alignment of the resonant intermediate state is then determined using lowest-order perturbation theory for these weak field excitations. For a single photon $X^2\Pi \rightarrow A^2\Sigma^+$ transition, the relative population $\rho_{ii}(M_J)$ is determined by the 3- j coefficient through^{12,13}

$$\rho_{ii}(M_J) \propto \begin{pmatrix} J' & 1 & J'' \\ M_J & 0 & -M_J \end{pmatrix}^2 A, \quad (2)$$

where J' and J'' are the rotational quantum number of the $A^2\Sigma^+$ and the $X^2\Pi$ states, respectively. M_J is the corresponding projection of J' on the z axis. The constant A is the one-photon line strength as given by Earls.¹⁴ The relative values of ρ_{ii} do not depend on the line strengths for pure rotational branches. The total photoionization probability, $P(J', N', J'', N'', N_+)$, is given by an incoherent sum over the individual M_J levels' $\Gamma_i(J', N', N_+)$, weighted with the corresponding relative populations ρ_{ii}

$$P(J', N', J'', N'', N_+) = \sum_i \rho_{ii} \Gamma_i(J', N', N_+). \quad (3)$$

In Eq. (3) $\Gamma_i(J', N', N_+)$ is proportional to $\langle f | \mu | i \rangle^2$, the square of the dipole matrix element between the final continuum state $|f\rangle$, and the resonant intermediate state $|i\rangle$. Following Eq. (6) of Ref. 9, this matrix element can be written as ($\Lambda_i = \Lambda_+ = 0$)

$$\langle f | \mu | i \rangle = \sum_{N_i, \zeta} R(\zeta, N_i) \sum_{\mu} r_{fi}^{\mu} (-1)^{\mu} \times \begin{pmatrix} N_+ & N_i & N_i \\ 0 & 0 & 0 \end{pmatrix} \begin{pmatrix} N_i & 1 & l \\ 0 & \mu & -\mu \end{pmatrix}, \quad (4)$$

where N_+ , N_i are the angular momentum of the ion and the resonant intermediate state (exclusive spin), respectively, N_i is the angular momentum transfer, l is the partial wave of the photoelectron orbital, and μ is its magnetic quantum number ($\mu = 0$ for the σ channel and $\mu = \pm 1$ for the π channels). $R(\zeta)$ represent products of 3- j coefficients and other angular momentum factors (see Refs. 9 and 11 for further details). The one-electron dipole matrix element r_{fi}^{μ} between the orbital of the resonant state and partial wave l of the photoelectron wave function, is defined by Eq. (13) of Ref. 9.

Using the properties of 3- j symbols¹⁵ and the symmetry relationship $r_{fi}^{\mu} = r_{fi}^{\mu - \mu - \mu}$, it can be shown that the summation over μ in Eq. (4) vanishes unless $N_i + N_i + N_+ = \text{even}$ and $N_i + l = \text{odd}$. These conditions lead to the selection rule⁸

$$N_+ - N_i + l \equiv \Delta N + l = \text{odd}. \quad (5)$$

This selection rule is independent of the excitation scheme to the intermediate state, and it is therefore applicable to any $(n+1)$ REMPI process with a final $\Sigma \rightarrow \Sigma$ transition.⁸ The $3s\sigma$ Rydberg character of the $A^2\Sigma^+$ state of NO leads to a dominance of odd partial waves in the continuum (see later) and hence to a propensity rule of $\Delta N = \text{even}$ for the REMPI via the $A^2\Sigma^+$ state. This predicted propensity rule has been seen to be valid both experimentally and theoretically.^{2,4,9,13}

For the $A^2\Sigma^+$ state we use a SCF wave function obtained using an extensive Gaussian basis set, described elsewhere.¹² This basis contains diffuse functions to ensure the correct behavior of the tail region of the 6σ orbital. A single center expansion of the 6σ orbital of NO about the center of mass has the following partial wave components: 94.0% s , 0.2% p , 5.5% d , and 0.1% f , in agreement with previous calculations by Kaufmann *et al.*¹⁶ The photoelectron wave functions were obtained using the iterative Schwinger method^{17,18} in the frozen-core approximation and retaining up to $l = 6$ in the partial wave expansion of the photoelectron wave function. All matrix elements were determined at $R_e(A^2\Sigma^+) = 2.0095$ bohr.¹⁹ To model the ZEKE spectra we used a photoelectron energy of 50 meV. At this kinetic energy we do not expect any serious breakdown of the fixed-nuclei approximation for these rotational studies. The cross sections were also seen to be relatively insensitive to changes in kinetic energy in this region. The partial wave decomposition of the photoelectron matrix element ($|r_{fi}^{\mu}|$) for the $k\sigma$ channel is (normalized to the value of the p wave in the $k\pi$ channel): 0.1512, 0.2522, 0.2145, 0.3273, and 0.0069 for $l = 0, 4$, respectively, and for the $k\pi$ channel: 1.0000, 0.0373, 0.4927, and 0.0094 for $l = 1, 4$, respectively. The $l = 1$ channel is seen to be dominant, as anticipated on the basis of the bound state's high s character. The even- l waves, however, contribute significantly to these matrix elements. The rotationally unresolved cross sections are $\sigma_e = 0.316$ Mb and

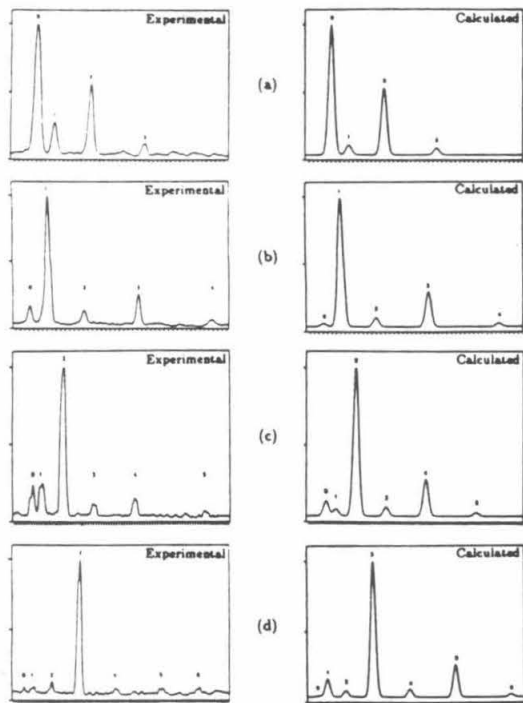


FIG. 1. (a) Experimental (Ref. 7) and calculated photoelectron spectra for REMPI via the $P_{11}(3/2)$ branch of the 0-0 band of the $X^2\Pi-A^2\Sigma^+$ transition, $J_A = 1/2$, $N_A = 0$. The value of N_+ is shown above each peak; (b) same as (a), but via the $P_{11}(5/2)$ branch, $J_A = 3/2$, $N_A = 1$; (c) same as (a), but via the $P_{11}(7/2)$ branch, $J_A = 5/2$, $N_A = 2$; (d) same as (a), but via the $P_{11}(9/2)$ branch, $J_A = 7/2$, $N_A = 3$.

$\sigma_v = 0.819$ Mb with a total cross section of $\sigma_{\text{tot}} = 1.135$ Mb ($1\text{Mb} = 10^{-18}\text{cm}^2$), similar to earlier results at higher energies.⁹

III. RESULTS

In Fig. 1, we compare the ZEKE spectra of Sander *et al.*⁷ for $(1 + 1')$ REMPI via the $P_{11}(J)$ ($J = 3/2, 5/2, 7/2, 9/2$) branches with our calculated spectra at a photoelectron kinetic energy of 50 meV. The calculated branching ratios have been normalized to the most intense peak ($\Delta N = 0$) and folded with a Gaussian detector function (FWHM = 1.0 meV), with a constant background signal added for experimental comparison. The position of the lines are calculated using molecular constant for the $A^2\Sigma^+$ state of NO from Ref. 19. The dominance of even ΔN peaks in these spectra reflects the strong contribution of odd partial waves to the photoelectron wave function. The nontrivial magnitudes of the odd ΔN peaks are a consequence of the nonspherical character of the molecular ion potential which leads to strong coupling of the partial waves of the photoelectron wave function.^{9,10,12,13}

The agreement between the experimental and calculated PES of Figs. 1(a)–1(b) for ionization via the $P_{11}(3/2)$ and $P_{11}(5/2)$ branch, respectively, is remarkably good. One of the more striking features in the comparison of the spectra for $J_i = J_A = 1/2$ and $J_i = J_A = 3/2$ is the decrease in the relative intensity of the $\Delta N = 0$ to 2 peaks. This behavior can be understood in terms of angular momentum constraints imposed by Eqs. (4) and (5). In the case of the $P_{11}(3/2)$ branch where $N_i = 0$, the only partial wave that can contribute to the $\Delta N = 0$ peak is $l = 1$ due to the requirement $N_+ = N_i = N_t = 0$. The $\Delta N = 0$ signal for the $P_{11}(3/2)$ line is therefore a direct measure of the strength of the p

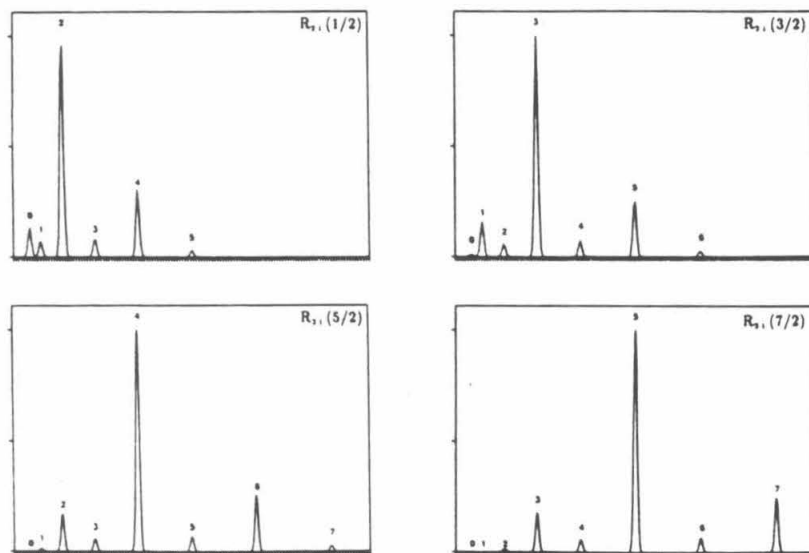


FIG. 2. Calculated photoelectron spectra for REMPI via the $R_{11}(J)$ branches, $J = 1/2 - 7/2$, of the 0-0 band of the $X^2\Pi-A^2\Sigma^+$ transition. The value of N_+ is shown above each peak. $J_A = J_i + 1$, $N_A = J_i + 1/2$.

wave. Correspondingly, the value of the β_2 coefficient in the photoelectron angular distributions would be 2. All higher β coefficients must be zero for the $J_i = J_A = 1/2$ state. However, for the $P_{11}(5/2)$ line both $l = 1$ and 3 partial waves contribute to the $\Delta N = 0$ peak. Similarly, the $\Delta N = +2$ signals for these $P_{11}(3/2)$ and $P_{11}(5/2)$ lines will also have contributions from higher odd partial waves ($l = 1, 3, \dots$). The magnitude of the $\Delta N = 0$ peak relative to the $\Delta N = +2$ is hence expected to be larger for the $P_{11}(5/2)$ case than for the $P_{11}(3/2)$. This argument can be further elaborated by considering the rotational branching ratios expected in REMPI via the pure $R_{21}(J = 1/2, 3/2, 5/2, 7/2)$ lines. Branching ratios for these are shown in Fig. 2. In this case the F_2 component of the $J_i = J_A = 3/2$ level corresponds to $N_i = 2$, and the $l = 1$ and 3 partial waves therefore also contribute to $\Delta N = 0$. The relative branching ratios for $\Delta N = 0$ and 2 peaks hence would not be expected, as seen in Fig. 2, to show the strong decrease with J , in contrast to the behavior of the P_{11} lines.

The experimental ZEKE spectra of Fig. 1 show that the $\Delta N \neq 0$ peaks die off rapidly with increasing N_i . This behavior is in contrast to the calculated spectra. Although these

spectra do show an initial decrease in the $\Delta N \neq 0$ peaks, the calculated relative peak heights approach the high- J limit by $N_i = 3$. This high- J limit ($J \approx 21.5$) of the branching ratios agrees with recent PES measurements.^{2,4,5} This result implies that the observed low- J low-kinetic energy ratios, as seen in Figs. 1(a)–1(d) would ultimately have to increase with J so as to reproduce this high- J behavior.

Finally, the calculated $\Delta N = \text{odd}$ branching ratios are generally smaller than those seen experimentally. The selection rule in Eq. (5) shows that even photoelectron partial waves contribute to these peaks. The discrepancy between the calculated and measured branching ratios for the $\Delta N = \text{odd}$ peaks may be due to the threshold behavior of the $l = 0$ wave.

In Fig. 3, we show the rotationally resolved photoelectron angular distributions (PAD) for the spectra of Fig. 1. These have been normalized, so that $\beta_0 \equiv 1.00$. In the weak-field approximation the maximum β_2 is β_4 . The PADs are dramatically state-dependent. As predicted, the PAD for $N_i = N_+ = 0$, has a pure p -wave character. Note that the PADs for the same $|\Delta N|$'s, as a function of J , are similar for different J_i , reflecting similarities in the contributing waves of the continuum in the high- J limit.

IV. CONCLUSION

We have reported rotational branching ratios for very low photoelectron energies (50 meV) resulting from $(1 + 1')$ REMPI via low J levels of the $X^2\Sigma^+(3s\sigma)$ state of NO. Comparison with experimental spectra at zero-kinetic energy (ZEKE) of Sander *et al.*⁷ shows good agreement for ionization through the $N_i = 0$ and 1 levels, but significant discrepancies remain for $N_i = 2$ and 3 where the rapid die off of the $\Delta N \neq 0$ peaks seen experimentally is not reproduced by the present results. A possible cause of this discrepancy is other state-dependent competing processes, such as autoionization and predissociation. The experimental spectra, however, do not seem to support the presence of autoionization.⁷ The trends in the calculated branching ratios can also be understood in terms of simple angular momentum (l, N_i, N_+) changes in the ionization step. Calculated photoelectron angular distributions also show a strong dependence on ΔN reflecting the changing composition of the photoelectron wave function. These results serve to underscore the molecular nature of the photoionization process.

ACKNOWLEDGMENTS

This material is based on research supported by the National Science Foundation under Grant No. CHE-8521391, by AFOSR under Grant No. 87-0039, and by the Office of Health and Environmental Research of DOE (DE-FG03-87ER60513). The authors also acknowledge use of the resources of the San Diego SuperComputer Center which is supported by the National Science Foundation. Work done by S.N.D. was performed under the auspices of the U.S. Department of Energy by Lawrence Livermore National Laboratory under Contract No. W-7405-Eng-48. H.R. gratefully acknowledges the support of the Danish Natural Science Research Council.

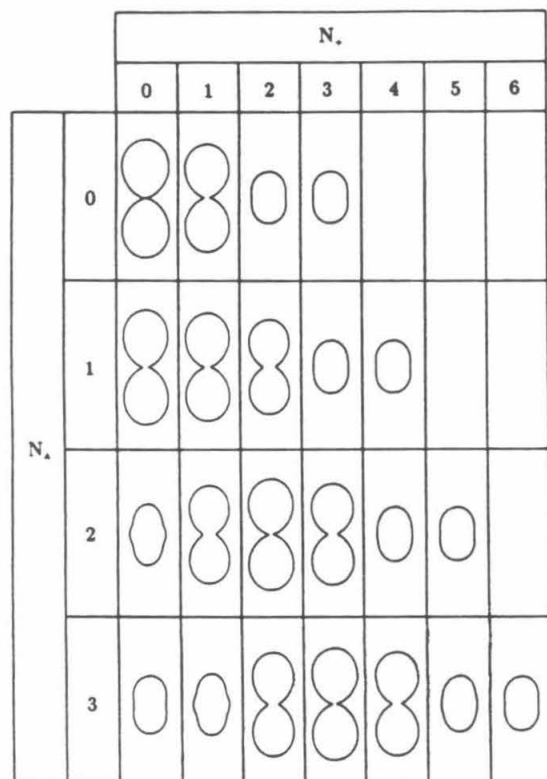


FIG. 3. Photoelectron angular distributions for REMPI via the $P_{11}(J)$ branches, $J = 3/2 - 9/2$, of the 0-0 band of the $X^2\Sigma^+ - A^2\Sigma^+$ transition as a function of N_+ , where N_+ is the rotational quantum number, less spin, of the intermediate state. $\theta = 0^\circ$ is vertical.

- ¹S. T. Pratt, P. M. Dehmer, and J. L. Dehmer, *J. Chem. Phys.* **78**, 4315 (1983).
- ²W. G. Wilson, K. S. Wiswanathan, E. Sekreta, and J. P. Reilly, *J. Phys. Chem.* **88**, 672 (1984).
- ³J. E. Pollard, D. J. Trevor, J. E. Recett, Y. T. Lee, and D. A. Shirley, *J. Chem. Phys.* **77**, 34 (1982).
- ⁴K. S. Wiswanathan, E. Sekreta, E. R. Davidson, and J. P. Reilly, *J. Phys. Chem.* **90**, 5078 (1986).
- ⁵S. Allendorf, D. Leahy, and R. N. Zare (private communication).
- ⁶K. Müller-Dethlefs, M. Sander, and E. W. Schlag, *Chem. Phys. Lett.* **112**, 291 (1984); *Z. Naturforsch. Teil A* **39**, 1089 (1984).
- ⁷M. Sander, L. A. Chewter, K. Müller-Dethlefs, and E. W. Schlag, *Phys. Rev. A* **36**, 4543 (1987).
- ⁸S. N. Dixit and V. McKoy, *Chem. Phys. Lett.* **128**, 49 (1986).
- ⁹S. N. Dixit, D. L. Lynch, V. McKoy, and W. M. Huo, *Phys. Rev. A* **32**, 1267 (1985).
- ¹⁰H. Rudolph, S. N. Dixit, V. McKoy, and W. M. Huo, *Chem. Phys. Lett.* **137**, 521 (1987).
- ¹¹S. N. Dixit and V. McKoy, *J. Chem. Phys.* **82**, 3546 (1985).
- ¹²H. Rudolph, S. N. Dixit, V. McKoy, and W. M. Huo, *J. Chem. Phys.* **88**, 637 (1988).
- ¹³H. Rudolph, S. N. Dixit, V. McKoy, and W. M. Huo, *J. Chem. Phys.* **88**, 1516 (1988).
- ¹⁴L. T. Earls, *Phys. Rev.* **48**, 423 (1935).
- ¹⁵A. R. Edmonds, *Angular Momentum in Quantum Mechanics*, 2nd ed. (Princeton University, Princeton, NJ, 1974).
- ¹⁶K. Kaufmann, C. Nager, and M. Jungen, *Chem. Phys.* **95**, 385 (1985).
- ¹⁷R. R. Lucchese and V. McKoy, *Phys. Rev. A* **21**, 112 (1980).
- ¹⁸R. R. Lucchese, G. Raseev, and V. McKoy, *Phys. Rev. A* **25**, 2572 (1982).
- ¹⁹K. P. Huber and G. Herzberg, *Constants of Diatomic Molecules* (Van Nostrand Reinhold, New York, 1979).

Chapter 4: Rotationally-resolved photoelectron angular dis-
tributions in resonance enhanced multiphoton ioniza-
tion of NO

[The text of this chapter appeared in: H. Rudolph and V. McKoy, submitted to J. Chem. Phys. (contribution no. 7937)]

I. INTRODUCTION

Resonance enhanced multiphoton ionization (REMPI), coupled with high resolution photoelectron spectroscopy, has in recent years proven to be an important state-specific probe of the photoionization dynamics of molecular excited states. While vibrationally-resolved spectra have been measured for many systems with conventional photoelectron spectroscopy,¹⁻² rotational resolution has been achieved in just a few cases.³⁻⁵ When combined with photoelectron angular detection such rotationally-resolved spectra provide a very detailed dynamical picture of the photoionization process. For example, the photoelectron angular measurements parallel and perpendicular to the polarization vector by Reilly *et al.*⁵ in rotationally-resolved REMPI via the $D^2\Sigma^+(3p\sigma)$ state of NO, made it possible to explicitly identify the surprisingly large p-wave character of the photoelectron wave function.

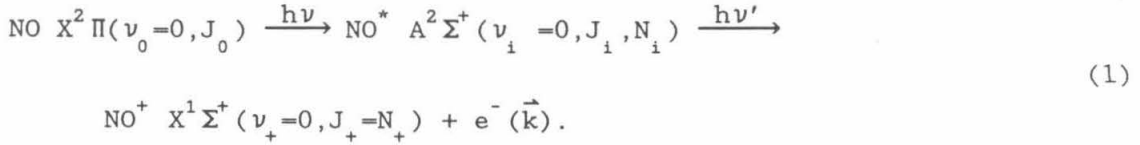
The preceding paper⁶ reports the results of measurements of photoelectron angular distributions and ionic rotational branching ratios for $(1+1')$ REMPI via the $A^2\Sigma^+(3s\sigma)$ of NO.⁷ In this paper we present calculated rotational branching ratios along with photoelectron angular distributions associated with these same REMPI processes. This work extends our earlier studies⁸⁻¹⁵ where we addressed underlying dynamical features associated with measurements of rotationally resolved REMPI spectra of the $^2\Sigma^+$ Rydberg states of NO.^{4-5, 15-16} These features included: (i) ion rotational distributions which manifest the significant non-atomic-like character of molecular photoelectron orbitals e.g., a strong $\Delta N=0$ peak in the rotational branching ratios seen in photoionization of the essen-

tially atomic 3p orbital of the $D^2\Sigma^+$ state of NO, implying a $3p \rightarrow kp$ transition in accordance with the $\Delta N + \ell = \text{odd}$ selection rule,^{11,14-15} (ii) dependence of ion rotational branching ratios on intermediate state alignment,¹² and (iii) strong dependence of rotational branching ratios at low J-values of the resonant state.¹³

Our ionic rotational branching ratios and photoelectron angular distributions are calculated at a photoelectron energy of ≈ 180 meV for (1+1') REMPI via the $R_{21}(20.5)$, $P_{21}+Q_{11}(25.5)$, and $P_{11}(22.5)$ branches of the $A^2\Sigma^+$ state of NO. The photoelectron angular distributions are branch-dependent with branching ratios symmetric around $\Delta N=0$ for the high J branches accessed in the present study ($J \approx 20.5$). This is in contrast to the behavior at low-J where the branching ratios show a strong asymmetry and dependence on J.^{13,16} The calculated branching ratios and photoelectron angular distributions are found to agree well with the experimental results of Allendorf *et al.*,⁶⁻⁷ although some disagreement is seen for the $\Delta N=-2$ signal of the $R_{21}(20.5)$ branch.

II. THEORY

The theoretical method used in the present studies has been described previously.^{9,17} Here we only discuss a few pertinent details. The (1+1') REMPI process of interest here is viewed as a one-photon excitation from an initially unaligned (all M_J -levels equally populated) ground state ($X^2\Pi$) to an aligned resonant intermediate state ($A^2\Sigma^+$) with subsequent one-photon ionization out of this state,



For linearly polarized light and in the absence of collisions and other M_J -mixing interactions, each M_J -level can be treated as an independent ionization channel. For the present weak-field studies the relative population of the M_J -levels (ρ_{ii}) of the intermediate state is adequately described by,

$$\rho_{ii} \propto \begin{pmatrix} J_0 & 1 & J_i \\ M_i & 0 & -M_i \end{pmatrix}^2 A, \quad (2)$$

where A is the line strength given in Ref. 18. The probability $P(\theta, \phi)$ of photoelectron ejection in the direction (θ, ϕ) with respect to the laser polarization vector ($\vec{\epsilon}$) is then given by an incoherent sum over both the photoionization probability Γ_i of the individual M_J -levels and rotational branches (for mixed branches),

$$P(\theta, \phi) = \sum_{\text{branches } i} \sum \rho_{ii} \Gamma_i(J_i, N_i, N_+) = \sum_{L=0}^{L_{\max}/2} \beta_{2L} P_{2L}(\cos\theta). \quad (3)$$

In the second summation the photoelectron angular distributions are expressed as a weighted sum over Legendre polynomials of even order. L_{\max} is determined by the dynamics of the particular REMPI process and is 4 for the present $(1+1')$ low intensity high- J experiments. In the evaluation of Eq. (3) it is assumed that the polarization vectors of the two photons in the $(1+1')$ REMPI scheme are parallel. It is simple to extend

Eq. (2) to allow for an arbitrary angle between the vectors. In the following we assume the lasers to be polarized parallel to each other unless otherwise specified. Changing the angle between the polarization vectors of the excitation and ionization lasers simply probes the dependence of the cross sections (and angular distributions) on the alignment of the intermediate state.

We assume the $X^2\Pi$ state to be intermediate between Hund's case (a) and Hund's case (b), and the resonant $^2\Sigma^+$ and final $^1\Sigma^+$ states to be adequately described by Hund's case (b) coupling. In the present frozen-core and orbital approximation,⁹ the photoionization probability for a particular M_j level Γ_i is proportional to $\langle f|\mu|i\rangle^2$, the square of the one-electron matrix element between the final continuum orbital, $|f\rangle$, and the resonant Rydberg orbital, $|i\rangle$. For the REMPI process of Eq. (1) $\langle f|\mu|i\rangle$ can then be written as,¹³

$$\langle f|\mu|i\rangle = \sum_{N_t, \zeta} R(N_t, \zeta) \sum_{\mu} r_{fi}^{\ell\mu\mu} (-1)^{\mu} \begin{pmatrix} N_+ & N_i & N_t \\ 0 & 0 & 0 \end{pmatrix} \begin{pmatrix} N_t & 1 & \ell \\ 0 & \mu & -\mu \end{pmatrix}, \quad (4)$$

where N_+ and N_i are the angular momenta of the ion and the resonant intermediate state (exclusive of spin) respectively. N_t is the angular momentum transfer, ℓ is a partial wave of the photoelectron wave function, and μ is its corresponding projection on the molecular axis ($\mu=0$ and ± 1 for the $k\sigma$ and $k\pi$ -channels respectively). $R(\zeta)$ and ζ represent other variables and summation indices. Details are given in Ref. 9.

The bound-free matrix element, $r_{fi}^{\ell\mu\mu}$, of Eq. (4) between the intermediate state and the photoelectron continuum wave function can be written as

$$r_{fi}^{\ell\mu\mu} = \sum_{l', l_0} \langle \Psi_{k\ell\ell'}(r) Y_{\ell', \lambda}(\hat{r}') | r Y_{1\mu} | \Phi_{i\ell_0}(r) Y_{\ell_0, 0}(\hat{r}') \rangle. \quad (5)$$

For a central potential $\ell'=\ell$. However, for the non-central potential of molecular ions, $\ell \neq \ell'$ terms are present and can be substantial due to the anisotropy of the molecular ion potential. This ℓ -coupling in the photoelectron wave function in turn influences the ionic rotational distributions. Using the symmetry relationship, $r_{fi}^{\ell\mu\mu} = r_{fi}^{\ell-\mu-\mu}$, and the properties of the 3-j symbols,¹⁹⁻²⁰ it can be shown that the summation in Eq. (4) vanishes for the $(1+l')$ process of Eq. (1) unless $N_t + N_i + \ell = \text{even}$ and $N_t + \ell = \text{odd}$. This leads to the selection rule,¹⁴

$$N_t - N_i + \ell \equiv \Delta N + \ell = \text{odd}, \quad (6)$$

where ΔN is the difference between the angular momentum of the intermediate state (exclusive of spin) and the final ionic state. An atomic-like picture would predict that photoionization of the $A^2\Sigma^+(3s\sigma)$ state should occur primarily via the p-wave ($3s \rightarrow kp$) and Eq.(6) therefore predicts a $\Delta N = \text{even}$ propensity rule.

For the electronic wave function of the intermediate $A^2\Sigma^+$ state we used the improved virtual orbital approximation (IVO)²¹ with an extensive Gaussian basis set that ensures the correct nodal and long-range behavior of the diffuse Rydberg state.¹¹ Single-center expansion of the

6σ ($3s\sigma$) orbital of the $A^2\Sigma^+$ state around the center-of-mass (CM) has the following partial wave composition: 94.0% s-, 0.2% p-, 5.5% d-, and 0.1% f-character. The photoelectron continuum functions were calculated using the iterative Schwinger method in the frozen-core approximation.²²⁻²³ All matrix elements are evaluated numerically for the equilibrium internuclear distance of 2.0069 a.u. of the $A^2\Sigma^+$ state.²⁴ The photoelectron energy in the (1+1') REMPI experiments of Allendorf *et al.*⁶⁻⁷ is ~183 meV for the $\Delta N=0$ signal. We have previously found the bound-free matrix elements, $r_{fi}^{\ell\mu\mu}$, and the ionic rotational branching ratios to be rather energy independent for REMPI via the $A^2\Sigma^+$ state¹¹ and hence the branching ratios are all evaluated assuming a single photoelectron energy of 183 meV.

The calculated partial wave composition of the resulting photoelectron matrix elements and their relative phases are listed in Table I. These can be compared with the experimentally derived elements shown in Table IV of the preceding paper. The p-wave ($\ell=1$) of the $k\pi$ continuum is the most dominant. The d-wave of the $k\sigma$ continuum is seen to be stronger than expected from the atomic picture ($\ell=\ell_0\pm 1$). This mixing arises from the non-isotropic nature of the molecular potential.

III. RESULTS

In Fig. 1 we compare the photoelectron angular distributions of Allendorf *et al.*⁶ for (1+1') REMPI of the NO $A^2\Sigma^+$ state via the rotationally clean $R_{21}(20.5)$ branch with our calculated distributions.

Also shown are the angular distributions via the magic-angle-(54.7° between the polarization direction of the two photons)-excited $R_{21}(20.5)$ branch (see Ref. 6 for details). The intermediate state is unaligned for this excitation geometry i.e., all M_J levels are equally populated, and the β_4 coefficient of Eq. (3) is hence zero (see Table II). The calculated and experimental photoelectron angular distributions are generally in good agreement, although there is some discrepancy for the $\Delta N=-2$ signal via the $R_{21}(20.5)$ branch for both excitation geometries. The branching ratios and angular distributions are expected to be almost symmetric around $\Delta N=0$ for these high-J studies. We are not able to account for this discrepancy within the context of the present theoretical framework.

Fig. 2 compares the experimental⁶ and calculated photoelectron angular distributions for the mixed $P_{21}+Q_{11}(25.5)$ branch. Also shown are the calculated results for the pure $P_{11}(22.5)$ branch. The agreement between the predicted and measured photoelectron angular distributions is very good for the mixed $P_{21}+Q_{11}(25.5)$ branch. Note that the angular distributions for this mixed branch ($P_{21}+Q_{11}(25.5)$) are distinctly different from those of the $R_{21}(20.5)$ branch (see Fig. 1). This reflects the importance and influence of the intermediate state's alignment on the rotationally-resolved photoelectron angular distributions.

The rotationally-unresolved distributions are (see Figs. 1 and 2) almost branch independent. This stresses the difficulty of probing alignment of the intermediate state with such distributions.²⁵⁻²⁶ The calculated asymmetry parameters in Table II also illustrate this since

the rotationally unresolved signals are dominated by the strong $\Delta N=0$ signal. Recent rotationally unresolved (2+1) REMPI experiments via the $E^2\Sigma^+$ state of NO have also shown the photoelectron angular distributions to be rather insensitive to the intermediate state's alignment,^{2,5} in agreement with the present case. Theoretical calculations confirm that the rotationally unresolved angular distributions via the E-state are alignment independent and that the rotationally resolved distributions are very branch dependent.^{2,6}

The model employed by Allendorf *et al.*⁶ to fit the experimental angular distributions as in Fig. 9-12 of Ref. 6, is based on the same theoretical framework used in our analysis. The photoelectron matrix elements are treated there as adjustable fitting parameters.⁶ Within this model these branching ratios and angular distributions should be almost symmetric around $\Delta N=0$. The asymmetry of the $\Delta N=\mp 2$ angular distributions for the $R_{2,1}(20.5)$ branch in Fig. 5 of Ref. 6 can therefore not be accounted for on the basis of the present model or fits based on it. The asymmetry between the measured and the "model" fits must therefore be due to perturbations not included in the model or to experimental uncertainties.

Table III lists the calculated angle-integrated ionic rotational branching ratios. The $\Delta N=0$ signal is dominant for all branches and is more than five times stronger than the $\Delta N=\pm 2$ signals and ~20 times stronger than the $\Delta N=\pm 1$ signals. These $\Delta N=\pm 1$ signals had not been resolved in earlier experiments,⁴⁻⁵ but were predicted theoretically^{9,11} to be ~5% of the $\Delta N=0$ signal. This agrees well with the experimental results.

IV. CONCLUSION

We have reported the ionic rotational branching ratios and photoelectron angular distributions for low photoelectron energies resulting from $(1+1')$ REMPI via the $R_{21}(20.5)$, $P_{11}(22.5)$, and $P_{21}+Q_{11}(25.5)$ branches of the $A^2\Sigma^+(3s\sigma)$ state of NO. Comparison with the experimental high resolution experimental results of Allendorf *et al.*⁶⁻⁷ shows quantitative agreement between the calculated and measured values. The ionic rotational branching ratios are seen to be weakly branch dependent. However, the rotationally resolved photoelectron angular distributions are very branch (alignment) dependent, whereas the rotationally unresolved ones are less so. This makes it difficult to probe the alignment of intermediate states via rotationally unresolved measurements. The rotationally resolved photoelectron angular distributions are clearly important for elucidating the dynamical details of the REMPI process.

ACKNOWLEDGMENTS

This material is based on research supported by the National Science Foundation under Grant NO. CHE-8521391, by AFOSR under Grant. NO. 87-0039 and by the Office of Health and Environmental Research of DOE (DE-FG03-87ER60513). The authors also acknowledge use of the resources of the San Diego Supercomputer which is supported by the National Science Foundation. H.R. gratefully acknowledges support from the NATO Science Fellowship Programme.

TABLE I

Bound-free matrix element, $r_{fi}^{\ell\mu\mu}$, and relative phases for a photoelectron kinetic energy of $E_{kin}=183$ meV, as defined by Eq. (5). The magnitudes and phases are normalized to $\ell=1$ (p-wave) of the $k\pi$ continuum.

<u>m=0 (kσ-channel)</u>			<u> m =1 (kπ-channels)</u>	
ℓ	r	$\theta(\text{rad})$	r	$\theta(\text{rad})$
0	0.294	4.88	—	—
1	0.519	2.97	$\equiv 1.000$	$\equiv 0.00$
2	0.412	4.77	0.037	0.00
3	0.667	4.78	0.500	1.61
4	0.016	0.15	0.011	3.31

TABLE II

Calculated asymmetry parameters (β_{2L}) for the $R_{21}(20.5)$, $R_{21}(20.5)$ (unaligned), $P_{21}+Q_{11}(25.5)$, and the $P_{11}(22.5)$ branches, as defined by Eq. (3), with $\beta_0 \equiv 1.000$.

	$R_{21}(20.5)$		$R_{21}(20.5)^\dagger$		$P_{21}+Q_{11}(25.5)$		$P_{11}(22.5)$	
	β_2	β_4	β_2	β_4	β_2	β_4	β_2	β_4
ΔN								
-2	0.676	0.251	0.580	0.000	0.387	-0.507	0.665	0.222
-1	1.724	0.111	1.492	0.000	0.824	-0.318	1.699	0.100
0	1.794	-0.068	1.835	0.000	1.886	0.087	1.800	-0.059
+1	1.730	0.099	1.492	0.000	0.829	-0.280	1.704	0.088
+2	0.666	0.222	0.580	0.000	0.409	-0.450	1.704	0.195
rot.								
unres.	1.458	0.027	1.486	0.000	1.548	-0.040	0.655	0.195

† 'unaligned' (54.7°), see text for details

TABLE III

Calculated angle-integrated rotational branching ratios normalized to the $\Delta N=0$ signal

ΔN	$R_{21}(20.5)$	$R_{21}(20.5)^\dagger$	$P_{21}+Q_{11}(25.5)$	$P_{11}(22.5)$
-2	0.199	0.167	0.126	0.194
-1	0.053	0.040	0.024	0.051
0	$\equiv 1.00$	$\equiv 1.00$	$\equiv 1.00$	$\equiv 1.00$
+1	0.055	0.042	0.025	0.053
+2	0.216	0.182	0.138	0.211

† 'unaligned' (54.7°), see text for details

REFERENCES

- 1 S.T. Pratt, P.M. Dehmer, and J.L. Dehmer, Chem. Phys. Lett. 105, 28 (1984).
- 2 K. Kimura in *Photodissociation and Photoionization* (John Wiley & Sons, 1985) p. 161, and references therein.
- 3 S.T. Pratt, P.M. Dehmer, and J.L. Dehmer, J. Chem. Phys. 78, 4315 (1983).
- 4 W.G. Wilson, K.S. Viswanathan, E. Sekreta, and J.P. Reilly, J. Phys. Chem. 88, 672 (1984).
- 5 K.S. Viswanathan, E. Sekreta, E.R. Davidson, and J.P. Reilly, J. Phys. Chem. 90, 5078 (1986).
- 6 S.W. Allendorf, D.J. Leahy, D.C. Jacobs, and R.N. Zare, J. Chem. Phys. (preceding paper).
- 7 S.W. Allendorf, Bull. of Am. Phys. Soc. 33 (4), 920 (1988).
- 8 V. McKoy *et al.*, Bull. of Am. Soc. Phys. 33 (4), 919 (1988).
- 9 S.N. Dixit, D.L. Lynch, V. McKoy, and W.M. Huo, Phys. Rev. A 32, 1267 (1985).

- 10 H. Rudolph, S.N. Dixit, V. McKoy, and W.M. Huo, Chem. Phys. Lett. 137, 521 (1987).
- 11 H. Rudolph, S.N. Dixit, V. McKoy, and W.M. Huo, J. Chem. Phys. 88, 637 (1988).
- 12 H. Rudolph, S.N. Dixit, V. McKoy, and W.M. Huo, J. Chem. Phys. 88, 1516 (1988).
- 13 H. Rudolph, S.N. Dixit, and V. McKoy, J. Chem. Phys. 90, 2570 (1989).
- 14 S.N. Dixit and V. McKoy, Chem. Phys. Lett. 128, 49 (1986).
- 15 Xinbei Song, Ellen Sekreta, James P. Reilly, H. Rudolph, and V. McKoy (to be published).
- 16 M. Sander, L.A. Chewter, K. Müller-Dethlefs, and E.W. Schlag, Phys. Rev. A 36, 4543 (1987).
- 17 S.N. Dixit and V. McKoy, J. Chem. Phys. 82, 3546 (1985).
- 18 L.T. Earls, Phys. Rev. 48, 423 (1935).
- 19 A.R. Edwards, *Angular Momentum in Quantum Mechanics*, 2nd ed. (Princeton University, Princeton, N.J. 1974).

- 20 R.N. Zare, *Angular Momentum, understanding spatial aspects in chemistry and physics* (John Wiley & Sons, N.Y. 1988).
- 21 W.J. Hunt and W.A. Goddard III, *Chem. Phys. Lett.* **24**, 464 (1974).
- 22 R.R. Lucchese and V. McKoy, *Phys. Rev. A* **21**, 112 (1980).
- 23 R.R. Lucchese, G. Raseev, and V. McKoy, *Phys. Rev. A* **25**, 2572 (1982).
- 24 K.P. Huber and G. Herzberg, *Constants of Diatomic Molecules* (Van Nostrand Reinhold, New York, 1979).
- 25 J.R. Appling, M.G. White, W.J. Kessler, R. Fernandez, and E.D. Poliakoff, *J. Chem. Phys.* **88**, 2300 (1988).
- 26 H. Rudolph and V. McKoy, *J. Chem. Phys.* (to be published).

FIGURE CAPTIONS

Figure 1 Rotationally resolved (ΔN) and unresolved experimental (from Ref. 6) and calculated photoelectron angular distributions for the $R_{21}(20.5)$ and unaligned $R_{21}(20.5)$ branch, see text for details.

Figure 2 Same as Fig.1, but for the mixed $P_{21}+Q_{11}(25.5)$ branch. Also shown are the calculated photoelectron angular distributions for the pure $P_{11}(22.5)$ branch.
























	ΔN					unres.
	-2	-1	0	+1	+2	
$R_{21}(20.5)$ experimental						
$R_{21}(20.5)$ calculated						
$R_{21}(20.5)$ 'unaligned' experimental						
$R_{21}(20.5)$ 'unaligned' calculated						

FIGURE 1



















	ΔN					unres.
	-2	-1	0	+1	+2	
$P_{21} + Q_u(25.5)$ experimental						
$P_{21} + Q_u(25.5)$ calculated						
$P_u(22.5)$ calculated						

FIGURE 2

INTRODUCTION

In recent years, the technique of resonant enhanced multiphoton ionization (REMPI) combined with high resolution photoelectron spectroscopy (PES) has proven useful in elucidating both the characteristics of intermediate electronic states and the dynamics of excited-state photoionization.¹⁻¹⁹ While considerable interest has been focussed on the vibrational state distribution of the ions formed, and how that relates to differences between excited state and ion potential energy surfaces, a few recent experiments have achieved rotational resolution in the photoelectron spectra and provided valuable insight into the propensity rules for these processes.^{4,6,10,12} These experiments are possible because specific single rovibrational levels of a certain electronic state can be excited with a pulse of narrowband laser radiation, the excited molecule ionized with the same light pulse, and the kinetic energies of the ejected electrons measured with a resolution sufficient to resolve the different rotational states of the ions. This approach to extracting rotational photoionization propensity rules has several advantages over photoionization of ground state molecules. First, ionization takes place from a single rotational state rather than from a thermal distribution of rotational levels, so the resulting spectra are simpler to interpret. Second, different types of electronic states can be excited and their varying characteristics probed. Third, by using different colors of light for the excitation and ionization steps, it is possible to study the effect of ionizing wavelength, and thus electron kinetic energy, on the rotational propensity rules.

Selection rules governing the changes in rotational angular momentum, ΔN , of a diatomic molecule upon ionization can be obtained via angular momentum and parity considerations.^{6, 21-22} Although such selection rules provide no information about the relative intensities of the peaks predicted to appear in a particular spectrum, they have been useful in interpreting our earlier experimental results on NO.^{10, 12} In particular, they correctly predict the observed $\Delta N=0, \pm 2$ propensity when ionizing from the $A^2\Sigma^+(3s\sigma)$ state, and the $\Delta N=0, \pm 2$ and $\Delta N=0, \pm 3$ propensities observed when ionizing from different spin components of the $C^2\Pi(3p\pi)$ state. However, when ionizing from the $D^2\Sigma^+(3p\sigma)$ state of NO, in addition to the anticipated $\Delta N=\pm 1, \pm 3$ peaks, we observed a very intense and unexpected $\Delta N=0$ peak.¹² Although the simplest explanation for such a peak in the photoelectron spectrum is that the $D^2\Sigma^+(3p\sigma)$ Rydberg state might have a non-negligible amount of s character, SCF calculations conclusively demonstrated that this was not the case.^{12, 20, 22} We then suggested, and through calculations later verified, that ℓ -mixing in the continuum can lead to a detectable $\Delta N=0$ peak.^{12, 23, 24} The fact that the $\Delta N=0$ peak completely vanished when the photoelectron spectrum was recorded with light polarized perpendicular to the electron flight direction¹² is consistent with this hypothesis. Calculations further suggested that the relative magnitudes of all of the observed peaks, including the $\Delta N=0$ feature, must depend on the kinetic energy of the ejected electron, and that this effect is much more pronounced in ionization of the $D^2\Sigma^+(3p\sigma)$ state of NO than the $A^2\Sigma^+(3s\sigma)$ state.^{23, 24} In the present work, a particular rotational level of the $D^2\Sigma^+(3p\sigma)$ state is excited and photoelectron spectra

measured with one of five different ionizing wavelengths. Calculations predicting the observed rotational state distributions are performed for precisely the photoionization wavelengths used experimentally. Although comparison of the predicted and observed spectra is encouraging, several discrepancies remain suggesting that a proper description of the $D^2\Sigma^+(3p\sigma)$ electronic state of NO may be more complicated than had been anticipated.

EXPERIMENTAL

In our previous rotationally-resolved photoelectron experiments, selected rotational levels of the $D^2\Sigma^+$ state of NO were reached by a two-photon process, and one additional photon was sufficiently energetic to induce ionization. The high light intensities required to two-photon excite the $D^2\Sigma^+$ state very efficiently ionized the excited molecules. This high photoionization efficiency becomes a problem in any two-color experiment in which the photoionization wavelength is varied; ionization of the NO by the intense light that two-photon excited it cannot be avoided! To circumvent this problem we chose in the present experiments to excite the $D^2\Sigma^+$ state of NO by a one-photon process using light at approximately 1871Å. Since the lifetime of the $D^2\Sigma^+$ state of NO is known to be rather short (about 20 ns),²⁵ very little time jitter between the excitation and tunable photoionization light pulses can be tolerated. This suggests that a single pump laser should be used to generate both the excitation and ionization radiation needed in these experiments. The method employed is schematically displayed in Fig. 1.

A Quanta Ray Nd:YAG laser acted as our primary light source producing 1.064 μm radiation with a repetition rate of 10 Hz. This radiation was frequency doubled in a Quanta Ray Model HG-2 harmonic generator. The resulting 532 nm light pumped a rhodamine 6G dye laser whose output was frequency doubled and mixed with the fundamental of the YAG laser in a Quanta Ray Wavelength Extension System (WEX). Wavelengths in the region of 2210-2230 \AA were thus obtained. The output from the WEX was focussed near the center of a high pressure (200 psi) hydrogen Raman shifting cell. The beams emerging from the Raman cell were collimated by a lens and dispersed by an equilateral prism. The first and second anti-Stokes lines and the first through fifth Stokes lines were all observed. The light wavelengths and pulse energies for all of these lines are listed in Table I. The second anti-Stokes line at 1871 \AA was appropriate for initially exciting the $D^2\Sigma^+(3p\sigma)$ Rydberg state. This radiation was refracted directly into the spectrometer by a second equilateral prism. The other Stokes lines, used as ionizing radiation, were reflected by four right angle prisms and focussed into the spectrometer in a counterpropagating direction. The light arrived in the photoelectron spectrometer 4 nanoseconds after the initial excitation pulse. The plane of polarization of all radiation was parallel to the electron flight direction. The reason that perpendicular polarization was not also used in the present experiment, as in the past,^{1,2} is that the count rate in the perpendicular direction is much smaller, so these experiments take longer than the parallel polarization experiments, and it was difficult to stabilize the complicated nonlinear optical light production for such extended periods. In addition, the small signals obtained in the perpendicular direction could hardly be distinguished

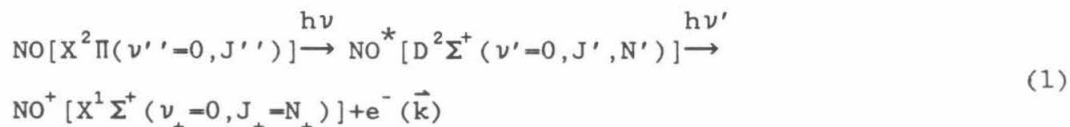
from the spectrometer photoemission background.

In order to know when we were exciting a particular rotational level of the $D^2\Sigma^+$ excited electronic state, it was necessary to record and assign a wavelength scan of an entire vibrational band. The $D^2\Sigma^+ \leftarrow X^2\Pi$ 0-0 band was recorded using a 1+1' REMPI process with the second anti-Stokes and the second Stokes radiation produced as described above. During the wavelength scan, acceleration grids were used to collect a substantial fraction of the electrons generated.

Nitric oxide gas (Matheson Grade CP) was purified by several freeze-thaw cycles to remove residual air and other oxides of nitrogen. An effusive beam of NO was streamed through a 30- μ m nozzle into the ionization chamber of the photoelectron spectrometer which was maintained at a pressure of 5.0×10^{-5} torr by a CTI model CRYO-TORR 8 high vacuum pump. The spectrometer, which operates on the time of flight principle, has been previously described.²⁶ The second anti-Stokes radiation was tuned to a particular $D^2\Sigma^+ \leftarrow X^2\Pi$ rovibrational line to excite molecules that were then ionized with one of the 8 available UV and visible colors. Electrons were detected with two Varian-8900 microchannel plates in tandem. The resulting signals were amplified and digitized with a Biomation 6500 waveform recorder and LeCroy 2228A and 4208 time to digital converters (TDCs) with time resolution of 250 ps per channel and 1 ns per channel respectively. The data were stored in a PC's Limited AT-compatible computer. Spectra were subsequently converted from linear in time to linear in kinetic energy and then transferred to a plotter.

THEORETICAL

The (1+1') REMPI via the $D^2\Sigma^+$ state of NO,



can be viewed as a two-step process: a one-photon excitation from an initially unaligned $X^2\Pi$ ground state (all M_J -levels equally populated) to the aligned $D^2\Sigma^+$ intermediate state, followed by subsequent one-photon ionization out of this aligned state. Details of the theory of molecular REMPI processes used in these studies have been described in ref. 27, while the general aspects of REMPI of NO have been discussed in refs. 21 and 22.

Under the collision-free conditions of the current experiments alignment of the resonant state is preserved and each (allowed) M_J -channel can be treated as an independent ionization channel. The total probability $P(\theta, \phi)$ for photoelectron ejection in the direction (θ, ϕ) with respect to the polarization vector $(\vec{\epsilon})$ of the laser light is given by

$$P(\theta, \phi) = \sum_{J'} \sum_{M_{J'}} \Gamma_{M_{J'}, M_{J'}} \rho_{M_{J'}, M_{J'}} \quad (2)$$

where the incoherent sum over allowed J' -levels accounts for the mixed rotational branches via the $D^2\Sigma^+$ state ($J'=N'\pm 1/2$) (e.g. $Q_{21}+R_{11}(J')$),

$\Gamma_{M_J, M_J'}$ is the ionization probability out of the M_J level, and $\rho_{M_J, M_J'}$ its population. For the low intensity experiments of interest here, $\rho_{M_J, M_J'}$ is adequately described by a product of 3-j coefficients and the line-strength $A(J'', N'', J', N')^{28}$

$$\rho_{M_J, M_J'} \propto \begin{pmatrix} J'' & 1 & J' \\ M_J & 0 & M_J' \end{pmatrix}^2 A(J'', N'', J', N'). \quad (3)$$

The photoionization probability, $P(\theta)$, can be expanded in Legendre polynomials $P_L(\cos(\theta))$ as

$$P(\theta) = \sum_{L=0}^{L_{\max}/2} \beta_{2L} P_{2L}(\cos(\theta)). \quad (4)$$

For the present 2-photon (1+1') REMPI study, with relatively high values of J' and low laser intensity, L_{\max} is 4. The photoelectron signal detected along the direction of polarization of the laser is therefore $P(\theta=0^\circ) = \beta_0 + \beta_2 + \beta_4$, and the perpendicular signal is $P(\theta=90^\circ) = \beta_0 - \frac{1}{2}\beta_2 + \frac{3}{8}\beta_4$.

The electronic wave function for the intermediate $D^2\Sigma^+$ state is obtained via diagonalization of the static-exchange potential associated with the $X^1\Sigma^+$ ground state of NO^+ .^{12, 20, 24, 29} We used the same Gaussian basis as in Ref. 24, except that the functions at the center-of-mass (CM) were taken from ref. 20 (s-, p-, and d-functions with exponents larger than 0.0008). This basis gives a calculated total energy of

-129.03587 a.u. for the $D^2\Sigma^+(3p\sigma)$ state at $R=2.0069$ a.u. A partial wave decomposition of the resulting $3p\sigma$ orbital about the CM gives 0.6% s-, 98.8% p-, 0.4% d-, and 0.1% f-character, respectively, in agreement with previous calculations.^{12,21,24} This same basis set gives a total energy of -129.07363 a.u. for the $A^2\Sigma^+(3s\sigma)$ state at $R=2.0069$ a.u., and a single-center expansion of the $3s\sigma$ orbital around the CM of 94.0% s-, 0.2% p-, 5.5% d-, and 0.1% f-character, respectively.

Determination of the M_J -resolved photoionization probability Γ_{M_J, M_J} , involves sums of the square of the bound-free matrix elements $r_{fi}^{\ell\lambda\mu}$,

$$r_{fi}^{\ell\lambda\mu} = \sum_{\ell', \ell_0} \langle \Psi_{k\ell\ell'}(r) Y_{\ell'\lambda}(\hat{r}') | r Y_{1\mu}(\hat{r}') | \Phi_{i\ell_0}(r) Y_{\ell_0 0}(\hat{r}') \rangle \quad (5)$$

between the resonant Rydberg and photoelectron orbitals. The photoelectron continuum functions are calculated using the iterative Schwinger variational method.^{30,31} These photoelectron orbitals are obtained as solutions of a one-electron Schrödinger equation containing the non-spherical, non-local potential of the molecular ion. The partial wave coupling in these molecular photoelectron orbitals is important for the description of the non-atomic nature of molecular photoionization. All matrix elements are evaluated for a fixed internuclear distance of $R=2.0069$ a.u. corresponding to the equilibrium distance of the $^2\Sigma^+$ Rydberg states.³²

RESULTS AND DISCUSSION

The wavelength dependence of the NO^+ ion yield is displayed in Fig. 2a. The simulation of this band, obtained using spectroscopic constants of NO that are known in both the ground and excited vibronic states,³² is shown in Fig. 2b. This simulation assumes that the $\text{D}^2\Sigma^+$ state is described by Hund's case (b) and that the $\text{X}^2\Pi$ state is intermediate between Hund's cases (a) and (b).³³ There is a 119.7 cm^{-1} separation between the $\text{X}^2\Pi_{1/2}$ and $\text{X}^2\Pi_{3/2}$ levels of the NO ground state, leading to $\text{D}^2\Sigma^+ \leftarrow \text{X}^2\Pi_{1/2}$ and $\text{D}^2\Sigma^+ \leftarrow \text{X}^2\Pi_{3/2}$ sub-bands. In addition, the interaction between rotation of the nuclei and electronic orbital angular momentum (Λ -doubling) splits each rotational level of the Π state into two components. Because of the large energy-level separation in the NO ground state, the selection rule $\Delta N=0, \pm 1$ does not apply and all transitions consistent with the selection rule $\Delta J=0, \pm 1$ and $+ \longleftrightarrow -$ are possible. Therefore, R_1 , Q_1 , P_1 , $^s\text{R}_{21}$, $^r\text{Q}_{21}$ and $^q\text{P}_{21}$ branches are formed from $\text{X}^2\Pi_{1/2}$ levels, and R_2 , Q_2 , P_2 , $^q\text{R}_{12}$, $^p\text{Q}_{12}$ and $^o\text{P}_{12}$ branches from the $\text{X}^2\Pi_{3/2}$ level. The intensities of the rotational lines were calculated using Earls' equation.²⁸ As can be seen from a comparison of figs. 2a and 2b, it is quite evident that an additional transition must be occurring in this wavelength region. This transition can be assigned as the $\text{A}^2\Sigma^+ \leftarrow \text{X}^2\Pi$ 4-0 band whose absolute position and rotational structure were calculated from other known spectroscopic constants. A simulation of the $\text{A}^2\Sigma^+ \leftarrow \text{X}^2\Pi$ 4-0 band is separately displayed in Fig. 2c. In the absorption spectrum of nitric oxide between 1700 Å and 2300 Å, the $\text{D}^2\Sigma^+ \leftarrow \text{X}^2\Pi$ 0-0 band, the $\text{A}^2\Sigma^+ \leftarrow \text{X}^2\Pi$ 4-0 band and the $\text{B}^2\Pi \leftarrow \text{X}^2\Pi$ 8-0 band have been found to be overlapped.³⁴ The former two bands are

more intense than the third. The presence of this overlapping absorption introduced considerable congestion into the spectrum and severely limits the number of non-overlapping rotational transitions that can be cleanly excited. Nevertheless, towards the short wavelength end of the spectrum it was possible to assign a rather weak, relatively resolvable feature. An expanded view of this area of the spectrum is displayed in Fig. 3. Based on the slit function used in our spectral simulation, it is possible to estimate that the linewidth of our tunable VUV radiation was about 1.2 cm^{-1} .

The particular spectral line that we chose to focus on (labelled "II" in Fig. 3) actually involves two overlapping transitions: R_1 (17.5) and ${}^RQ_{2,1}$ (17.5). This line was selected because of its relatively small overlap with lines in the $A^2\Sigma^+ \leftarrow X^2\Pi$ (4,0) band referred to previously. Although the two overlapping transitions involve different J levels in the $D^2\Sigma^+$ state, the rotational quantum number N in both of these upper levels is 18. Therefore, this mixed line can be used to study rotational photoionization propensities.

With approximately $2.4 \mu\text{J}$ of the second antistokes radiation alone we recorded the photoelectron spectrum displayed in Fig. 4. As can be seen from Table I, with such a short ionizing wavelength the kinetic energies of the ejected electrons are near 4 eV, and our TOF electron spectrometer's resolution is insufficient to distinguish ions generated in different rotational states. Nevertheless, it is quite apparent that ions are being produced in more than one vibrational state. The separation between the two principal features displayed in Fig. 4 is

approximately 1.15 eV, which corresponds to the separation between the $v=0$ and $v=4$ ion vibrational states. Since the Franck-Condon factor connecting the $v=4$ level of an ion with the $v=0$ level of an excited Rydberg state is extremely small, the most likely explanation for their appearance is that there is sufficient overlap between the $D^2\Sigma^+ \leftarrow X^2\Pi$ (0,0) and $A^2\Sigma^+ \leftarrow X^2\Pi$ (4,0) bands so that a substantial fraction of the initially excited molecules are in the A-state. This could be due to overlapping spectral transitions or simply because the $v=0$ level of the $D^2\Sigma^+$ state vibronically mixes with the nearby $v=4$ level of the $A^2\Sigma^+$ state. The latter hypothesis will be further considered below.

The limited electron energy resolution attainable when electrons are ejected with rather substantial kinetic energies is not the only problem associated with using short wavelength radiation. A second one is that the light induces a substantial photoemission that appears as a background over a wide range of electron energies. Because of these two problems we did not record two-color laser photoelectron spectra with either the fundamental or the first anti-Stokes line. Instead, we concentrated on photoionizing with the first, second, third, fourth, and fifth Stokes lines whose wavelengths and photon energies are listed in Table I. In order to record these two-color photoelectron spectra, it was important to strictly limit the fluence of second anti-Stokes radiation with a small aperture, while using substantially higher intensity Stokes radiation pulses. In this way, most of the $D^2\Sigma^+$ state NO molecules were ionized with Stokes light.

Photoelectron spectra obtained by exciting with the second anti-

Stokes line and ionizing with the fifth, fourth, third, second, and first Stokes lines are displayed in figs. 5a-5e. Only that part of each spectrum corresponding to ions produced in their ground vibrational state is displayed. Although in a few cases the peaks corresponding to $v=4$ ions were rotationally resolved, the resulting rotational state distributions were not so simple as those associated with $v=0$ ions since no effort was made to excite a single level characterized by just one N quantum number.

We have previously studied branching ratios for (2+1) REMPI via the $D^2\Sigma^+$ state.^{12,24} The agreement between the calculated and measured branching ratios was quite good except for an anomalously strong $\Delta N=0$ signal seen experimentally for parallel ($\theta=0$) photoelectron detection, indicating, by virtue of the selection rule $\Delta N+\ell=\text{odd}$, the presence of a strong p-wave in the continuum.²² Our calculated rotational branching ratios and total cross sections for (2+1') REMPI of NO via the $D^2\Sigma^+$ state were also highly dependent on the photoelectron kinetic energy. The branching ratios of the present (1+1') REMPI experiments can also be expected to display a similar dependence on photoelectron energy. Fig. 5 shows the experimental (a-e) and calculated (f-j) branching ratios for parallel detection in (1+1') REMPI via the mixed $Q_{21}+R_{11}(17.5)$ branch of the $D^2\Sigma^+$ state. These calculated branching ratios have been convoluted with a Lorentzian detector function with a FWHM determined from the experimental resolution (5.5-14 meV). The measured and calculated branching ratios are strongly dependent on the photoelectron kinetic energy. The $\Delta N=0$ signal is significant at all photoelectron energies and most dominant at $\sim 0.85\text{eV}$. The high ΔN peaks ($\pm 4, \pm 5$), experimentally observed

at higher kinetic energies, are not seen in the calculated spectra. In the calculated branching ratios the $\Delta N=0$ signal is significant throughout the whole energy range but not as dominant as seen experimentally. The presence of the $\Delta N=0$ signal in the calculated branching ratios probes the $\ell=1$ character of the photoelectron orbital. To illustrate this, we give the partial wave decomposition of the bound-free matrix elements, proportional to $|r_{fi}^{\ell\lambda\mu}|^2$, as a function of ℓ and energy in Table II. The $k\pi$ -channel is dominant at lower energies. Further, as expected from an atomic-like photoionization picture ($\ell=\ell_0\pm 1$), the d-wave ($\ell=2$) is substantial throughout. The $p\sigma$ -wave ($\ell=1, m_\ell=0$) is, however, far from negligible and is primarily responsible for the $\Delta N=0$ signal.

At these low energies the $\Delta N=0$ signal is a measure of the contribution of the $\ell=1$ wave of the photoelectron orbital to the transition moment. Comparison of the predicted and measured $\Delta N=0$ signals indicates that this component of the photoelectron matrix element is being underestimated in the calculations. Our experience in studies of REMPI of other $^2\Sigma^+$ states of NO suggests that this behavior is not due to inaccuracies in the photoelectron orbitals.^{12,20,24,35} The vibronic spectrum of the D-state shows some differences from that of the other Rydberg states which suggest a possible explanation for these discrepancies. As a Rydberg state the D-state is expected to have vibrational constants similar to those of the $\text{NO}^+ X^1\Sigma^+$ ground state, despite the slight anti-bonding character of the 7σ orbital, i.e. $\omega_e \approx 2376 \text{ cm}^{-1}$ and $\omega_e \chi_e \approx 16 \text{ cm}^{-1}$.³² The D-state's vibrational constants are, however, $\omega_e \approx 2324 \text{ cm}^{-1}$ and $\omega_e \chi_e \approx 23 \text{ cm}^{-1}$.³² The $v_D=0$ level is almost degenerate with the $v_A=4$ level of the $A^2\Sigma^+$ state suggesting possible perturbations between these

$\nu_D=0$ and $\nu_A=4$ levels. Several perturbations have been identified among the Rydberg states of NO,³⁶⁻⁴¹ but, to our knowledge, perturbations between the $\nu_D=0$ and $\nu_A=4$ levels have not been addressed. The D-state is known to be perturbed in different parts of the vibronic manifold, e.g., the complicated indirect heterogeneous perturbation between the $B^2\Pi-C^2\Pi-L^2\Pi-D^2\Sigma^+$ states⁴⁰⁻⁴² and the possible perturbation by the dissociative $A'^2\Sigma^+$ ($2p\sigma_u$) state.^{37,43} Neither of these perturbations can give rise to the almost pure s-character ($\ell_0=0$) in the resonant electronic state necessary to explain the anomalously large $\Delta N=0$ signal arising from $\ell=1$ character of the photoelectron wavefunction since the $^2\Pi$ states and the $A'^2\Sigma^+$ state have essentially no s-character.

This apparently direct homogeneous Rydberg-Rydberg perturbation between the A and D states is unusual, since they have different "atomic symmetries" (ℓ_0), $3s\sigma$ and $3p\sigma$, and it does not obey the vibrational propensity rule for Rydberg-Rydberg interactions: $\Delta\nu=\pm 1$.⁴² But similar interactions have been found in the PO molecule (valence-shell-isoelectronic with NO) by Ngo *et al.*⁴⁴ for the corresponding states $A^2\Sigma^+(4s\sigma, \nu=12)$ and $H^2\Sigma^+(4p\sigma, \nu=0)$. This perturbation arises via second-order van Vleck corrections with a leading term from interactions with the $F^2\Sigma^+$ valence state.⁴² It is possible that similar interactions are present in the NO molecule. However, there is insufficient spectroscopic data to sustain this theory.

A determination of the interaction of the $\nu_A=4$ and $\nu_D=0$ levels would require a careful deperturbation study, as described by Lefebvre-Brion,⁴² or a knowledge of highly accurate potential curves so far only

obtainable for H_2 .⁴⁵ Assuming the two Rydberg states interact, the only good quantum numbers would be parity, energy, and the rotational quantum number J . A crude model for the effect of the perturbation is to allow the two adiabatic electronic wave functions $\Psi_A^{ad.}$ and $\Psi_D^{ad.}$ to mix, forming an "effective" diabatic wave function for the D-state,

$$\Psi_D = c_1 \Psi_D^{ad.} + c_2 \Psi_A^{ad.} \quad (6)$$

where $c_2 = (1 - c_1^2)^{1/2}$. In the present frozen-core approximation this amounts to a mixing of the 6σ and 7σ orbitals. Assuming the two sublevels, $N' \pm 1/2$, in the D-state have the same coupling, we can assess the perturbation from the strength of the observed $\Delta N=0$ signal. We determine c_1 and c_2 by adjusting them so as to reproduce the observed branching ratio $\eta \equiv (\Delta N=0)/(\Delta N=+1)$ of ~ 1.5 at 0.85 eV. This gives values of $c_1 = 0.990$ and $c_2 = 0.142$ i.e., Ψ_D ($v_D=0, J'=17.5, 18.5$) level is $\sim 98\%$ "D-state" and $\sim 2\%$ "A-state". Single-center expansion of this state yields a 2.8 % s-, 96.7% p-, and 0.3% d-character.

In Fig. 5 k-o we show the calculated branching ratios using this mixed state for parallel detection of $(1+1')$ REMPI via the mixed $Q_{2,1}+R_{1,1}(17.5)$ branch of the $D^2\Sigma^+$ state. The calculated branching ratios are again convoluted with a Lorentzian detector function with a FWHM determined from the experimental resolution. The agreement between the experimental and the calculated results is much better than for the unperturbed state. The calculated $\Delta N=0$ signal now increases with increasing photoelectron energy and the intensity of the $\Delta N=\pm 3$ peaks decreases going from 0.85 to 1.36 eV photoelectron kinetic energy. This is primarily due to the insensitivity of the "A-state" component's cross section

to photoelectron energy for this perturbed state and to the strong energy dependence of the "D-state" component. The significant increase in the $\Delta N=0$ signal for this mixed D-state, arising from the small (~2%) admixture of the A-state, is due to the very strong $\Delta N=0$ propensity rule of the A-state, as observed experimentally in (1+1) REMPI via the $A^2\Sigma^+(3s\sigma)$ state.^{10,12-13}

A few experimentally observed trends were not reproduced very well in the calculated spectra. The calculated spectra do not show the same strong asymmetry at low photoelectron kinetic energy (0.33 eV) nor the high angular momentum transfer peaks ($\Delta N=\pm 4, \pm 5$) at higher energies (1.88 and 2.39 eV) seen experimentally. In table III we show the calculated, normalized, partial wave decomposition of the bound-free matrix elements, proportional to $|r_{fi}^{\ell\lambda\mu}|^2$, for the $k\sigma$ and $k\pi$ channels. The p-wave is, as expected, more dominant for this "mixed" state, and the angular distribution for the $\Delta N=0$ signal, dominated by this component, therefore has a large β_2 value. In Fig. 6 we show the calculated branching ratios for detection perpendicular to the polarization for the perturbed, Fig. 6 (a)-(e), and the unperturbed D-state, Fig. 6 (f)-(j). The two sets of results are virtually identical, reflecting the perpendicular signals' insensitivity ($\cos^2\theta$) to the presence of the $\ell_0=0$ component in the resonant state. This is in agreement with our earlier experimental¹² and theoretical²⁴ results for (2+1) REMPI via the $S_{21}(11.5)$ and $R_{21}+S_{11}(15.5)$ branches of $D^2\Sigma^+$ state, where agreement between the experimental and theoretical results was excellent for perpendicular detection. However, the strong $\Delta N=0$ signal observed experimentally in parallel detection,¹² was not well-reproduced theoretically.²⁴

Other mechanisms for the presence of the strong $\Delta N=0$ signal include correlation effects in the intermediate state that may introduce s-character into the $D^2\Sigma^+$ state. Bergeman and Zare³⁹ have measured the 'effective' dipole moment of the $A^2\Sigma^+$ ($v_A=3$) state to be $|\mu^{exp}|=1.10\pm0.03$ D, which differs significantly from the SCF value, $\mu^{SCF}=0.66$ D ($N^{\delta+}O^{\delta-}$), and that of earlier configuration interaction (CI) calculations,⁴⁶ $\mu\approx0.40$ D. Bergeman and Zare attribute this disagreement to possible perturbations between the $A^2\Sigma^+$ and the $D^2\Sigma^+$ states, either by "dipole borrowing" or non-adiabatic couplings possibly via the repulsive $A'^2\Sigma^+$ state⁴³ consistent with the assumptions we have made here. More extensive CI calculations have since determined the dipole moment of the $A^2\Sigma^+$ state to be ~ 1.4 D,^{47,48} a value much closer to the experimental value. The transition moments between the Rydberg states are known, however, to be quite insensitive to inclusion of correlation effects,^{12,49} and the CI calculated dipole moment for the $D^2\Sigma^+$ state $\mu^{CI} = -2.2$ D ($N^{\delta}-O^{\delta+}$)⁴⁷ agrees well with the value obtained from the present IVO calculations $\mu^{IVO} = -2.0$ D. Furthermore, if this were purely an adiabatic electronic effect, and therefore independent of J' and N' , the mixed D-state obtained above should then be suitable for describing branching ratios for other rotational branches of the D-state. A calculation of the branching ratios via the previously studied $S_{21}(11.5)$ and $R_{21}+S_{11}(17.5)$ branches¹² with this perturbed D-state leads, however, to a poorer agreement with the experimental results. Finally, it could be due to final state effects such as autoionization, predissociation etc. However, the agreement between theory and experiment over an energy range of ~ 2 eV, using the perturbed intermediate state does not

support this possibility. We therefore believe the "dynamic" coupling between the A- and D-state is a likely cause of the large $\Delta N=0$ signal observed here.

The obvious asymmetry that is displayed in the experimental spectrum of Fig. 5a but is missing from its theoretical counterparts (Figs. 5f and 5k) is highly reproducible and perhaps noteworthy. There are a few reasons why it is not likely to be due to variations in the electron spectrometer transmission. First, our spectrometer's transmission tends to cut off between 50 and 100 meV, depending on its condition, which is well below the lowest energy peak (~ 300 meV) in Fig. 5a. Second, the asymmetry in the middle of the spectrum involving the $\Delta N=+1$ and -1 peaks appears to be more dramatic than at the edges where the $\Delta N=+3$ and -3 peaks are involved. Third, the $\Delta N=-1$ peak, which appears to be smaller than the $\Delta N=+1$ peak, actually occurs at higher electron energy than the latter and thus is less likely to be discriminated against. Finally, the asymmetry is also present to a small degree in Fig. 5b and to a considerable degree in Figs. 9a and 10a of Ref. 13. The combination of these facts suggests that the observed asymmetry is a real effect and not an experimental artifact.

ACKNOWLEDGMENTS

The research at Indiana University was supported by the National Science Foundation under Grant NO. CHE-8800991. The research at the California Institute of Technology was supported by the National Science Foundation under Grant NO. CHE-8521391, by AFOSR under Grant NO. 87-0039, and by the Office of Health and Environmental Research of DOE (DE-FG03-87ER60513). The authors also acknowledge use of the resources of the San Diego SuperComputer Center which is supported by the National Science Foundation. HR and VM would like to thank Dr. H. Lefebvre-Brion and Dr. R. Cave for helpful discussions. HR gratefully acknowledges the support of the Danish Natural Science Research Council and a NATO Science Fellowship.

REFERENCES

1. J.T. Meek, S.R. Long, and J.P. Reilly, *J. Phys.* **86**, 2809 (1982).
2. S.L. Anderson, D.M. Rider, R.N. Zare, *Chem. Phys. Lett.* **93**, 11 (1982).
3. J. Kimman, P. Krust, and M.J. Van der Wiel, *Chem. Phys. Lett.* **88**, 576 (1982).
4. J.E. Pollard, D.J. Trevor, J.E. Reutt, Y.T. Lee, and D.A. Shirley, *J. Chem. Phys.* **77**, 34 (1982).
5. S.R. Long, J.T. Meek, and J.P. Reilly, *J. Chem. Phys.* **79**, 3206 (1983).
6. S.T. Pratt, P.M. Dehmer, J.L. Dehmer, *J. Chem. Phys.* **78**, 4315 (1983).
7. P. Kruit, H.G. Muller, J. Kimman, and M.J. Van der Wiel, *J. Phys. B: At. Mol. Phys.* **16**, 2359 (1983).
8. Y. Achiba, K. Sato, K. Shobatake, and K. Kimura, *J. Chem. Phys.* **78**, 5474 (1983).
9. S.L. Anderson, G.D. Kubiak, and R.N. Zare, *Chem. Phys. Lett.* **105**,

22 (1984).

10. W.G. Wilson, K.S. Viswanathan, E. Sekreta, and J.P. Reilly, *J. Phys. Chem.* **88**, 672 (1984).
11. J. Kimman, M. Lavollee, and M.J. Van der Wiel, *Chem. Phys.* **97**, 137 (1985).
12. K.S. Viswanathan, E. Sekreta, E.R. Davidson, and J.P. Reilly, *J. Chem. Phys.* **90**, 5078 (1986).
13. K.S. Viswanathan, E. Sekreta, and J.P. Reilly, *J. Phys. Chem.* **90**, 5658 (1986).
14. A. Sur, C.V. Ramana, W.A. Chupka, and S.D. Colson, *J. Chem. Phys.* **84**, 69 (1986).
15. T.M. Orlando, L. Li, S.L. Anderson, and M.G. White, *Chem. Phys. Lett.* **129**, 31 (1986).
16. J.C. Miller and R.N. Compton, *J. Chem. Phys.* **84**, 675 (1986).
17. J. Kimman, J.W.J. Verschuur, M. Lavollee, H.B. van Linden van den Heuvell, and M.J. van der Wiel, *J. Phys. B:At. Mol. Phys.* **19**, 3909 (1986).
18. P. Chen, J.B. Pallix, W.A. Chupka, and S.D. Colson, *J. Chem. Phys.*

- 86, 516 (1987).
19. D.T. Biernacki, E.E. Eyler, and S.D. Colson, *J. Chem. Phys.* **88**, 2099 (1988).
20. K. Kaufmann, C. Nager, and M. Jungen, *Chem. Phys.* **95**, 385 (1985).
21. S.N. Dixit, D.L. Lynch, V. McKoy, and W.M. Huo, *Phys. Rev. A* **32**, 1267 (1985).
22. S.N. Dixit and V. McKoy, *Chem. Phys. Lett.* **128**, 49 (1986).
23. H. Rudolph, S.N. Dixit, V. McKoy, and W.M. Huo, *Chem. Phys. Lett.* **137**, 521 (1987).
24. H. Rudolph, S.N. Dixit, V. McKoy, and W.M. Huo, *J. Chem. Phys.* **88**, 637 (1988).
25. A.B. Callear, M.J. Pilling, and I.W.M. Smith, *Trans. Faraday Soc.* **64**, 2296 (1968).
26. S.R. Long, J.T. Meek, J.P. Reilly, *J. Chem. Phys.* **79**, 3206 (1983).
27. S.N. Dixit and V. McKoy, *J. Chem. Phys.* **82**, 3546 (1985).
28. L.T. Earls, *Phys. Rev.* **48**, 423 (1935).

29. W.J. Hunt and W.A. Goddard III, *Chem. Phys. Lett.* 24, 464 (1974).
30. R.R. Lucchese, G. Raseev, and V. McKoy, *Phys. Rev. A* 25, 2572 (1982).
31. R.R. Lucchese, K. Takatsuka, and V. McKoy, *Phys. Rep.* 131, 147 (1986).
32. K.P. Huber and G. Herzberg '*Constants of Diatomic Molecules*', (Van Nostrand Reinhold, New York, 1979).
33. J.B. Halpern, H. Zacharias, and R. Wallenstein, *J. Mol. Spectrosc.* 79, 1 (1980).
34. G.W. Bethke, *J. Chem. Phys.* 31, 662 (1959).
35. H. Rudolph, S.N. Dixit, V. McKoy, and W. M. Huo, *J. Chem. Phys.* 88, 1516 (1988).
36. C. Jungen and E. Miescher, *Can. J. Phys.* 46, 987 (1968).
37. E. Miescher, *Can. J. Phys.* 49, 2350 (1971).
38. Y. Ben-Aryeh, *J. Quant. Spectrosc. Radiat. Transfer.* 13, 1441 (1973).
39. T. Bergeman and R.N. Zare, *J. Chem. Phys.* 61, 4500 (1974).

40. R. Gallusser and K. Dressler, *J. Chem. Phys.* **76**, 4311 (1982).
41. J. Kimman, M. Laollée and M.J. Van der Wiel, *Chem. Phys.* **97**, 137 (1985).
42. H. Lefebvre-Brion and R.W. Field '*Perturbations in the Spectra of Diatomic Molecules*' (Academic Press, 1986).
43. F.R. Gillmore, *J. Quant. Spectr. Radiat. Transfer.* **5**, 369 (1965).
44. T.A. Ngo, M. DaPaz, B. Coquart, C. Couet, *Can. J. Phys.* **52**, 154 (1974).
45. K. Dressler, R. Gallusser, P. Quadrelli, and L. Wolniewicz, *J. Mol. Spectrosc.* **75**, 205 (1979).
46. S. Green, *Chem. Phys. Lett.* **23**, 115 (1973).
47. S.P. Walch and W.A. Goddard III, *Chem. Phys. Lett.* **33**, 18 (1975).
48. S.R. Langhoff, C.W. Bauschlicher, Jr., and H. Partridge, *J. Chem. Phys.* **89**, 4909 (1988).
49. R. de Vivic and S.D. Peyerimhoff, *J. Chem. Phys.* **89**, 3028 (1988).

Table I

Photon and electron energetics				
Raman line	Ionizing λ	Pulse energy	Photon E	Electron K. E.*
	(Å)	(μ J)	(eV)	(eV)
2nd anti-Stokes	1871	2.4	6.626	3.940
1st anti-Stokes	2029	----	6.111	3.425
main beam	2216	320	5.596	2.910
1st Stokes	2440	240	5.081	2.395
2nd Stokes	2716	160	4.565	1.879
3rd Stokes	3061	60	4.050	1.364
4th Stokes	3507	12	3.535	0.849
5th Stokes	4106	0.8	3.020	0.334

* Electron kinetic energy was calculated for $\Delta N = 0$ peak of each photoelectron spectrum.

Table II

Value of $|r_{fi}^{l\lambda\mu}|^2$ as a function of l , normalized to the dominant wave for each energy.

E (eV) (Photoelectron energy)						
	l	0.33	0.85	1.36	1.88	2.35
$k\sigma$	0	0.0880	0.1544	0.3864	0.3340	0.3278
	1	0.1472	0.2647	0.4914	0.2886	0.1984
	2	0.0146	0.2113	0.9785	≈ 1.00	≈ 1.00
	3	0.0129	0.0247	0.0457	0.0260	0.0174
	4	0.0003	0.0005	0.0009	0.0005	0.0003
$k\pi$	1	0.0053	0.0090	0.0167	0.0098	0.0066
	2	≈ 1.00	≈ 1.00	≈ 1.00	0.2807	0.0747
	3	0.0192	0.0396	0.0765	0.0448	0.0301
	4	0.0001	0.0001	0.0002	-	-

Table III

Value of $|r_n^{L\mu}|^2$ as a function of l , for ionization via mixed D-state, normalized to the dominant wave for each energy.

E (eV) (Photoelectron energy)						
	l	0.33	0.85	1.36	1.88	2.39
$k\sigma$	0	0.0791	0.1539	0.3632	0.3275	0.3311
	1	0.1930	0.3767	0.6556	0.4151	0.3088
	2	0.0203	0.2634	≈ 1.00	≈ 1.00	≈ 1.00
	3	0.0010	0.0008	0.0010	0.0033	0.0059
	4	0.0002	0.0005	-	0.0006	0.0005
$k\pi$	1	0.0475	0.1111	0.2256	0.1622	0.1330
	2	≈ 1.00	≈ 1.00	0.8639	0.2394	0.0620
	3	0.0034	0.0047	0.0041	0.0009	0.0004
	4	0.0001	0.0002	0.0002	-	-

FIGURE CAPTIONS

Figure 1 Apparatus employed to generate UV laser radiation and to record time of flight laser photoelectron spectra. WEX is a Quanta Ray wavelength extension system. MCP is the micro-channel plate detector.

Figure 2 (A) Wavelength dependence of NO ionization yield obtained under effusive beam conditions using the second anti-Stokes line to excite and the second Stokes to ionize. (B) The calculated simulation of the rotational structure of the $D^2\Sigma^+ \leftarrow X^2\Pi$ 0-0 band. (C) The calculated simulation of the rotational structure of the $A^2\Sigma^+ \leftarrow X^2\Pi$ 4-0 band.

Figure 3 Wavelength scan near the region of the $R_1(17.5)+^RQ_{21}(17.5)$ mixed line of the 0-0 band of the $D^2\Sigma^+ \leftarrow X^2\Pi$ transition. Peak I involves the $R_1(12.5)$, $^RQ_{21}(12.5)$ and $^SR_{21}(7.5)$ lines of the $A^2\Sigma^+ \leftarrow X^2\Pi$ 4-0 band. Peak II is the $R_1(17.5)+^RQ_{21}(17.5)$ mixed line of the $D^2\Sigma^+ \leftarrow X^2\Pi$ 0-0 band. Peak III is the result of overlapping $R_1(13.5)$, $^RQ_{21}(13.5)$ and $^SR_{21}(8.5)$ lines of the $A^2\Sigma^+ \leftarrow X^2\Pi$ 4-0 band.

Figure 4 Photoelectron spectrum recorded with laser tuned to peak II of Fig. 3.

Figure 5 Comparison of experimentally observed and theoretically predicted photoelectron spectra obtained by exciting the

$R_1(17.5)+^RQ_{21}(17.5)$ mixed line of the $D^2\Sigma^+ \leftarrow X^2\Pi$ transition. (a)-(e) Experimental data obtained by exciting with the second anti-Stokes line and ionizing with the fifth, fourth, third, second and first Stokes lines respectively. (f)-(j) Spectra calculated by assuming the same photoelectron kinetic energies as in Fig. 5 (a)-(e). (k)-(o) Spectra calculated by assuming mixing between $A^2\Sigma^+$ and $D^2\Sigma^+$ Rydberg states.

Figure 6 Calculated branching ratios for (1+1') REMPI via the $R_1(17.5)+^RQ_{21}(17.5)$ branch of the $D^2\Sigma^+$ state of NO, assuming the same photoelectron kinetic energies as in Fig. 5 (a)-(e). Detection perpendicular to the polarization of the light ($\theta=90^\circ$). (a)-(e) Calculated assuming no mixing between the $A^2\Sigma^+$ and $D^2\Sigma^+$ states. (f)-(j) Calculated assuming the existence of mixing between $A^2\Sigma^+$ and $D^2\Sigma^+$ states, see text for details.

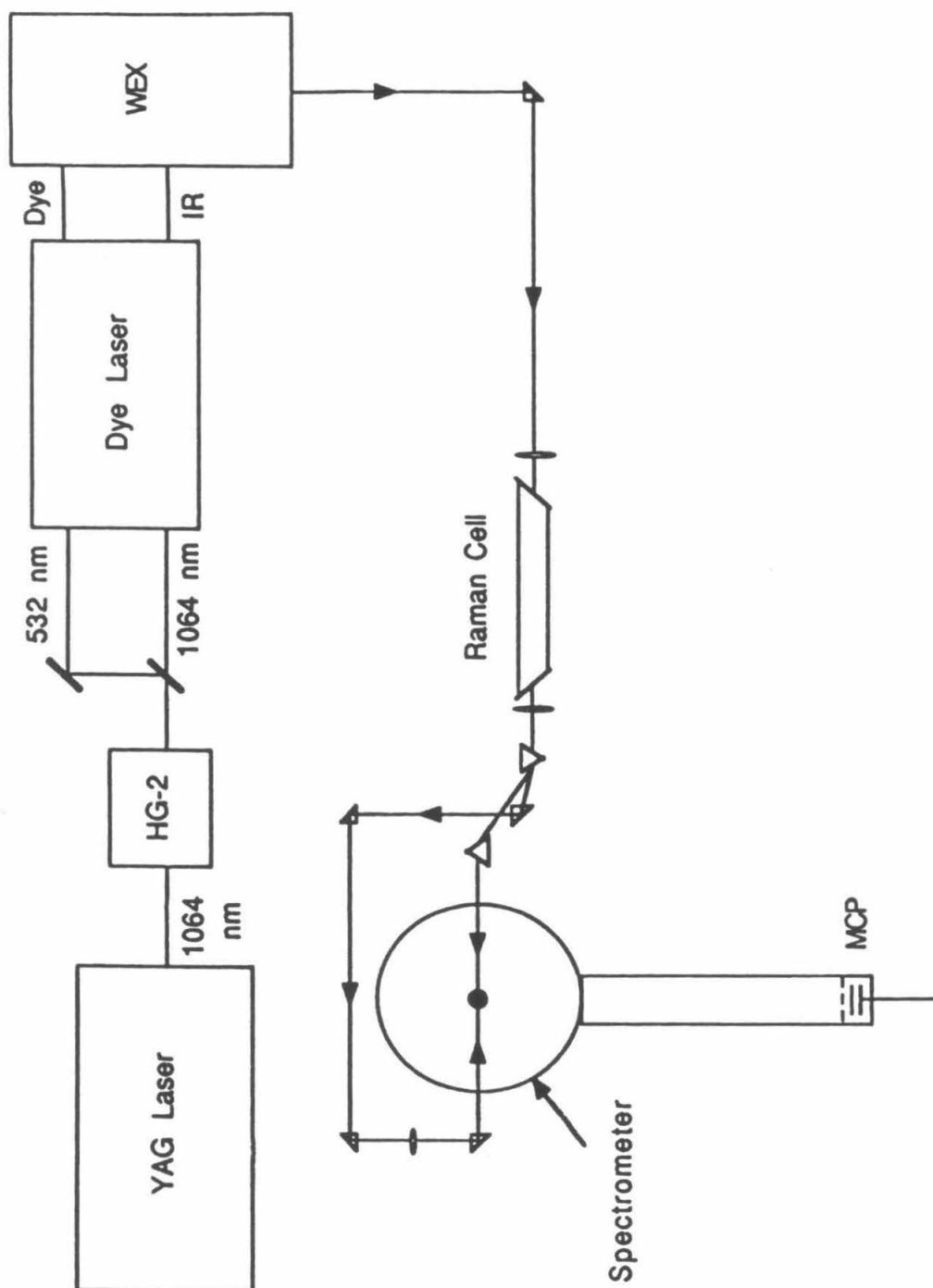


FIGURE 1

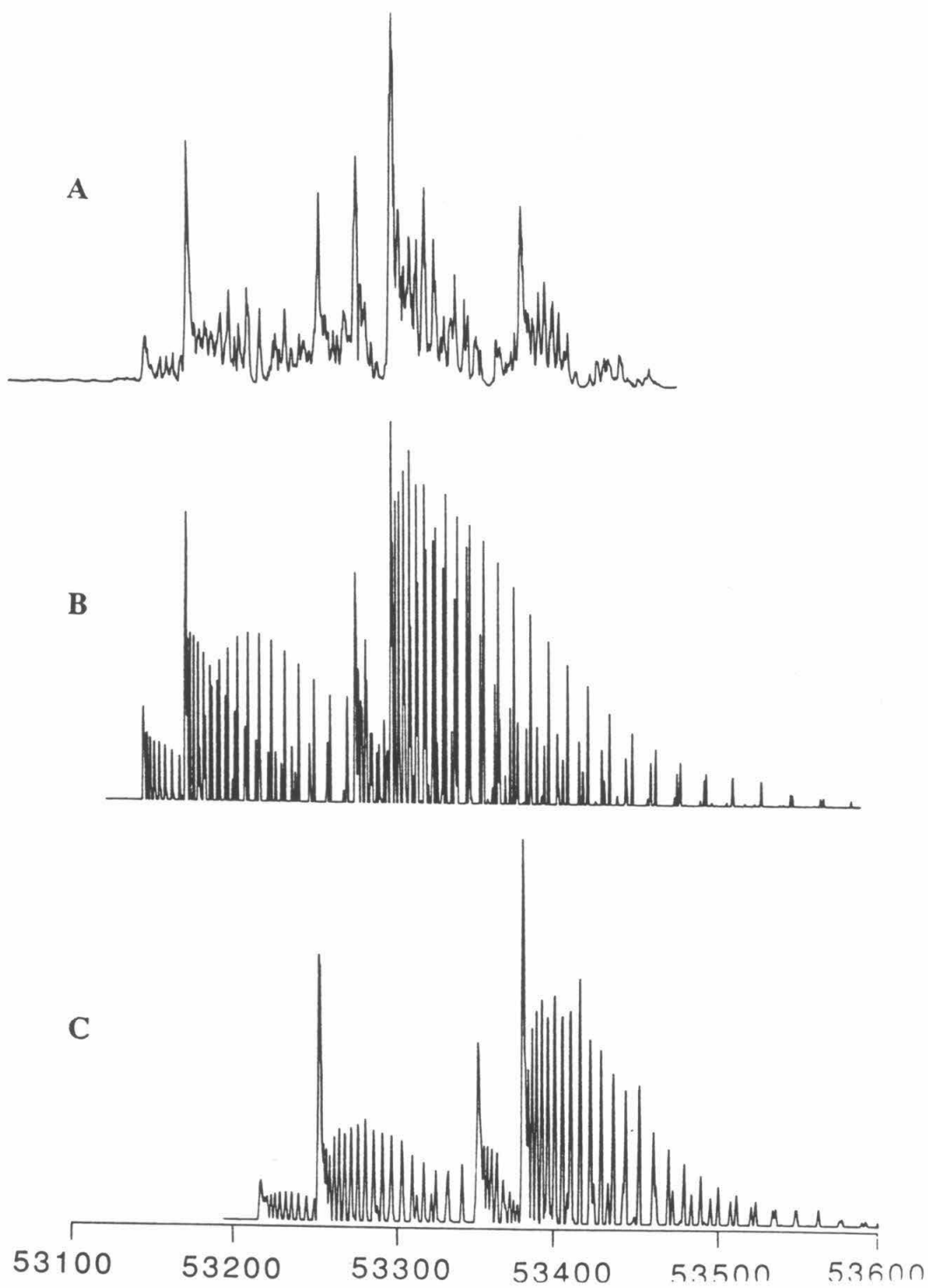


FIGURE 2

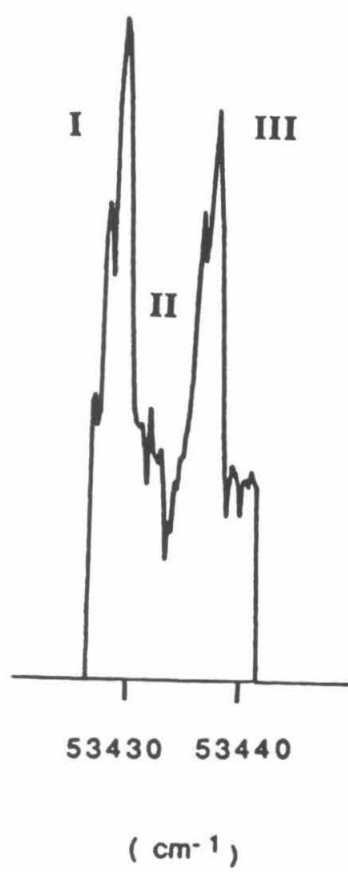


FIGURE 3

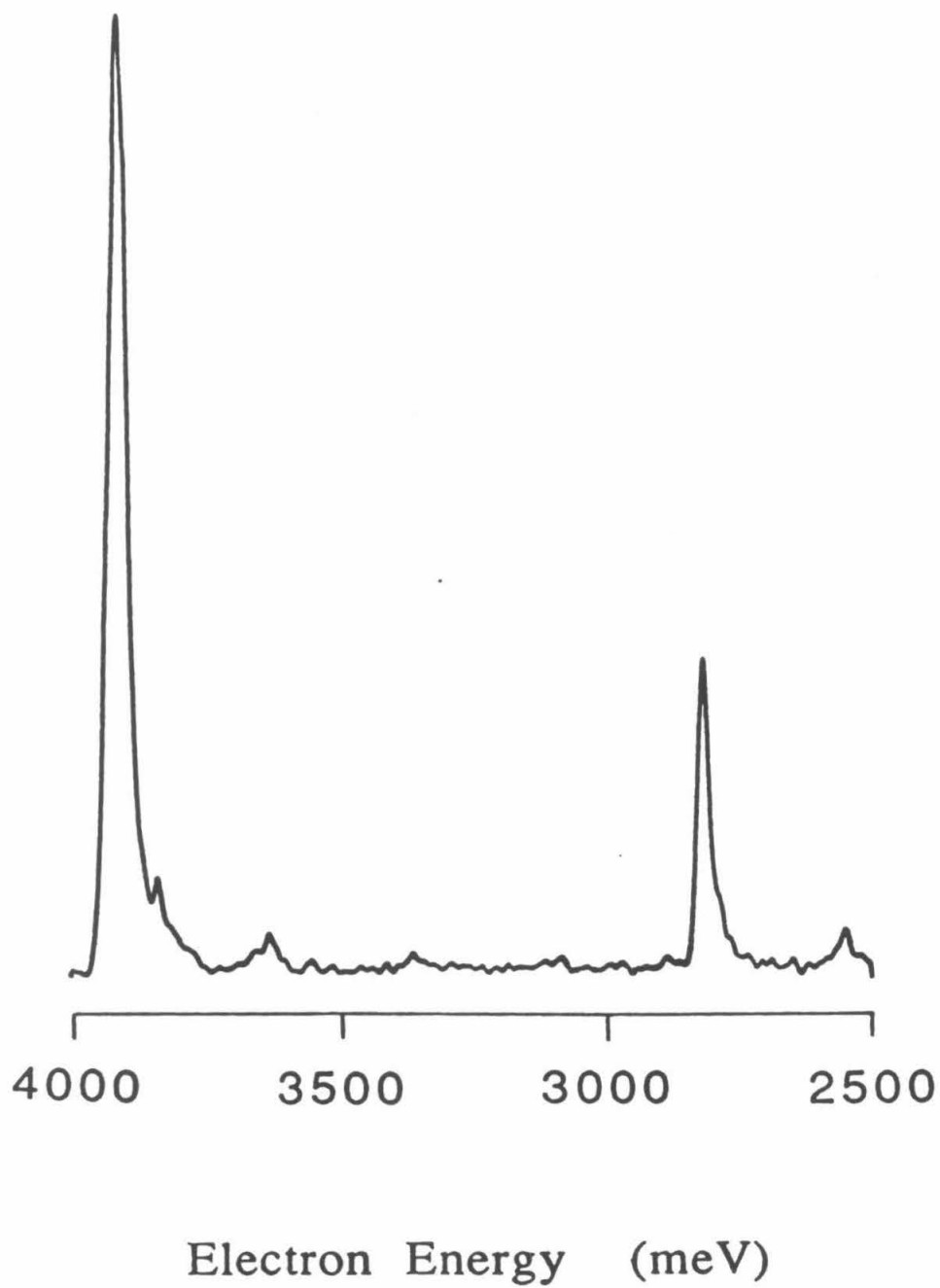


FIGURE 4

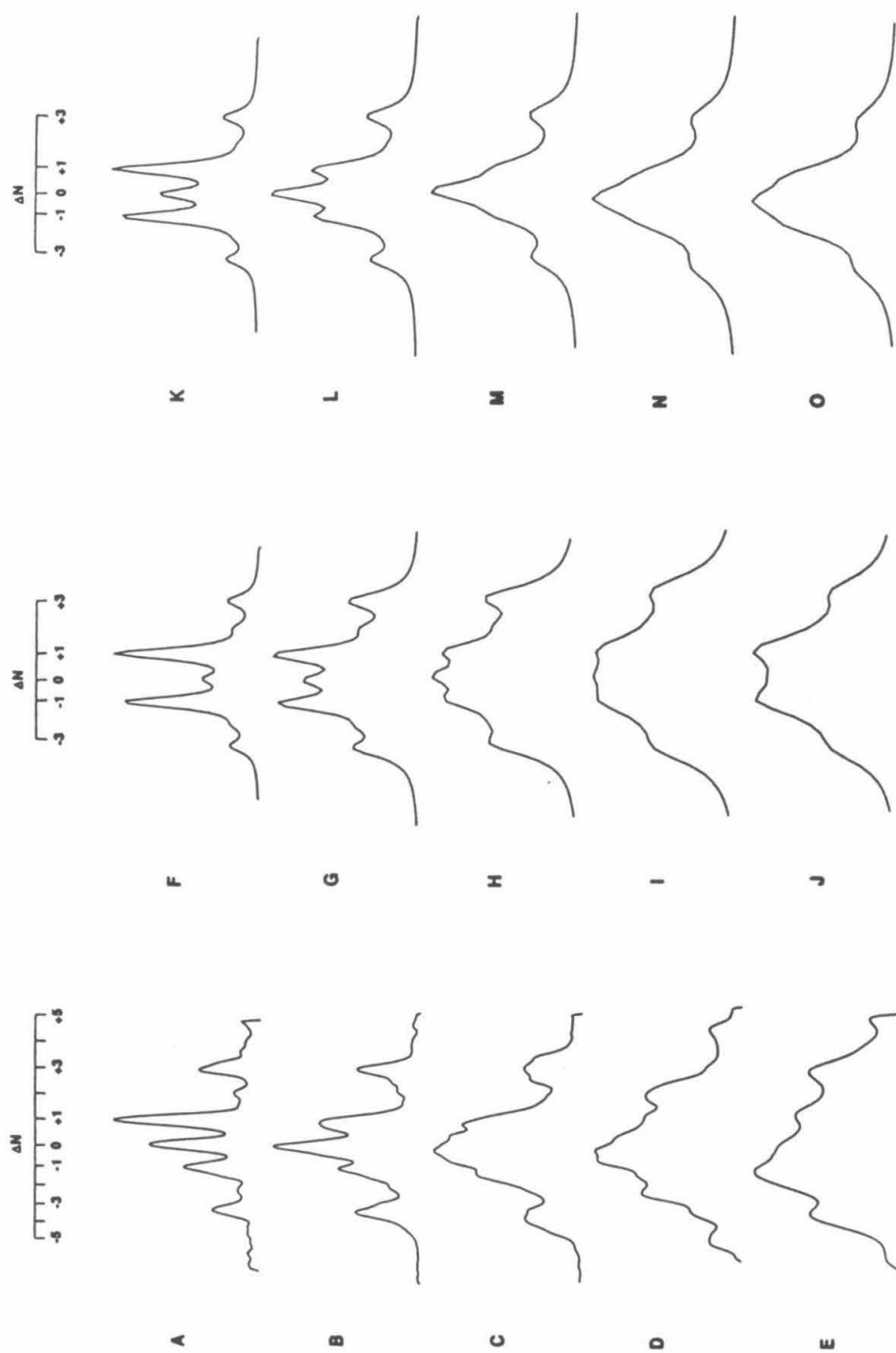


FIGURE 5

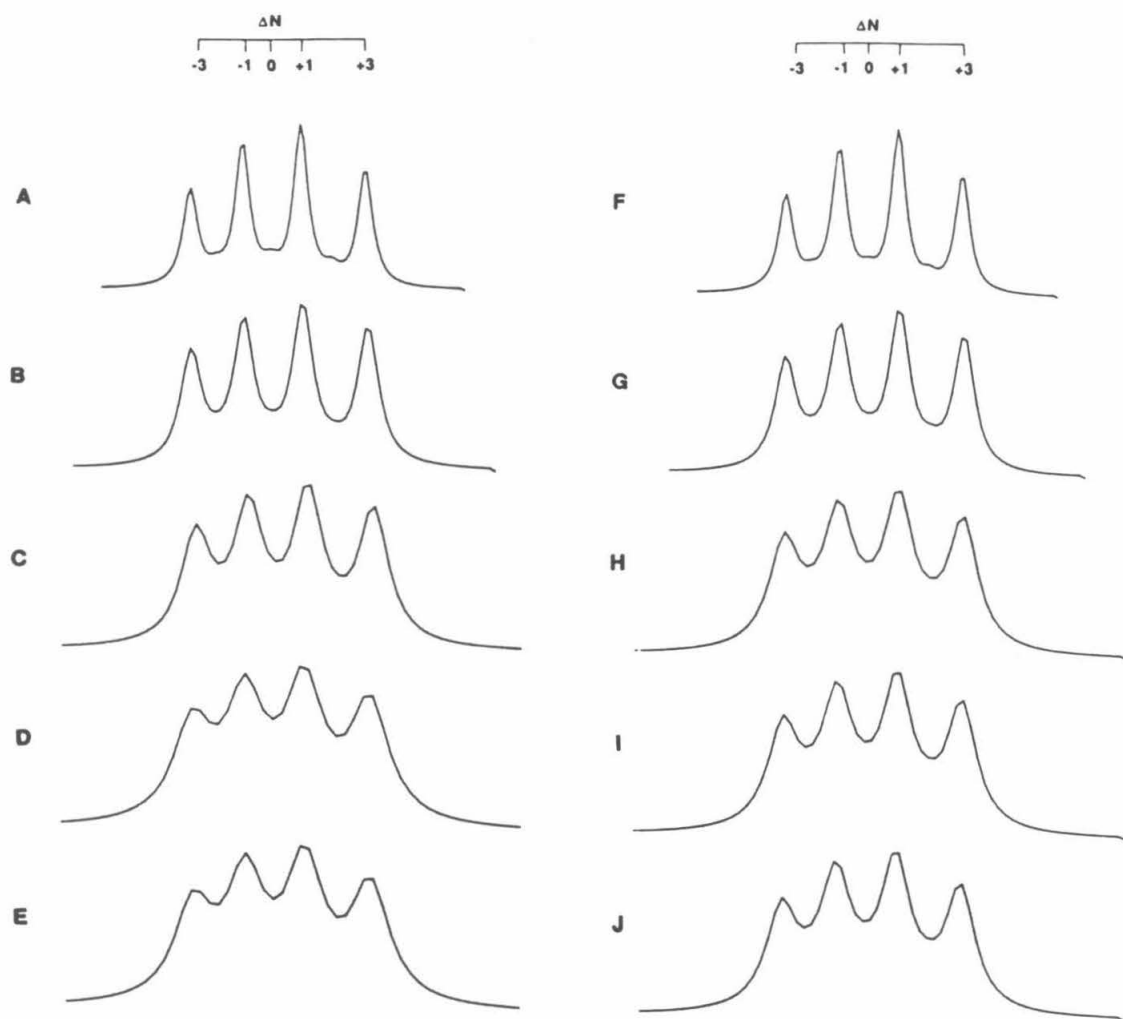


FIGURE 6

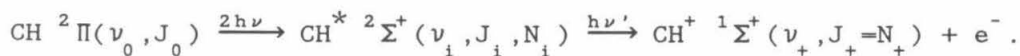
**Chapter 6: Vibrational state dependence of ionic rotational
branching ratios in resonance enhanced multiphoton
ionization of CH**

[The text of this chapter appeared in: H. Rudolph, J.A. Stephens, V. McKoy, and M.-T. Lee, submitted to J. Chem. Phys. (contribution no. 7939)]

Combined with high-resolution photoelectron spectroscopy, resonance enhanced multiphoton ionization (REMPI) is an important probe of the photoionization dynamics of excited molecular states at a quantum-state-specific level.¹⁻³ Whereas much interest has been focused on vibrationally-resolved REMPI spectra and the insight such spectra provide on the resonant and ionized state dynamics, rotationally-resolved spectra not only extend our understanding of the underlying ionization dynamics but also obviously play a role in the use of this technique for state-specific production of ions.⁴⁻⁶ Among small molecules, the REMPI spectra of diatomic hydrides such as CH, NH, and OH are of particular interest because of their importance as dissociation fragments and reactive intermediate species. The Rydberg states of diatomic hydrides share a common, rather simple, electronic structure: the first Rydberg state is repulsive (σ -type Rydberg orbitals consist mainly of a mixture between $3s_A$ and antibonding $2p_{z_A} - 1s_B$ orbitals), followed by a set of Rydberg states whose potential energy curves closely resemble that of the associated ion.⁷ Recently we have shown that rapid evolution of the Rydberg orbital with internuclear distance (further enhanced by the presence of a Cooper minimum) can lead to strong non-Franck-Condon effects in ion vibrational branching ratios measured in REMPI, as predicted for OH and other diatomic hydrides.⁸

The purpose of this Letter is to illustrate the striking and significant influence this rapid orbital evolution of the resonant Rydberg state has on the ionic rotational distributions as the level of vibrational excitation in the resonant state increases. As a specific example of this effect we present results of *ab initio* calculations of these branching ratios for (2+1') REMPI of CH via the $E'^2\Sigma^+(3p\sigma)$ state. This

is similar to the excitation scheme used in the recent work by Chen et al.⁹ in which the E' state was probed by REMPI for the first time:



Here we choose excitation via the $O_{11}(20.5)$ branch, i.e. $J_0=20.5$, $J_i=18.5$, and $N_i=18$. For a Σ - Σ transition as in the photoionization step of the above reaction, a $\Delta N + \ell = \text{odd}$ selection rule applies,¹⁰ where ΔN is the change of the rotational quantum number (excluding spin) between the intermediate and final state, and ℓ denotes a partial-wave component of the photoelectron orbital. For the $E'^2\Sigma^+(3p\sigma)$ state of CH, this selection rule therefore predicts a $\Delta N = \text{odd}$ propensity rule, since an atomic photoionization picture would predict dominance of even partial waves in the photoelectron orbital (i.e. $3p \rightarrow ks, kd, \dots$).

The electronic wave function for the $E'^2\Sigma^+(3p\sigma)$ state of CH, (with the dominant configuration¹¹ $1\sigma^2 2\sigma^2 3\sigma^2 5\sigma$) was determined using the improved virtual orbital method¹² with the CH^+ orbitals for the core. The continuum photoelectron orbitals were obtained using the iterative Schwinger method.¹³ The explicit R-dependence of the transition moment between the initial state $|i\rangle$ and the final state $|f\rangle$ was included via the transition moment $\int dR \chi_f^*(R) r_{fi}(R) \chi_i(R)$ where $r_{fi}(R)$ is the bound-free electronic transition moment at an internuclear distance R. The electronic wave functions and transition moments were calculated over a range of internuclear distances from $R=1.6 a_0$ to $R=3.2 a_0$, and the vibrational wave functions χ_f and χ_i were obtained numerically using the potential curves calculated by van Dishoeck¹¹ for the $E'^2\Sigma^+$ state, and by Green et al.¹⁴ for the $X^1\Sigma^+$ state of CH^+ . The coupling between partial waves of the continuum orbital and the molecular rotation was

treated explicitly, employing a method previously described.⁴⁻⁶ Both the intermediate state and the final state were treated in Hund's case (b) coupling scheme.¹⁵ Further details of the calculations will be reported in a separate paper.

The evolution of the 5σ orbital of the $E'^2\Sigma^+$ state is very rapid as a function of internuclear distance: it changes from predominantly $3p$ character at small internuclear distances to predominantly $3s$ character at larger internuclear distances. A single-center expansion of the 5σ orbital around the center-of-mass yields a 14.8% s -, 84.7% p -, and 0.5% d -character at $R=1.6 a_0$, and a 81.6% s -, 5.3% p -, and 10.6% d -character at $R=3.2 a_0$. This orbital evolution is similar to that for the $D^2\Sigma^-$ ($3p\sigma$) state of OH,⁸ and in the present case also leads to strong non-Franck-Condon behavior in ion vibrational branching ratios (not shown). This orbital evolution also results in a dramatic dependence of the partial-wave composition of the transition moment as a function of internuclear distance. An atomic photoionization picture would therefore predict, as a function of internuclear distance, the even ℓ partial waves (s, d, \dots) to be dominant at small internuclear distances and the odd partial waves (p, f, \dots) at larger internuclear distances.

In Fig. 1 we show calculated ionic rotational branching ratios for the $O_{11}(20.5)$ branch via the $E'^2\Sigma^+$ state of CH, for the $v_1=0-3$ vibrational levels of the resonant intermediate state. The branching ratios have been convoluted with a Gaussian detector function with a FWHM of 6 meV. Only the diagonal ($\Delta v=v_+-v_1=0$) vibrational branches are presented since these are predicted to have the strongest signals, as expected on basis of the Rydberg nature of the E' state. The ionic rotational branching ratios are determined for the $O_{11}(20.5)$ branch because it is a

"clean" branch, and it has reached the high-J limit, where the rotational branching ratios are symmetric around $\Delta N=0$. Since $N_i=18$, the $\Delta N=0$ peak corresponds to $N_+=18$. The rotational branching ratios are seen to be very dependent on the vibrational level accessed in the intermediate state, with a strong $\Delta N=\text{odd}$ (i.e. $\ell=\text{even}$) propensity rule apparent in lower vibrational levels and a $\Delta N=\text{even}$ (i.e. $\ell=\text{odd}$) propensity rule for higher vibrational excitation. This vibrational dependence of the propensity rule is caused by the extended portion of the potential well sampled by the higher vibrational levels, i.e. the region of R where the Rydberg orbital itself has evolved from $3p\sigma$ to mainly $3s\sigma$ type. The photoelectron kinetic energy is kept constant (100 meV in the present calculations). The branching ratios are somewhat (but not strongly) dependent on the final kinetic energy, and results indicate (not shown) that this effect remains very pronounced at higher kinetic energies. In conclusion, we point out that this vibrational dependence of the ionic rotational propensity rule should be quite general, and is expected to occur in the other diatomic hydrides in which the Rydberg orbital of the resonant intermediate state exhibits rapid evolution with internuclear distance. The hydrides are particularly suitable for ionic rotationally resolved experiments, since the large rotational constant of the ion makes the required rotational resolution feasible at lower N_+ levels.

We would like to thank Professor W. Chupka for several helpful discussions. We acknowledge support from the National Science Foundation (Grant No. CHE-8521391), Air Force Office of Scientific Research (Contract No. 87-0039), and the Office of Health and Environmental Research of the U.S. Department of Energy (Grant No. DE-FG03-87ER60513). We also

made use of resources of the San Diego SuperComputer Center, which is supported by the National Science Foundation. H.R. gratefully acknowledges support from the NATO Science Fellowship Programme (Denmark).

References

- 1 S.T. Pratt, P. M. Dehmer, and J. L. Dehmer, Chem. Phys. Lett. 105, 28 (1984).
- 2 K. S. Viswanathan, E. Sekreta, E. R. Davidson, and J. P. Reilly, J. Phys. Chem. 90, 5078 (1986), and references therein.
- 3 M. Sander, L. A. Chewter, K. Müller-Dethlefs, and E. W. Schlag, Phys. Rev. A 36, 4543 (1987).
- 4 S. N. Dixit, D. L. Lynch, V. McKoy, and W. M. Huo, Phys. Rev. A 32, 1267 (1985).
- 5 H. Rudolph, S. N. Dixit, V. McKoy, and W. M. Huo, J. Chem. Phys. 88, 637 (1988).
- 6 H. Rudolph, V. McKoy, and S. N. Dixit, J. Chem. Phys. 90, 2570 (1989).
- 7 H. Lefebvre-Brion and R. W. Field, *Perturbations in the Spectra of Diatomic Molecules* (Academic, Orlando, 1986), Chap. 4, Sec. 2. Rydberg states may deviate considerably from their associated ion under conditions of strong Rydberg-valence mixing. The present discussion pertains to Rydberg states which are well described by a single electronic configuration, over a range of internuclear distance typically spanning several lower vibrational levels.

- 8 J. A. Stephens and V. McKoy, Phys. Rev. Lett. 62, 889 (1989).
- 9 P. Chen, J. B. Pallix, W. A. Chupka, and S. D. Colson, J. Chem. Phys. 86, 516 (1987).
- 10 S. N. Dixit and V. McKoy, Chem. Phys. Lett. 128, 49 (1986).
- 11 E. F. van Dishoeck, J. Chem. Phys. 86, 196 (1987).
- 12 W. J. Hunt and W. A. Goddard III, Chem. Phys. Lett. 24, 464 (1974).
- 13 R. R. Lucchese, G. Raseev, and V. McKoy, Phys. Rev. A 25, 2572 (1982).
- 14 S. Green, P. S. Bagus, B. Liu, A. D. McLean, and M. Yoshimine, Phys. Rev. A 5, 1614 (1972).
- 15 G. Herzberg, *Spectra of Diatomic Molecules* (Van Nostrand Reinhold, New York, 1950).

Figure caption

Ionic rotational branching ratios for (2+1') REMPI via the $O_{11}(20.5)$ branch of the $E'^2\Sigma^+(3p\sigma)$ state of CH for various vibrational levels of the E' state. The value of ν_i and ν_+ is indicated ($\Delta\nu=0$) in the upper right corner of each frame. The value of N_+ is indicated over each photoelectron peak. The photoelectron kinetic energy is 100 meV.

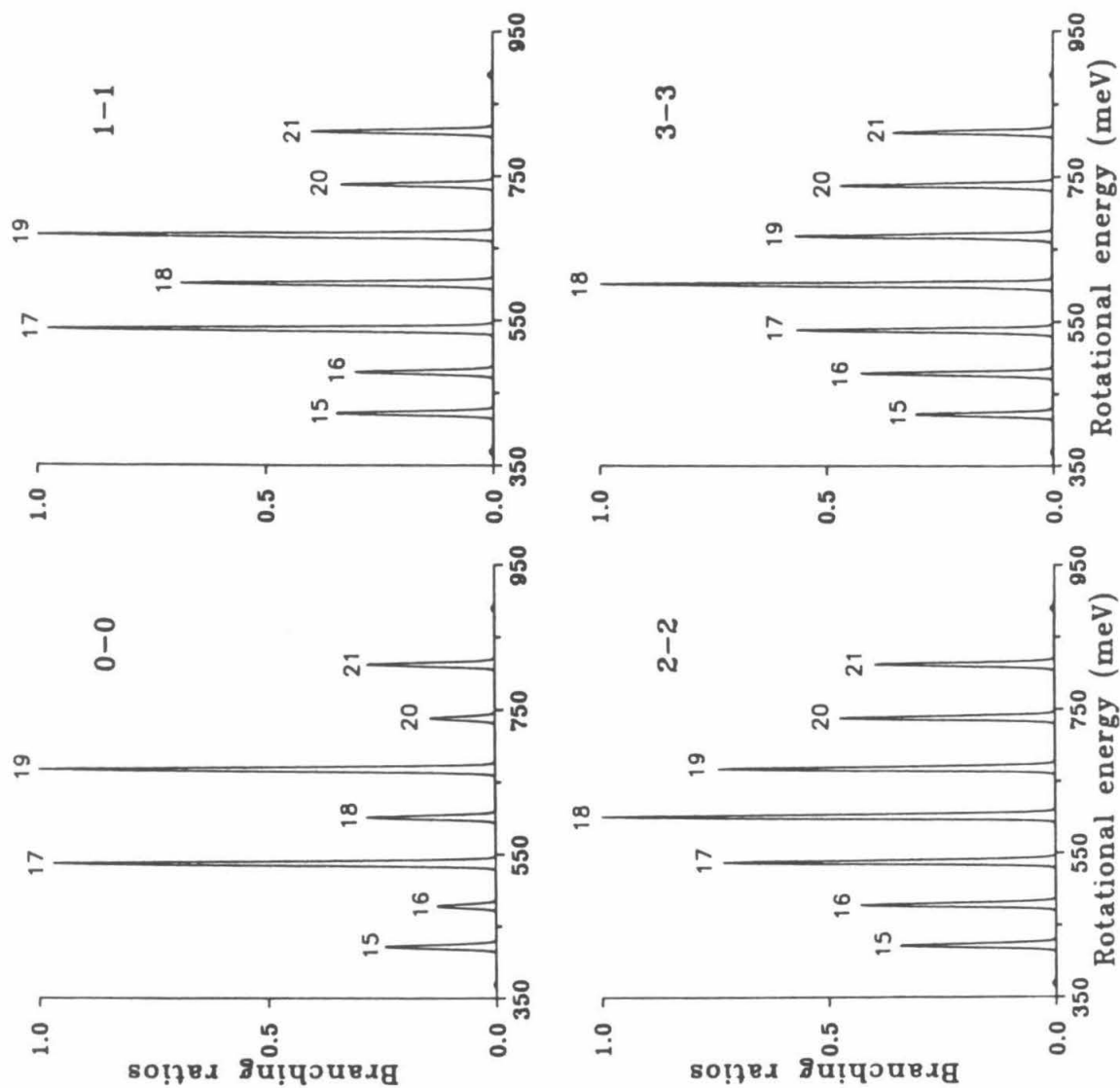


FIGURE 1

Chapter 7: **(2+1) resonant enhanced multiphoton ionization of H_2**
 via the $E,F,^1\Sigma_g^+$ state

[The text of this chapter appeared in: H. Rudolph, D.L. Lynch, S.N. Dixit, and V. McKoy, J. Chem. Phys. **86**, 1748 (1987)]

(2+1) resonant enhanced multiphoton ionization of H₂ via the $E,F\ ^1\Sigma_g^+$ state

H. Rudolph, D. L. Lynch,^{a)} S. N. Dixit, and V. McKoy

Arthur Amos Noyes Laboratory of Chemical Physics,^{b)} California Institute of Technology,
Pasadena, California 91125

Winifred M. Huo^{c)}

Radiation Laboratory, University of Notre Dame, Notre Dame, Indiana 46556

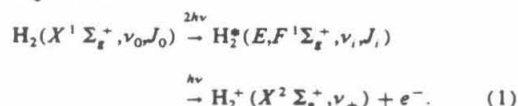
(Received 30 September 1986; accepted 7 November 1986)

In this paper, we report the results of *ab initio* calculations of photoelectron angular distributions and vibrational branching ratios for the (2 + 1) REMPI of H₂ via the $E,F\ ^1\Sigma_g^+$ state, and compare these with the experimental data of Anderson *et al.* [Chem. Phys. Lett. **105**, 22 (1984)]. These results show that the observed non-Franck-Condon behavior is predominantly due to the R dependence of the transition matrix elements, and to a lesser degree to the energy dependence. This work presents the first molecular REMPI study employing a correlated wave function to describe the Rydberg-valence mixing in the resonant intermediate state.

INTRODUCTION

Resonant enhanced multiphoton ionization (REMPI) techniques provide a useful tool for the study of highly excited states and of the dynamics of the photoionization of these rovibrationally selected states. Furthermore, for systems with inversion symmetry, REMPI studies can be effectively used to access dipole-forbidden bound and continuum states. Several groups have experimentally exploited these advantages to demonstrate interesting aspects of REMPI dynamics.¹⁻⁹ In a previous paper,¹⁰ we have discussed the development of our theoretical framework for analyzing REMPI processes in diatomic molecules. In this theory, an $(n + m)$ REMPI is viewed as a two-step process with n -photon absorption to the resonant intermediate state followed by an m -photon ionization out of it. Coupling the formalism with *ab initio* calculations of molecular properties, we have analyzed several recent REMPI experiments with encouraging results.¹¹⁻¹⁴

Recently Zare and co-workers¹⁵ have measured the photoelectron angular distributions and vibrational branching ratios in a one-color (2 + 1) REMPI of H₂ via the $E,F\ ^1\Sigma_g^+$ state:



The low resolution (150 meV) photoelectron spectra display highly non-Franck-Condon behavior as seen by the departure of the vibrational branching ratios from Franck-Condon values and by a strong vibrational state dependence of the photoelectron angular distributions. The potential energy curve of the $E,F\ ^1\Sigma_g^+$ state has the well-known double-well structure^{16,17} with the nature of the electronic wave

function changing from Rydberg-like in the inner well (E state) to valence-like in the outer well (F state). This presents an interesting situation for theoretical investigation as the electronic wave function for the E,F state has to be described in a multiconfigurational scheme to incorporate the continuous change of its character with internuclear distance (R). We have, therefore, carried out *ab initio* calculations of photoelectron angular distributions and vibrational branching ratios for the REMPI process of Eq. (1). Our results are in general agreement with the measured values¹⁵ and indicate that the observed non-Franck-Condon behavior results primarily from the R dependence of the electronic transition moments. In contrast to our earlier REMPI studies in which the resonant state was described by a single electronic configuration, i.e., the improved virtual orbital (IVO) approximation,¹⁸ we have used a correlated wave function to describe the Rydberg-valence mixing in the E,F state. Rydberg-valence mixing is a common feature in the spectrally congested region and must influence REMPI processes through the highly excited states.⁵⁻⁹ As such, the present study, due to the isolated and "clean" nature of the E,F state, forms a prelude to forthcoming investigations of such effects in heavier diatomic molecules. An additional motivation for investigation of the REMPI process of Eq. (1) is the proposed use of this REMPI scheme for detecting product H₂ molecules in reactions.¹⁹

In the following we briefly review our theoretical approach and present the relevant details of the calculations. In the last section we discuss the calculated vibrational branching ratios and photoelectron angular distributions and compare them to the experimental results of Anderson *et al.*¹⁵

THEORY

The general theory for REMPI molecular processes is given in Ref. 10, and here we briefly describe only those details which are necessary for the specific scheme given in Eq. (1). As in the experiments, we assume that the molecules are excited from an isotropic ground state by linearly polarized light of weak intensity. Under these conditions the

^{a)} Present address: Theoretical Division, Los Alamos National Laboratory, Los Alamos, New Mexico 87545.

^{b)} Contribution No. 7490.

^{c)} Mailing address: NASA-Ames Research Center, MS230-3, Moffett Field, California 94035.

are primarily located in the E well and look like $v_E = 0, 1$ wave functions for a Rydberg state. The wave function for $v_i = 6$ has considerable spread over the F well but still looks somewhat like a $v_E = 2$ wave function.^{15,20} The plotted values are proportional to the probability of photoelectron ejection along the direction of the polarization of the light, $P(\theta = 0, \phi = 0)$. For each vibrational level of the ion four bars are shown. The experimental data is taken from Ref. 15. The three bars labeled Franck-Condon, non-Franck-Condon, and full correspond to our calculated results using different levels of approximation,¹¹ i.e., (1) neglecting the energy and internuclear distance dependence of the bound-free matrix elements, (2) neglecting the energy dependence but retaining the internuclear distance dependence, and (3) including both the internuclear distance and energy dependence, respectively. The plots are normalized to the most intense peak determined experimentally,¹⁵ which, as expected from the Rydberg character of the E state, is $\Delta v \equiv v_+ - v_E = 0$, where v_E is the vibrational quantum number defined for the inner-well levels. The similarity between the non-Franck-Condon and full branching ratios indicates the weak dependence of the results on the kinetic energy of the photoelectron. However, the larger difference between the Franck-Condon and non-Franck-Condon results indicate a greater sensitivity to the internuclear distance dependence of the photoionization matrix elements. This points to the inadequacy of the Franck-Condon approximation.¹⁵ The disagreement between the calculated and measured vibrational branching ratios are substantial, although it is difficult to be very specific at this time, the disagreement could arise, on the theoretical side, from our neglect of autoionization and saturation effects. On the other hand they may also be due to inherent difficulties in the experimental determination of such branching ratios.

We compare the calculated and experimental photoelectron angular distributions for the $Q(0)$, and $Q(1)$ branches via the $v_{E,F} = 3$ vibrational levels in Figs. 2 and 3, respectively. In these figures the vertical direction corresponds to $\theta = 0^\circ$. The non-Franck-Condon behavior for

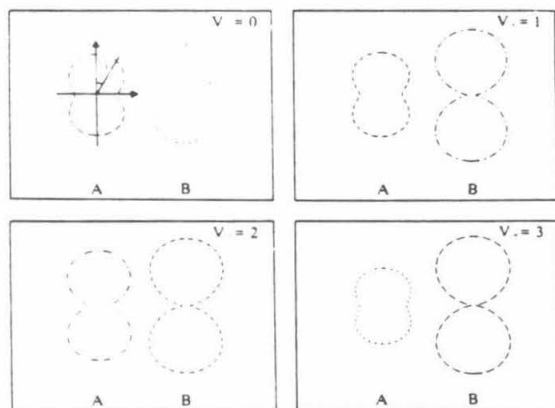


FIG. 2. Photoelectron angular distributions for the $Q(0)$ branch via the $v_{E,F} = 3$ level. (A) Experimental results of Ref. 15, and (B) present full results. $\theta = 0^\circ$ is vertical.

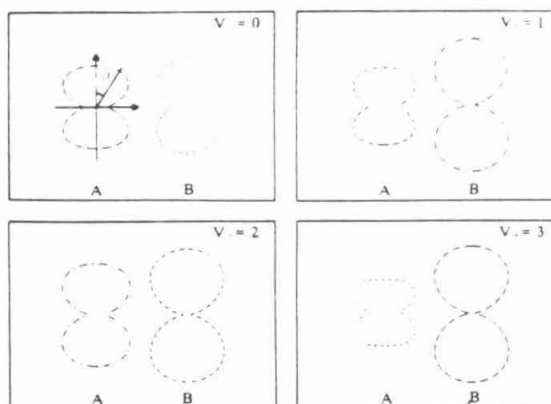


FIG. 3. Same as Fig. 4 but via the $Q(1)$ branch.

these transitions is seen by the dependence of the angular distributions on the final vibronic levels particularly for $v_+ = 0$ to $v_+ = 1$. Recent $(3 + 1)$ REMPI studies in H_2 via the $C^1\Pi_u$ state have also demonstrated such non-Franck-Condon effects on the photoelectron angular distribution.²⁶ The calculated distributions reported are the "full" results where both the internuclear and photoelectron kinetic energy dependence are retained in the evaluation of the transition moments. A quantitative comparison between the calculated and measured angular distributions is difficult for reasons discussed in Ref. 15; however, the general trends are reproduced. The lack of "sharpness" around 90° for some of the experimental distributions may be attributed to the finite angular resolution ($\approx 3^\circ$) of the photoelectron detector.

It is clear from the Figs. 2 and 3 that the angular distributions for the $Q(0)$ and $Q(1)$ excitations are almost identical. The β_4 of Eq. (4) in the latter case is about 5%–10% of the β_2 coefficient. This implies that either the alignment in the $Q(1)$ excitation is small or, that the partial waves larger than the p wave are contributing weakly to the photoionization. Indeed, our calculations confirm that both these effects contribute significantly to the REMPI, resulting in a suppression of β_4 .

CONCLUSION

We have presented results for the photoelectron angular distributions and vibrational branching ratios resulting from a $(2 + 1)$ one-color REMPI of H_2 via the $v_E = 0, 3, 6$ vibrational levels of the $E, F^1\Sigma_g^+$ state. A correlated electronic wave function has been used to consistently describe the Rydberg-valence mixing in the $E, F^1\Sigma_g^+$ state. The calculated vibrational branching ratios are in general agreement with the experimental results of Anderson *et al.*¹⁵ indicating that the pronounced non-Franck-Condon behavior observed is primarily due to the internuclear distance dependence of the electronic transition moments. General agreement between the theoretical and experimental angular distributions is obtained. We have, in the present work, neglected the effects of saturation and the possible presence of autoionization features in the continuum. In a previous pa-

population ρ_{ii} of each $|J_i, M_i\rangle$ level of the resonant intermediate state is proportional to¹⁰

$$\rho_{ii} \propto \sum_{M_0} \left| \frac{\langle J_i, M_i | \mu \cdot \epsilon | J_0, M_0 \rangle \langle J_i, M_i | \mu \cdot \epsilon | J_0, M_0 \rangle}{E_i - E_0 - h\nu} \right|^2, \quad (2)$$

where $|J_0, M_0\rangle$ is the ground $X^1\Sigma_g^+$ state with angular momentum J_0 and its z projection M_0 , $|J_i, M_i\rangle$ is a virtual state connected to the ground state by a one-photon transition and $h\nu$ is the photon energy. In the absence of M -mixing interaction, e.g., collisions, each $|J_i, M_i\rangle$ level will form an independent ionization channel, and the probability $P(\theta, \phi)$ of ejecting an electron in the direction (θ, ϕ) with respect to the polarization vector (ϵ) of the light is given by¹⁰

$$\frac{dP(\theta, \phi)}{dt} = \sum_{M_i} \Gamma_{M_i, M_i}(\theta, \phi) \rho_{ii}, \quad (3)$$

where $\Gamma_{M_i, M_i}(\theta, \phi)$ is the ionization width defined by Eq. (29) of Ref. 10. $P(\theta, \phi)$ itself can be expanded in Legendre polynomials $P_L(\cos \theta)$ as

$$P(\theta) = \sum_{L=0}^{L_{\max}} \beta_L P_L(\cos \theta). \quad (4)$$

For these weak field studies L_{\max} is determined by the rotational quantum state of the intermediate level and is, for the $(2+1)$ REMPI process of Eq. (1), the smaller of $2J_i + 2$ or 6. The infinite summation in Eq. (2) goes over the complete set of rovibrational electronic states $|J_i, M_i\rangle$ of H_2 . We have included in this summation only the lowest states of ungerade symmetry ($B^1\Sigma_g^+$, $C^1\Pi_u$) and kept up to $v = 9$ in the vibrational manifolds at the one-photon level. The relative vibrational branching ratios for $Q(0)$ excitation are unaffected by this truncation. For the $Q(1)$ excitation, based on the study of Huo and Jaffe,²⁰ we estimate the truncation error to be about 10% in the relative populations of the $M_j = 0$ and $M_j = 1$ levels. The summation over rotational states was performed implicitly using closure relations.²¹ The bound-bound transition moments were taken from previous calculations by Wolniewicz²² and Wolniewicz and Dressler,²³ and the vibrational wave functions were obtained numerically using the potential curves compiled by Sharp.¹⁷ The electronic wave function for the $E,F^1\Sigma_g^+$ state was determined from a configuration interaction (CI) calculation using a $(6s5p1d)$ uncontracted Gaussian basis set. This calculation produces 240 configurations of the proper overall $^1\Sigma_g^+$ symmetry. The wave function was determined at the internuclear distances R (a.u.) = 1.00, 1.401, 1.911, 2.50, 3.12, 3.70, 4.39, 5.00 which cover the relevant range of the potential. The resulting energies are within 0.6% of the accurate calculated values.¹⁷ The photoelectron continuum wave functions for the $k\sigma_u$ and $k\pi_u$ channels were calculated in the frozen-core Hartree-Fock approximation using the iterative Schwinger variational method.²⁴ Finally, the bound-free electronic transition moments $\langle X^2\Sigma_g^+; k\sigma_u, k\pi_u | \mu \cdot \epsilon | E,F^1\Sigma_g^+ \rangle$ were calculated for each R and for a range of photoelectron kinetic energies, $k^2/2$, between 1.22 and 4.12 eV. Interpolation was performed in both R and k to obtain the necessary matrix elements for integration over the numerical vibrational wave functions and for specific kinetic energies.

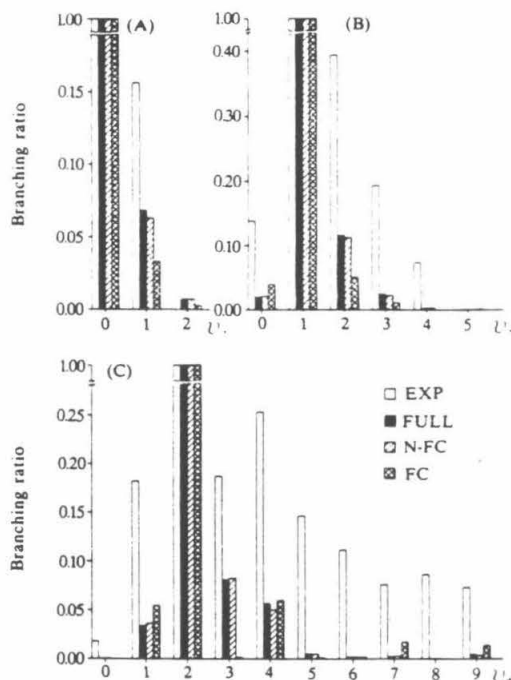


FIG. 1. Vibrational branching ratios for $(2+1)$ REMPI via (A) $v_{E,F} = 0$, $Q(0)$ level; (B) $v_{E,F} = 3$, $Q(1)$ level; (C) $v_{E,F} = 6$, $Q(1)$ level.

RESULTS

Figure 1 shows our calculated vibrational branching ratios for the $v_i = v_{E,F} = 0, 3, 6$ levels of the E,F state. For convenience the plotted data are reproduced in tabular form in Table I. The vibrational wave functions for $v_i = 0, 3$ states

TABLE I. Comparison of the experimental and the theoretical vibrational branching ratios in three different approximations, as explained in the text. Entries less than 10^{-3} are not listed.

v_i	$v_{E,F}$	Exp ^a	Full	N-FC	FC
0	0	1.000	1.000	1.000	1.000
0	1	0.156	0.068	0.064	0.033
0	2	...	0.007	0.007	0.003
3	0	0.126	0.018	0.020	0.038
3	1	1.000	1.000	1.000	1.000
3	2	0.359	0.116	0.112	0.049
3	3	0.176	0.023	0.021	0.010
3	4	0.066	0.003	0.003	...
3	5	0.001	0.001
6	0	0.018
6	1	0.182	0.034	0.036	0.055
6	2	1.000	1.000	1.000	1.000
6	3	0.187	0.081	0.083	0.002
6	4	0.253	0.057	0.050	0.060
6	5	0.146	0.005	0.005	0.001
6	6	0.111	0.002	0.002	0.002
6	7	0.076	0.002	0.003	0.017
6	8	0.086
6	9	0.073	0.005	0.004	0.014

^a From Ref. 15.

per¹⁴ we have shown the sensitivity of the calculated results to the inclusion of saturation effects. The effects of the Rydberg-valence mixing on the photoelectron angular distributions and vibrational branching ratios are expected to be even more dramatic if the outer-well vibrational states $v_F = 0, 1, 2, 3$, i.e., $v_{E,F} = v_i = 1, 2, 4, 5$ were accessed. Further theoretical and experimental studies for ionization through the outer well would therefore be very useful in unraveling the dynamics of these molecular photoionization processes.

ACKNOWLEDGMENTS

This research was supported by the National Science Foundation under Grant No. CHE8521391. W. M. H. acknowledges support from the NASA Ames Cooperative Agreement NCC 2-147, and H. R. gratefully acknowledges support from the Danish Natural Science Research Council and the Carlsberg Foundation.

¹S. T. Pratt, P. M. Dehmer, and J. L. Dehmer, *J. Chem. Phys.* **78**, 4315 (1983); *Chem. Phys. Lett.* **105**, 28 (1984); (private communication).

²W. Meier, H. Rottke, H. Zacharias, and K. H. Welge, *J. Chem. Phys.* **83**, 4360 (1985); H. Zacharias, R. Schmiedl, and K. H. Welge, *Appl. Phys.* **21**, 127 (1980); H. Rottke and H. Zacharias, *J. Chem. Phys.* **83**, 4831 (1986).

³J. C. Miller and R. N. Compton, *J. Chem. Phys.* **75**, 22 (1981); *Chem. Phys. Lett.* **93**, 453 (1982); *J. Chem. Phys.* **84**, 675 (1986).

⁴W. G. Wilson, K. S. Viswanathan, E. Sekreta, and J. P. Reilly, *J. Phys. Chem.* **88**, 672 (1984); K. S. Viswanathan, E. Sekreta, E. R. Davidson,

and J. P. Reilly, *ibid.* **90**, 5078 (1986).

⁵M. G. White, M. Seaver, W. A. Chupka, and S. D. Colson, *Phys. Rev. Lett.* **49**, 28 (1982); M. G. White, W. A. Chupka, M. Seaver, A. Woodward, and S. D. Colson, *J. Chem. Phys.* **80**, 678 (1984).

⁶S. T. Pratt, P. M. Dehmer, and J. L. Dehmer, *J. Chem. Phys.* **80**, 1706 (1984); **81**, 3444 (1984).

⁷A. Sur, C. V. Ramana, W. A. Chupka, and S. D. Colson, *J. Chem. Phys.* **84**, 69 (1986).

⁸S. Katsumata, K. Sato, Y. Achiba, and K. Kimura (private communication).

⁹J. Kimman, M. Lavollée, and M. J. Van der Wiel, *Chem. Phys.* **97**, 137 (1985).

¹⁰S. N. Dixit and V. McKoy, *J. Chem. Phys.* **82**, 3546 (1985).

¹¹S. N. Dixit, D. L. Lynch, and V. McKoy, *Phys. Rev. A* **30**, 3332 (1984).

¹²S. N. Dixit, D. L. Lynch, V. McKoy, and W. M. Huo, *Phys. Rev. A* **32**, 1267 (1985).

¹³D. L. Lynch, S. N. Dixit, and V. McKoy, *Chem. Phys. Lett.* **123**, 315 (1986).

¹⁴H. Rudolph, D. L. Lynch, S. N. Dixit, and V. McKoy, *J. Chem. Phys.* **84**, 6657 (1986).

¹⁵S. L. Anderson, G. D. Kubiak, and R. N. Zare, *Chem. Phys. Lett.* **105**, 22 (1984).

¹⁶E. R. Davidson, *J. Chem. Phys.* **35**, 1189 (1961).

¹⁷T. E. Sharp, *At. Data* **2**, 119 (1971).

¹⁸W. J. Hunt and W. A. Goddard III, *Chem. Phys. Lett.* **24**, 464 (1974).

¹⁹E. E. Marinero, C. J. Rettner, and R. N. Zare, *Phys. Rev. Lett.* **48**, 1323 (1982); E. E. Marinero, R. Vasudev, and R. N. Zare, *J. Chem. Phys.* **78**, 692 (1983).

²⁰W. M. Huo and R. Jaffe, *Chem. Phys. Lett.* **101**, 463 (1983).

²¹J. B. Halpern, H. Zacharias, and R. Wallenstein, *J. Mol. Spectrosc.* **79**, 1 (1980).

²²L. Wolniewicz, *J. Chem. Phys.* **51**, 5002 (1969).

²³L. Wolniewicz and K. Dressler, *J. Mol. Spectrosc.* **96**, 195 (1982).

²⁴R. R. Lucchese, G. Raseev, and V. McKoy, *Phys. Rev. A* **25**, 2572 (1982).

²⁵S. N. Dixit, D. L. Lynch, and V. McKoy, in *Multiphoton Processes*, edited by P. Lambropoulos and S. J. Smith (Springer, New York, 1984).

**Chapter 8: Photoionization cross sections of rovibrational
 levels of the $B^1\Sigma_u^+$ state of H_2**

[The text of this chapter appeared in: H. Rudolph, D.L. Lynch, S.N. Dixit, and V. McKoy, J. Chem. Phys. **84**, 6657 (1986)]

Photoionization cross sections of rovibrational levels of the $B^1\Sigma_u^+$ state of H_2

H. Rudolph, D. L. Lynch, S. N. Dixit, and V. McKoy

Arthur Amos Noyes Laboratory of Chemical Physics, ^{*)} California Institute of Technology, Pasadena, California 91125

(Received 21 February 1986; accepted 7 March 1986)

We report theoretical cross sections for direct photoionization of specific rovibrational levels of the $B^1\Sigma_u^+$ electronic state of H_2 . The calculated cross sections differ considerably from values recently determined by resonant enhanced multiphoton ionization (REMPI) studies. In an attempt to understand the disagreement, we analyze in detail the REMPI dynamics and find that the multiphoton ionization probability is extremely sensitive to the spatial and temporal profiles of the laser pulses. Accurate characterization of laser profiles and their jitter is therefore necessary for a comparison between theory and experiment.

INTRODUCTION

In recent years, resonant enhanced multiphoton ionization (REMPI) coupled with photoelectron spectroscopy (PES) has become a highly sensitive technique for spectroscopic as well as dynamical studies. In addition to the observation of hitherto unknown excited states, several studies have illustrated important dynamical features such as the non-Franck-Condon behavior in ionic vibrational branching ratios,^{1,2} propensity rules in ionic rotational branching ratios,^{3,4} Rydberg-valence mixing and predissociation,⁵ and strong final state selectivity.⁶ REMPI processes are also being used for detection and characterization of species in unimolecular reactions⁷ and desorption from surfaces.⁸ In addition to the detection of new states, REMPI processes also offer the possibility of measuring photoionization cross sections for excited states. Often such studies probe the part of the photoelectron continuum inaccessible by single photon ionization out of the ground state. Moreover, extraction of absolute REMPI cross sections from measured ion/electron signals requires the knowledge of the atomic/molecular densities in the interaction volume and the characteristics of the laser pulses used. Recent experiments in atomic⁹ and molecular¹⁰⁻¹² systems have circumvented these difficulties in measuring absolute particle densities by studying the saturation behavior of the REMPI signal as a function of the laser intensity. Furthermore, measured values of the cross sections for ionization out of the $A^2\Sigma^+$ state of NO derived by this technique¹⁰ were seen to be within a factor of 2 of subsequent theoretical studies.¹³

In another, more recent, experiment Meier *et al.*¹¹ reported cross sections for photoionization out of specific rovibrational levels of the $B^1\Sigma_u^+$ state of H_2 . These cross sections were extracted by observing the saturation behavior of the ion signal as the intensity of the ionizing laser is varied in their two color (1 + 1) REMPI experiment. We have calculated the relevant cross sections using *ab initio* electronic wave functions and our calculated values are compared with the measured ones¹¹ in Table I. The experimental values seem to be consistently lower than the theoretical numbers by about an order of magnitude.

In an attempt to understand such a large discrepancy, we analyze the REMPI dynamics in detail using density matrix equations. Some limitations to the use of the rate equations in the analysis of Ref. 11 are discussed. In addition, we show that the REMPI signal is very sensitive to the spatial and temporal profiles of the laser. Proper analysis of the experimental data, therefore, requires a characterization of laser profiles and a subsequent incorporation of these into the dynamics. Laser characteristics for the experiment of Meier *et al.*¹¹ are needed for further comparison between theory and experiment.

THEORETICAL CALCULATIONS

In this section we discuss the results of our calculations of the ionization probability for the two color (1 + 1)

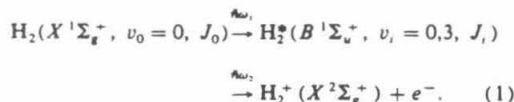
TABLE I. $B^1\Sigma_u^+(v, J, M_i) \xrightarrow{\omega} X^2\Sigma_g^+ + e^-$ photoionization cross sections (in 10^{-18} cm²) of H_2 at $\lambda = 266.05$ nm.

v_i	J_i	M_i	Calculated		Measured ^a σ
			σ_s	σ_L	
0	0	0	11.99	12.19	0.83 ± 0.17
0	1	0	13.10	13.65	
0	1	± 1	11.43	11.46	
0	2	0	12.79	13.23	1.19 ± 0.24
0	2	± 1	12.39	12.71	
0	2	± 2	11.19	11.15	
0	3	0	12.73	13.16	0.84 ± 0.17
0	3	± 1	12.55	12.92	
0	3	± 2	11.99	12.19	
0	3	± 3	11.06	10.98	
3	0	0	5.07	5.03	0.65 ± 0.13
3	1	0	5.55	5.60	
3	1	± 1	4.84	4.74	0.23 ± 0.05
3	2	0	5.41	5.43	
3	2	± 1	5.24	5.23	1.03 ± 0.20
3	2	± 2	4.73	4.62	
3	3	0	5.39	5.41	0.25 ± 0.05
3	3	± 1	5.31	5.31	
3	3	± 2	5.07	5.03	
3	3	± 3	4.68	4.55	

^a) Contribution No. 7368.

^a) Reference 11.

REMPI process in H_2 via the $B^1\Sigma_u^+$ state



The parameters required for the analysis of the dynamics of this REMPI process are, the X - B transition moment, the decay rates out of the B state, and photoionization cross sections out of specific rotational-vibrational levels of the B state. We have used the X - B transition moments given by Wolniewicz¹⁴ and vibrational wave functions obtained by the finite element method¹⁵ using the potential curves of Sharp.¹⁶ The spontaneous decay rate of the B state is taken to be $1.85 \times 10^9 \text{ s}^{-1}$.^{11,17} The electronic wave functions of the B state at various internuclear separations (R) were calculated using the improved virtual orbital (IVO) technique¹⁸ with sufficient number of diffuse functions included in the basis set. The resulting energies of the $B^1\Sigma_u^+$ state are within 5%–10% of the accurate values.¹⁶ As an additional check on the quality of the wave functions, the X - B transition moments were calculated and agree with those of Wolniewicz¹⁴ to within 7% up to $R = 2.0 \text{ a.u.}$ For larger R , the deviation between our values and the accurate ones increases because of the single configuration wave functions used by us. We believe, however, that for the vibrational states under consideration in the photoionization step, these large R errors will play a less significant role in the averaged bound-free transition moments. For the bound-bound moments necessary for the REMPI dynamics, we have used the accurate values of Wolniewicz.¹⁴

The photoelectron continuum wave functions were calculated within the frozen core Hartree-Fock approximation using the iterative Schwinger variational method.¹⁹ Combining these with the B state wave functions, the photoionization dynamical coefficients were calculated. We explicitly included both the energy and R dependence of these dynamical coefficients in averaging over the vibrational wave functions.²⁰ Finally, the photoionization cross sections for ionization out of specific $|v_i, J_i M_i\rangle$ levels of the B state are calculated using the detailed expression given in an earlier paper.²¹ Since Meier *et al.*¹¹ collected total ion signals, we have summed the cross sections over the symmetry allowed ionic rotational states and energetically allowed ionic vibrational states. The results are presented in Table I together with the experimentally deduced cross sections of Ref. 11. The agreement between the length and the velocity forms of cross sections indicates that the single determinant description of the B state as well as of the photoelectron continuum is sufficiently accurate. Moreover, calculations similar to those outlined here (different rovibrational states and kinetic energies but same basis set) have yielded good agreement with measured ionic vibrational-rotational branching ratios.²² This leads us to believe that, within our model, the theoretical cross sections quoted in Table I are fairly accurate.

As seen from Table I, there is clearly a disagreement between our calculated cross sections and the experimentally deduced values of Meier *et al.*¹¹ The theoretical values are

consistently higher than the experimental ones. Our calculations have not included autoionization. Although the influence of interference with competing autoionizing channels may account for the discrepancy for single rotational/vibrational levels, we feel that it is unlikely to explain the systematic differences observed. Several recent studies^{23–25} have demonstrated the sensitivity of REMPI signals to the dynamics and to the spatial-temporal characteristics of the laser employed. We believe that such effects could have influenced the results of Meier *et al.*¹¹ In the following section we address these questions.

REMPI DYNAMICS

In the experiment of Meier *et al.*¹¹ a low intensity laser was used for the X - B excitation while a (variable) high intensity laser was used to ionize the B state. The choice of frequencies and intensities eliminates the possibility of excitation by the high intensity laser and ionization by the low intensity one. Focusing on the case where both lasers were linearly polarized along the same direction, collision free conditions imply that the REMPI process originating from each $|J_0 M_0\rangle$ state forms an independent channel. The dynamics in each channel can be accurately described by the appropriate density matrix equations. These have been discussed by several authors^{12,21} and we will simply reproduce them here in the rotating wave approximation (RWA) for on-resonance excitation:

$$\dot{\rho}_{00} = -i \frac{1}{2} \Omega_{0i} (\rho_{0i} - \rho_{i0}) + \alpha \rho_{ii}, \quad (2a)$$

$$\dot{\rho}_{ii} = i \frac{1}{2} \Omega_{0i} (\rho_{0i} - \rho_{i0}) - (\Gamma_i + \alpha) \rho_{ii}, \quad (2b)$$

$$\dot{\rho}_{0i} = i \frac{1}{2} \Omega_{0i} (\rho_{ii} - \rho_{00}) - \frac{1}{2} (\Gamma_i + \alpha) \rho_{0i}, \quad (2c)$$

$$\dot{\rho}_{i0} = -i \frac{1}{2} \Omega_{0i} (\rho_{ii} - \rho_{00}) - \frac{1}{2} (\Gamma_i + \alpha) \rho_{i0}. \quad (2d)$$

In the above equations, $\alpha (= 1.85 \times 10^9 \text{ s}^{-1})$ denotes the spontaneous decay rate from the B state ($|J_i M_i\rangle \equiv |i\rangle$) to the X state ($|J_0 M_0\rangle \equiv |0\rangle$), Ω_{0i} the Rabi frequency for the $|0\rangle - |i\rangle$ transition and Γ_i the ionization rate out of $|i\rangle$. The latter two parameters are laser intensity dependent and can be written as

$$\frac{1}{2} \Omega_{0i} = \frac{E_1(t)}{\hbar} \langle 0 | \mu \cdot \epsilon_1 | i \rangle \quad (3a)$$

and

$$\Gamma_i = \sigma_i \frac{I_2(t)}{\hbar \omega_2}, \quad (3b)$$

where μ is the electronic dipole moment operator, $E_1(t)$ is the field envelope of the exciting laser, and $I_2(t)$ is the intensity of the ionizing laser. Detailed expressions for σ_i , the photoionization cross section, and the bound-bound dipole matrix element $\langle 0 | \mu \cdot \epsilon_1 | i \rangle$ have been given in Ref. 21. Both Ω_{0i} and Γ_i are M dependent quantities and, as such, the saturation behavior of each M_0 channel will be different. The total ionization probability is given by

$$P = 1 - \sum_{M_0} [\rho_{00}^{M_0}(t) + \rho_{ii}^{M_0}(t)]. \quad (4)$$

We will discuss the effect of different saturation behavior of M channels in a later publication. For simplicity, here we will treat the $P(1) v_0=0-v_i=3$ excitation case where only one M channel ($M_0=0$) exists.

Under conditions when the time rate of change of $\rho_{0\alpha}$ and $\rho_{0\beta}$ is small, $\rho_{0\alpha}$ and $\rho_{0\beta}$ can be adiabatically eliminated from Eq. (2) and one can obtain two rate equations for ρ_{00} and ρ_{ii} . As has been derived by Meier *et al.*¹¹ and by Rotke *et al.*,¹² these can be written as

$$\dot{\rho}_{00} = W_1(\rho_{ii} - \rho_{00}) + \alpha\rho_{ii}, \quad (5a)$$

$$\dot{\rho}_{ii} = -W_1(\rho_{ii} - \rho_{00}) - (W_2 + \alpha)\rho_{ii}, \quad (5b)$$

where

$$W_1 = \frac{\Omega_{0i}^2}{\Gamma_i + \alpha} \quad (6)$$

and $W_2 = \Gamma_i$. It is important to note that W_1 depends on W_2 . Equation (5) can be solved analytically for a uniform intensity pulse turned on at $t = 0$ and off at τ_p and the ionization probability $P = 1 - \rho_{ii} - \rho_{00}$ can be written as

$$P(\tau_p) = \left[1 - \frac{a+b}{2b} e^{-(a-b)\tau_p} + \frac{a-b}{2b} e^{-(a+b)\tau_p} \right], \quad (7)$$

where

$$a = W_1 + \frac{W_2 + \alpha}{2} \quad (8a)$$

and

$$b = [a^2 - W_1 W_2]^{1/2}. \quad (8b)$$

A Taylor expansion of $P(\tau_p)$ to first order in W_1 yields Eq. (1) of Meier *et al.*,¹¹ viz.

$$P(\tau_p) = \frac{W_1}{W_2 + \alpha} \tau_p W_2 \left[1 + \frac{e^{-(W_2 + \alpha)\tau_p} - 1}{(W_2 + \alpha)\tau_p} \right] \quad (9)$$

which, because of $\alpha\tau_p \approx 9.25 \gg 1$ ($\tau_p = 5$ ns), reduces to

$$P(\tau_p) = \frac{W_1}{W_2 + \alpha} \tau_p W_2. \quad (10)$$

While this is identical to Eq. (2) of Ref. 11, an important difference in the analysis arises by realizing that W_1 is a function of W_2 as shown in Eq. (6). The dependence of P on W_2 is then

$$P(\tau_p) = \frac{\Omega_{0i}^2}{(W_2 + \alpha)^2} \tau_p W_2 \quad (11)$$

or

$$P^{-1} = \frac{W_2^2 + 2W_2\alpha + \alpha^2}{\Omega_{0i}^2 \tau_p W_2} = \frac{W_2}{\Omega_{0i}^2 \tau_p} + \frac{2\alpha}{\Omega_{0i}^2 \tau_p} + \frac{\alpha^2}{\Omega_{0i}^2 \tau_p W_2}. \quad (12)$$

Clearly this is in disagreement with Eq. (3) of Ref. 11 used in their analysis which is a result of ignoring the W_2 dependence in W_1 . Equation (12) predicts a linear dependence of P^{-1} on W_2^{-1} only for W_2 small compared to α while P^{-1} increases with W_2 for large W_2 . Such a decrease of P with increasing W_2 is a consequence of the dynamics and has actually been observed in a two color (2 + 1) REMPI experiment in sodium.²⁵ It should be noted that such a decrease in the ion signal with increasing intensity will not arise in single color REMPI or when the two pulses do not overlap in time. The observation of a linear dependence of the inverse ion

signal on the inverse of the ionizing pulse energy by Meier *et al.*¹¹ then implies that the intensities used must correspond to $\Gamma_i \ll \alpha$. In the linear regime,

$$P^{-1} = \frac{2\alpha}{\Omega_{0i}^2 \tau_p} + \frac{\alpha^2}{\Omega_{0i}^2 \tau_p} \frac{\hbar\omega_2 \tau_p A}{\sigma_i E_2}, \quad (13)$$

where we have used the relation

$$E_2 = I_2 \tau_p A \quad (14)$$

between the ionizing laser pulse energy E_2 , its intensity I_2 , the (rectangular) pulse duration τ_p , and the (uniform intensity) beam cross section area A . A more careful analysis of the Taylor expansion of Eq. (7) will add a correction term $2\Omega_{0i}^2$ to α^2 in the second term in Eq. (13). The cross section can be calculated from the intercept and the slope of the linear part of P^{-1} vs E_2^{-1} graph using

$$\sigma_i = \frac{\text{intercept}}{\text{slope}} \cdot \hbar\omega_2 \alpha A \tau_p \frac{\alpha^2 + 2\Omega_{0i}^2}{2\alpha^2}. \quad (15)$$

Note that the third factor, absent in the analysis of Ref. 11, reduces the apparent cross section by about a factor of 2.

In Fig. 1, we compare the solution of the density matrix equations (2) with the solution of rate equations (5) for the $v_i = 3$ $P(1)$ excitation. The molecular parameters were calculated as mentioned in the previous section. In relating E_2 to I_2 in Eq. (14) we have used $\tau_p = 5$ ns and $A = 0.01\pi$ mm² quoted in Ref. 11. Both methods predict a linear regime for low E_2 and a diverging P^{-1} for high E_2 . However, the slopes of the two linear parts are different. This is a result of Ω_{0i} not being much smaller than α ($\Omega_{0i} = 2.5 \times 10^8$ rad/s, $\alpha = 1.85 \times 10^9$ s⁻¹). More interestingly, we see that the linear regime exists for pulse energies less than 0.25 mJ or so, whereas Meier *et al.*¹¹ have observed linear behavior for E_2 up to 2 mJ. This could be a result of using inaccurate values of A and τ_p and not incorporating the spatial and temporal

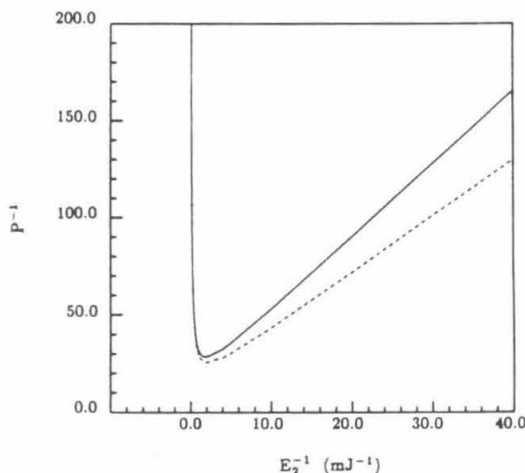


FIG. 1. Inverse of the ionization probability (P^{-1}) a function of the inverse of the ionizing pulse energy. The $X-B$ excitation is through the $v_0 = 0 \rightarrow v_1 = 3$ $J_0 = 1 \rightarrow J_1 = 0$ line. (—) density matrix solution, (---) rate equation solution. Uniform spatial and temporal profiles are assumed.

profiles of the laser. For uniform pulses, Eq. (15) implies that for a given value of (intercept/slope), the smaller the value of $A\tau_p$, the smaller the calculated cross section.

Since the actual temporal and spatial profiles of the lasers used have not been presented in Ref. 11, we shall assess the influence of these on the dependence of the ionization probability on the ionizing laser pulse energy. For nonuniform pulses, analytical solutions are not possible and therefore we have numerically integrated Eq. (2).

To discuss the effects of temporal pulse shape, we have integrated the density matrix equations (2) assuming Gaussian shaped exciting and ionizing pulses with $\text{FWHM} = \tau_p$. The results are displayed in Fig. 2 where we have also illustrated situations where the exciting laser pulse peaks before the ionizing laser peaks (+ jitter) and where the ionizing pulse peaks before the exciting pulse (- jitter). The jitter is fixed at ± 1 ns.¹¹ In reality, the jitter is probably a random variable changing from pulse to pulse in which case an averaging of P over the distribution of jitter has to be carried out. The ionization probability in the linear regime is seen to be more sensitive to the jitter than to the Gaussian nature of the pulse shape. Pulse shapes other than Gaussian would be expected to have a profound effect on the resulting ion signal. The spread between + and - jitters gives a measure of the uncertainty in the experimental measurements.

As for the effects of the spatial profile of the laser pulses, we find that a Gaussian spatial profile, as would be for a laser operating in a TEM_{00} mode, has a minor effect on the ion signal. However, as discussed in a later publication,¹² the ionizing laser seems to have an Airy function dependence on the transverse radius in the far-field region, i.e.,

$$I_2(x) = I_0 \left(\frac{2J_1(x)}{x} \right)^2, \quad (16)$$

where $J_1(x)$ is the Bessel function of first kind of order one and x is a normalized transverse coordinate.²⁶ If we equate

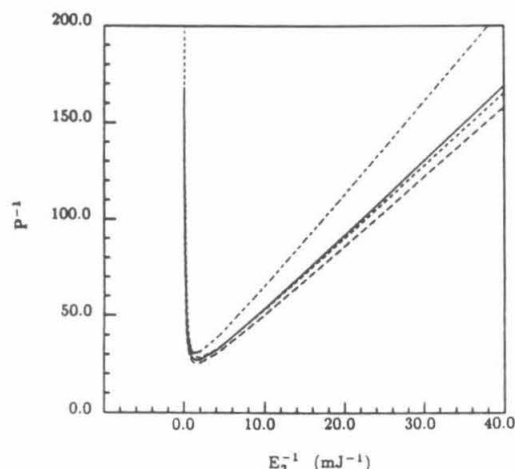


FIG. 2. Same as Fig. 1. (—) Gaussian temporal profile, no jitter; (---) uniform temporal profile, no jitter; (- - -) Gaussian temporal profile, + 1.0 ns jitter; (· · ·) Gaussian temporal profile, - 1.0 ns jitter. Uniform spatial profiles are assumed.

the energy contained in the central maximum of Eq. (16) to that contained in a uniform distribution of the same radius, we find that the peak intensity (at $x = 0$) in Eq. (16) is about 4.38 times higher than the peak intensity for a uniform intensity pulse. The influence of spatial variation is included by averaging $P[I_2(r)]$ over the distribution

$$\bar{P} = 2\pi \int_0^{\omega_0} P[I_2(r)] r dr / \pi \omega_0^2, \quad (17)$$

where ω_0 denotes the beam radius [taken to be the first zero of Eq. (16)]. The results are presented in Fig. 3. We see that an Airy function pulse is less efficient in ionization than a uniform pulse. This is because, although the intensity is much higher at the center, it is smaller than the uniform value over a larger area. The averaging is seen to reduce the slope and raise the intercept of the linear part. As in the case relating to the temporal profile, different spatial profiles will also have different effects on the averaged ion signal.

Finally, we should mention that a uniform spatial profile has been assumed for the exciting laser in the above calculations. Inclusion of the actual profile of this laser will undoubtedly give rise to additional changes. Although the exciting laser in Ref. 11 was ten times wider than the ionizing laser, the perpendicular propagation configuration used in that experiment actually probes the complete profiles of both lasers. A co/counter propagating geometry would make the broad exciting laser to appear to have a uniform profile.

CONCLUSIONS

We have presented photoionization cross sections for single-photon ionization of specific rovibrational levels of the $B^1\Sigma_u^+$ state of H_2 at $\lambda = 266.05$ nm. Good agreement between the length and velocity forms leads us to believe that these values are fairly accurate. However, recent measured

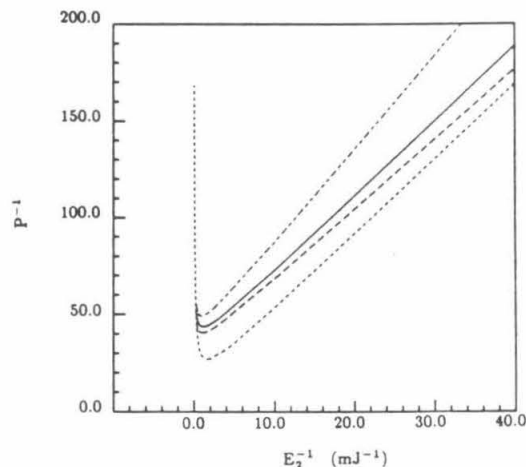


FIG. 3. Same as Fig. 1. (—) Airy function spatial profile no jitter; (---) uniform spatial profile no jitter; (- - -) Airy function spatial profile + 1.0 ns jitter; (· · ·) Airy function spatial profile, - 1.0 ns jitter. Gaussian temporal profiles are assumed.

values seem to be consistently lower than our calculated ones for all the levels considered. Although we have not included effects of autoionization, it is unlikely that their incorporation will lower all the calculated cross sections of Table I. On the other hand, we have shown through detailed dynamical calculations that the ion signal is very sensitive to the spatial and temporal profiles of the laser pulses and also to the jitter between the exciting and ionizing pulses. Lacking detailed information on these characteristics in the experiment by Meier *et al.*,¹¹ we have chosen examples to illustrate the sensitivity of the ion signal to these effects. Such information is essential for further comparison between theory and experiment.

ACKNOWLEDGMENTS

This research was supported by the National Science Foundation under Grant No. CHE8218166. One of us (H.R.) gratefully acknowledges support from the Danish Natural Science Research Council and the Carlsberg Foundation.

¹S. T. Pratt, E. D. Poliakov, P. M. Dehmer, and J. L. Dehmer, *J. Chem. Phys.* **78**, 65 (1983).

²S. T. Pratt, P. M. Dehmer, and J. L. Dehmer, *Chem. Phys. Lett.* **105**, 28 (1984).

³W. G. Wilson, K. S. Viswanathan, E. Sekreta, and J. P. Reilly, *J. Phys. Chem.* **88**, 672 (1984).

⁴K. S. Viswanathan, E. Sekreta, E. R. Davidson, and J. P. Reilly (pre-

print).

⁵A. Sur, C. V. Ramana, W. A. Chupka, and S. D. Colson, *J. Chem. Phys.* **84**, 69 (1985).

⁶S. T. Pratt, P. M. Dehmer, and J. L. Dehmer, *J. Chem. Phys.* **80**, 1706 (1984); **81**, 3444 (1984).

⁷See, for example, O. Benoist Dazy, F. Lahmani, C. Lardeux, and D. Solgadi, *Chem. Phys.* **94**, 247 (1985).

⁸A. H. Burns, *Phys. Rev. Lett.* **55**, 525 (1985).

⁹U. Heinzman, D. Schinkowski, and H. D. Zeman, *Appl. Phys.* **12**, 113 (1977); R. V. Ambartsumian, N. P. Furzikov, V. S. Letokhov, and A. A. Puretzky, *ibid.* **9**, 335 (1976); A. V. Smith, J. E. M. Goldsmith, D. E. Nitz, and S. J. Smith, *Phys. Rev. A* **22**, 577 (1980).

¹⁰H. Zacharias, R. Schmiedl, and K. H. Welge, *Appl. Phys.* **21**, 127 (1980).

¹¹W. Meier, H. Rotke, H. Zacharias, and K. H. Welge, *J. Chem. Phys.* **83**, 4360 (1985).

¹²H. Rotke and H. Zacharias, *J. Chem. Phys.* **83**, 4831 (1985).

¹³S. N. Dixit, D. L. Lynch, V. McKoy, and W. Huo, *Phys. Rev. A* **32**, 1267 (1985).

¹⁴L. Wolniewicz, *J. Chem. Phys.* **51**, 5002 (1969).

¹⁵D. J. Malik, J. Eccles, and D. Secrest, *J. Comput. Phys.* **38**, 157 (1980).

¹⁶T. E. Sharp, *At. Data* **2**, 119 (1971).

¹⁷H. Schmoranz and J. Imschwiler, *Phys. Lett. A* **100**, 85 (1984).

¹⁸W. J. Hunt and W. A. Goddard III, *Chem. Phys. Lett.* **24**, 464 (1974).

¹⁹R. R. Lucchese, G. Raseev, and V. McKoy, *Phys. Rev. A* **25**, 2572 (1982).

²⁰S. N. Dixit, D. L. Lynch, and V. McKoy, *Phys. Rev. A* **30**, 3332 (1984).

²¹S. N. Dixit and V. McKoy, *J. Chem. Phys.* **82**, 3546 (1985).

²²D. L. Lynch, S. N. Dixit, and V. McKoy, *Chem. Phys. Lett.* **123**, 315 (1986).

²³See, for example, M. Crance, *J. Phys. B* **13**, 101 (1980).

²⁴M. Crance and S. Feneuille, *Phys. Rev. A* **16**, 1587 (1977).

²⁵L. Allen, R. W. Boyd, J. Krasinski, M. S. Malcuit, and C. R. Stroud, Jr., *Phys. Rev. Lett.* **54**, 309 (1985).

²⁶M. Born and E. Wolf, *Principles of Optics*, 6th ed. (Pergamon, New York, 1980), p. 395.

**Chapter 9: (1+1) resonant enhanced multiphoton ionization via
the $A^2\Sigma^+$ state of NO: Ionic rotational branching
ratios and their intensity dependence**

[The text of this chapter appeared in: H. Rudolph, S.N. Dixit, V. McKoy, and W.M. Huo, J. Chem. Phys. **88**, 1516 (1988). Please note that due to a printing error Figs. 3-5 are in the wrong order. Figure 3 should be Fig. 4, Fig. 4 should be Fig. 5, and Fig. 5 should be Fig. 3. The figure captions remain as they are in the chapter]

(1+1) resonant enhanced multiphoton ionization via the $A^2\Sigma^+$ state of NO: Ionic rotational branching ratios and their intensity dependence^{a)}

H. Rudolph

Arthur Amos Noyes Laboratory of Chemical Physics, California Institute of Technology, Pasadena, California 91125

S. N. Dixit

Lawrence Livermore National Laboratory, L-401, Livermore, California 94550

V. McKoy

Arthur Amos Noyes Laboratory of Chemical Physics, California Institute of Technology, Pasadena, California 91125

W. M. Huo

NASA-Ames Research Center MS230-3, Moffett Field, California 94035

(Received 28 August 1987; accepted 20 October 1987)

Recent high resolution photoelectron spectroscopic studies of the (1+1) resonant enhanced multiphoton ionization (REMPI) of NO via the 0-0 transition of the $A-X$ band (γ band) have shown a pronounced $\Delta N = 0$ signal ($\Delta N \equiv N_+ - N_-$) and smaller, but measurable, $\Delta N = \pm 2$ peaks. The authors [K. S. Viswanathan *et al.*, *J. Phys. Chem.* **90**, 5078 (1986)] assign the excitation to be via an $R(21.5)$ line, with no further specification. We have performed *ab initio* calculations of the rotational branching ratios for the four possible " $R(21.5)$ " transitions, namely, the rotationally "clean" R_{21} and R_{22} , and the "mixed" $R_{12} + Q_{22}$ and $R_{11} + Q_{21}$ branches. We find the mixed $R_{12} + Q_{22}(21.5)$ branch to agree best with the observed photoelectron spectrum collected parallel to the polarization vector of the light. The discrepancy is larger for detection perpendicular to the polarization. To understand this difference, we have assessed the influence of laser intensity and polarization "contamination" on the branching ratios and photoelectron angular distributions.

INTRODUCTION

Within the past decade resonant enhanced multiphoton ionization spectroscopy (REMPI), combined with high resolution photoelectron spectroscopy (PES) has provided significant dynamical insight into several aspects of multiphoton ionization processes.¹⁻⁹ The REMPI-PES technique has been successfully employed in studies of diatomic molecules (H_2 , NO, CO, N_2 , I_2),⁶⁻¹⁸ exploiting their less congested vibrational and rotational manifolds, which allows a greater specificity in the excitation schemes. The spectral resolution of the PES detectors have been refined to a point where the rotational structure of the ion can be resolved in the photoelectron spectra, providing information about the character of the resonant intermediate state, and on the electronic continuum.^{6-8,14} Nitric oxide, NO, has attracted the most attention because of its low ionization potential (9.24 eV)¹⁹ and its well-studied bound-bound spectrum.²⁰ Reilly and co-workers have, in a series of recent papers,⁶⁻⁸ studied the lower Rydberg states of NO, with a photoelectron energy resolution (3 meV at best) sufficient to resolve the ionic rotational structure for medium to high rotational quantum numbers ($N \approx 10-25$). The agreement between the experimental and recently calculated²¹⁻²³ results has generally been quite good. Several important features in the PES were

shown to arise from the nonspherical nature of the molecular potential. In a previous paper²¹ we compared the calculated rotational branching ratios for (1+1) REMPI of NO via the $A^2\Sigma^+(3s\sigma)$ state of NO to the earlier results of Wilson *et al.*⁶ The agreement was moderately good and the observed photoelectron spectra could be explained on the basis of an "atomic-like" model, in which the $3s\sigma$ Rydberg state ejects a photoelectron primarily into the odd l partial waves of the electronic continuum. However, the analysis of the $D^2\Sigma^+$ state PES indicates that the photoionization dynamics is more complex and that the "atomic" picture may be inadequate.

In this paper we present further detailed results on the (1+1) REMPI-PES via the $A^2\Sigma^+$ state. As the rotational line in the data in Refs. 6 and 7 was identified as simply an $R(21.5)$ line, we present results for the four possible $R(21.5)$ transitions, two of which are "pure" and two are mixed rotational lines. The measured rotational branching ratios for parallel detection agree best with those calculated for the $R_{12} + Q_{22}(21.5)$ branch. The agreement in the perpendicular direction is less satisfactory. To assess the possible influence of saturation effects the solution of the rate equations for (1+1) REMPI is also analyzed.

THEORY

In this section we briefly describe the essential steps in the analysis of the (1+1) REMPI, and refer the reader to Refs. 24-26 for details. The (1+1) REMPI is viewed as a

^{a)} Contribution no. 7650.

one-photon excitation to a resonant intermediate state (the $A^2\Sigma^+$ state) from an (initially) unaligned ground state (the $X^2\Pi$ state), followed by subsequent one-photon ionization out of this aligned intermediate state. The problem therefore has two parts: (i) a bound-bound excitation dynamical part and (ii) a bound-free photoionization part. We have in previous papers concerning NO concentrated our effort on the latter since the bound-bound dynamics can be adequately described by a simple perturbative scheme, where the population ρ_{ii} of the intermediate state's M_j sublevels are proportional to^{24,26}

$$\rho_{ii} \propto \begin{pmatrix} J_0 & 1 & J_i \\ -M_i & 0 & M_i \end{pmatrix}^2. \quad (1)$$

Here J_0 and J_i denote the total angular momentum quantum number for the $X^2\Pi$ and $A^2\Sigma^+$ states, respectively, and M_i the corresponding magnetic quantum number. This approximation is valid in the low laser intensity regime, where saturation and depletion effects can be neglected and in the absence of M_j mixing terms (linearly polarized light and collision free conditions, etc.). However, for moderately high laser intensities, Eq. (1) does not adequately describe the population of the intermediate state due to saturation effects. In this regime one has to use the density matrix equations. As explained previously by us²⁷ and others,²⁸⁻³⁰ these reduce to a set of rate equations in the high intensity regime and under certain dephasing assumptions. The term high intensity regime is used rather loosely here, but generally refers to a situation where one or more of the excitation, fluorescence, or ionization rates are comparable to or larger than the reciprocal of the laser pulse duration (τ_p). In the saturation regime the REMPI process is quite sensitive to the laser characteristics and resonance conditions.

The ground $X^2\Pi$ state of NO belongs to the intermediate coupling case between Hund's cases (a) and (b), whereas the upper $A^2\Sigma^+$ state belongs strictly to Hund's case (b).^{19,38} In the intermediate coupling regime, neither N , the nuclear rotational quantum number, nor Ω , the projection of the total angular momentum J on the internuclear axis ($\Omega = |\Lambda + \Sigma|$), is a good quantum number.^{32,37,38} Each rotational level J is split into two components, f_1 and f_2 , whose splitting depends on the spin-orbit coupling constant A and the rotational constant B . A doubling causes a further splitting of each of these components, but this is quite small for the $X^2\Pi$ state and will be neglected. The $A^2\Sigma^+$ state is in a similar fashion split into two sublevels (F_1 and F_2). This splitting is much smaller ($R = 8 \times 10^{-5} \text{ cm}^{-1}$)²⁰ than in the $X^2\Pi$ state and is unresolved in the current experiments. The various branches allowed by the one-photon dipole selection rule $\Delta J = 0, \pm 1$ are shown in Fig. 1. The notation for labeling the branches is ΔJ_{ij} ,¹⁹ where i is the sublevel for the upper ($A^2\Sigma^+$) state and j for the lower ($X^2\Pi$) state. Whenever transitions to both J levels of a given N level in the A state are allowed one has a rotationally mixed branch. For a one-photon transition one therefore has rotationally clean P_{11} , R_{21} , P_{12} , and R_{22} branches, and rotationally mixed $Q_{11} + P_{21}$, $R_{11} + Q_{21}$, $Q_{12} + P_{22}$, and $R_{12} + Q_{22}$ branches as seen in Fig. 1. The photoionization dynamics therefore involves in the most general case a bound three level system: the initial

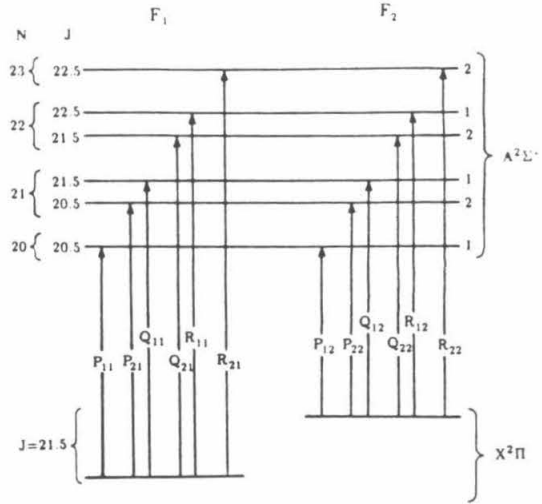


FIG. 1. The possible rotational branches originating from the $J = 21.5$ level of the $X^2\Pi$ state. The R_{11} branches are mixed with the corresponding Q_{21} ($X = 1$ or 2) branches because of the negligible splitting of the J -levels originating from the same N level of the upper state ($A^2\Sigma^+$ state).

state $|0\rangle$ and the two resonant intermediate states $|i\rangle$, and $|j\rangle$, which are coupled to the continuum $|k\rangle$ and described by the following rate equations³⁵:

$$\frac{d\rho_{00}}{dt} = -W_{0i}(\rho_{00} - \rho_{ii}) - W_{0j}(\rho_{00} - \rho_{jj}), \quad (2a)$$

$$\frac{d\rho_{ii}}{dt} = W_{0i}(\rho_{00} - \rho_{ii}) - \sum_{N'} \Gamma_i^{N'} \rho_{ii}, \quad (2b)$$

$$\frac{d\rho_{jj}}{dt} = W_{0j}(\rho_{00} - \rho_{jj}) - \sum_{N'} \Gamma_j^{N'} \rho_{jj}, \quad (2c)$$

$$\frac{d\rho_{kk}^{N'}}{dt} = (\Gamma_i^{N'} \rho_{ii} + \Gamma_j^{N'} \rho_{jj}). \quad (2d)$$

Here W_{0i} and W_{0j} are the excitation rates from the ground state to the two rotational sublevels

$$W_{0i} = K_{0i} S(J_0, J_i) \begin{pmatrix} J_0 & 1 & J_i \\ -M_i & 0 & M_i \end{pmatrix}^2 I(t), \quad (3a)$$

$$W_{0j} = K_{0j} S(J_0, J_j) \begin{pmatrix} J_0 & 1 & J_j \\ -M_j & 0 & M_j \end{pmatrix}^2 I(t), \quad (3b)$$

which are proportional to the laser intensity $I(t)$. The K_{0i} and K_{0j} factors depend on the ionization rates $\Gamma_i^{N'}$ and $\Gamma_j^{N'}$, as explained previously,²⁷ and on the laser bandwidth. In the following the K_{0i} and K_{0j} factors are assumed to be identical and their values taken from Ref. 31. $S(J_0, J_i)$ and $S(J_0, J_j)$ are the rotational line strengths as calculated originally by Earls.³² The ionization widths $\Gamma_i^{N'}$ and $\Gamma_j^{N'}$ are defined as²⁷

$$\Gamma_i^{N'} = \frac{\sigma^{N'}(M_i) I(t)}{h\nu}, \quad (4a)$$

$$\Gamma_j^N = \frac{\sigma^N(M_j)I(t)}{h\nu} \quad (4b)$$

The rate equations (2) are valid in the low to the medium high intensity regime. The long lifetime of the A state (~ 200 ns) permits us to ignore the spontaneous emission rates γ_i and γ_j of the intermediate states (see Fig. 2). The two rotational sublevels of the intermediate states $|i\rangle$ and $|j\rangle$ are assumed to be incoherently excited. This assumption is justified because of strong dephasing due to laser bandwidth effects, shot-to-shot fluctuations, etc. For the excitation of a rotationally clean branch, Eqs. (2) reduce to a set of three rate equations that can be solved in closed form, but the four-level mixed-branch system must be solved numerically. Since different laser temporal profiles have previously been shown to have a minor effect (5%–10%) on the final results,^{27,30} the shape of the laser pulse is assumed uniform. As seen by inspection, the rate equations of Eq. (2) do indeed yield the result of Eq. (1) in the low intensity regime.

The ionization cross section σ involves the sums of squares of the matrix element $r_{kl}^{\lambda\mu}$,

$$r_{kl}^{\lambda\mu} = \sum_{l',l''} \langle \Psi_{kl}(r) Y_{l'\lambda}(\hat{r}) | r Y_{l''\mu}(\hat{r}) | \Phi_{il}(r) Y_{l\lambda}(\hat{r}) \rangle, \quad (5)$$

between the bound $|i\rangle$ and the final $|k\rangle$ state.²¹ The electronic continuum wave function of the final state is calculated in the Hartree–Fock fixed-nuclei-frozen-core approximation using the variational Schwinger method³³ and includes the effects of the nonspherical, nonlocal nature of the molecular ion potential. The bound electronic wave function is calculated at the Hartree–Fock SCF level using a Gaussian basis set.²³

Finally, the M_j -resolved photoelectron distribution $P_i^M(\theta)$ is given by

$$\frac{dP_i^M(\theta)}{dt} = \Gamma_i^M(\theta) \rho_i^M(t). \quad (6)$$

$P_i^M(\theta)$ can furthermore be expanded in terms of Legendre polynomials $P_L(\cos \theta)$:

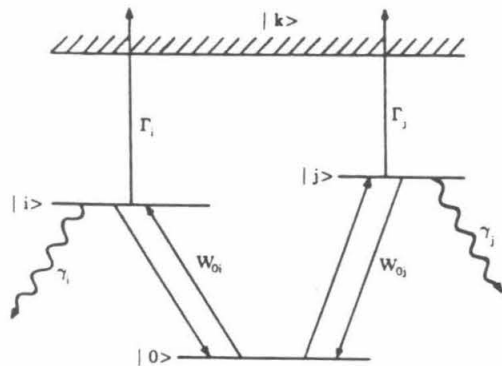


FIG. 2. Schematic picture of (1 + 1) REMPI via the $A^2\Sigma^+$ state via a mixed rotational branch. The different constants are explained in the text.

$$P_i^M(\theta) = \sum_{L=0,2} \beta_L^M(i) P_L(\cos \theta). \quad (7)$$

In the high intensity limit, the upper limit on the summation is determined by the smaller of $2(J_i + 1)$ or $2 \cdot l_{\max}$, where l_{\max} is the maximum partial wave retained in the expansion of the photoelectron continuum orbital. The resulting photoelectron angular distribution is the sum over all the M_j sublevels and branches (i) and integrated over the pulse duration τ_p ,

$$P(\theta) = \sum_L P_L(\cos \theta) \sum_i \sum_{M_j} \beta_L^M(i) \int_0^{\tau_p} dt \rho_i^M(t). \quad (8)$$

Saturation effects in $P(\theta)$ in Eq. (8) appear through the intensity dependence of ρ_i^M . The rotational branching ratios and the photoelectron angular distributions are obtained by the calculation of $P(\theta)$ for the different final rotational levels (N_+).

RESULTS

The recent experimental results by Viswanathan *et al.*⁷ illustrate the branching ratios for (1 + 1) REMPI of NO via a $R(21.5)$ branch of the $A^2\Sigma^+$ state. As in their previous experiment⁶ they observed only the even ΔN ($\Delta N \equiv N_+ - N_i$) terms, with the $\Delta N = 0$ signal as the dominating feature. The general selection rule for single photon ionization out of a Σ state leaving the ion in a Σ state,²⁵ is

$$\Delta N + l = \text{odd}, \quad (9)$$

where l is the partial wave of the photoelectron. Since the bound state is a $3s\sigma$ Rydberg state,^{7,34} the $l = 1$ wave is predicted to be dominant in an atomic-like model, and hence ΔN is even. The previously reported calculated branching ratios were for the isolated (although in reality mixed) $R_{12}(21.5)$ or $R_{11}(21.5)$ branches. These branches lead to identical rotational branching ratios in the perturbative limit.²¹ We have confirmed that the branching ratios are also essentially the same as those for the clean R_{22} and R_{21} branches, since the branching ratios change very little with N for such high values of J . The $\Delta N = 0$ signal indeed is the strongest, with a weak $\Delta N = \pm 1$ signal probably buried under the detection threshold. There are, however, as shown in Fig. 1, four possible $R(21.5)$ branches: the two clean R branches, R_{22} and R_{21} , and the two mixed branches, $R_{11} + Q_{21}$ and $R_{12} + Q_{22}$. The resonant wavelengths for these four branches are respectively, 2255.03, 2247.88, 2252.49, and 2259.67 Å.^{19,20} The photoelectron kinetic energies for a $\Delta N = 0$ transition via (1 + 1) REMPI are all around 1.70 eV. As the actual wavelength used in the experiments of Refs. 6 and 7 was not quoted, the closeness of photoelectron kinetic energies makes it difficult to identify the specific $R(21.5)$ branch accessed in the experiment. Furthermore, there seems to be a slight difference between the $\Delta N = 0$ kinetic energy positions in the two published photoelectron spectra,^{6,7} that may be caused by small changes in the surface potential in the electron spectrometer. In the following we will describe the calculation of the branching ratios via the four possible branches both in the perturbative limit and later in the high intensity limit.

The electronic wave function of the bound state is calcu-

lated with an extensive Gaussian basis set used in previous studies of higher members of the $^2\Sigma$ Rydberg series,^{22,23} yielding a total electronic energy of -129.076 58 a.u. for a bond length of 1.062 Å, the equilibrium internuclear distance of the $A^2\Sigma^+$ state.¹⁹ The single-center expansion of the 6σ orbital about the center of mass shows 94.0% s character, 0.3% p character, 5.4% d character, 0.1% f character, and 0.2% g character in agreement with our previous results²¹ and the results of Kaufmann *et al.*³⁴ For a kinetic energy of 1.67 eV, corresponding to the $\Delta N = 0$ signal of the observed $R(21.5)$ band, the relative magnitudes of the $|r_{kl}^A|^2$ of Eq. (5) are 0.038, 0.091, 0.048, 0.119, and 0.005 for $l = 0, 4$ in the $k\pi$ channel, and 0.299, 0.014, 0.173, and 0.007 for $l = 1, 4$ in the $k\pi$ channel. As expected the ionization out of the primarily gerade (even l) bound 6σ orbital gives rise to a primarily ungerade character of the continuum, and it is seen that the π channel contributes the major part (0.804 Mb) of the total cross section (1.158 Mb). These cross sections are in agreement with our previous results,²¹ and the experimental results of Rottke and Zacharias.²⁸

In Fig. 3, we compare the experimental and the calculated branching ratios for parallel and perpendicular (relative to the polarization of the radiation) detection for the three different branches. The $R_{22}(J)$ and $R_{21}(J)$ branches have

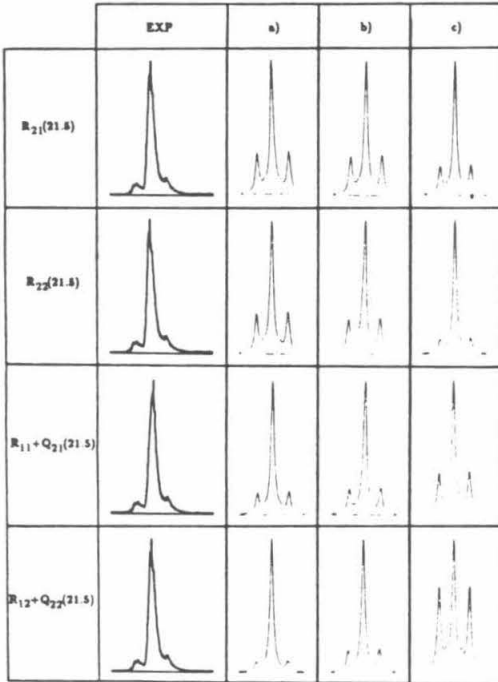


FIG. 3. Comparison of the experimental (left) and the calculated (right) rotational branching ratios for the three possible branches: (a) R_{21} or R_{22} ; (b) $R_{11} + Q_{21}$; and (c) $R_{12} + Q_{22}$ for the light polarization parallel ($\theta = 0^\circ$) and perpendicular ($\theta = 90^\circ$) to the direction of detection (perturbative limit).

TABLE I. Rotational branching ratios for the laser light polarized parallel ($\theta = 0^\circ$) and perpendicular ($\theta = 90^\circ$) to the detection direction (perturbative limit). The branching ratios are normalized to the $\Delta N = 0$ signal.

ΔN	Parallel detection ($\theta = 0^\circ$)			
	$R_{22}(21.5)$	$R_{21}(21.5)$	$R_{11} + Q_{21}(21.5)$	$R_{12} + Q_{22}(21.5)$
-2	0.292	0.292	0.142	0.050
-1	0.041	0.041	0.020	0.007
0	1.000	1.000	1.000	1.000
+1	0.042	0.042	0.021	0.008
+2	0.301	0.301	0.156	0.061

ΔN	Perpendicular detection ($\theta = 90^\circ$)			
	$R_{22}(21.5)$	$R_{21}(21.5)$	$R_{11} + Q_{21}(21.5)$	$R_{12} + Q_{22}(21.5)$
-2	1.916	1.916	1.388	0.881
-1	0.125	0.125	0.123	0.120
0	1.000	1.000	1.000	1.000
+1	0.125	0.125	0.129	0.132
+2	2.025	2.025	1.520	0.998

identical normalized branching ratios in the perturbative limit, since the only difference is the rotational line strength $S(J_0, J)$, which for clean branches is an overall factor. The rotational line strengths are³² $R_{11}(21.5) = 4.212$, $R_{12}(21.5) = 1.166$, $R_{21}(21.5) = 1.373$, $R_{22}(21.5) = 4.005$, $Q_{21}(21.5) = 2.596$, and $Q_{22}(21.5) = 8.398$. The mixed $R_{12} + Q_{22}$ and $R_{11} + Q_{21}$ branches have been weighted appropriately with these factors, and the resulting branching ratios convoluted with a Lorentzian detection function with a FWHM of 6 meV. They are shown on the same absolute energy scale as the experimental results.^{6,7} The normalized branching ratios for both directions of detection (normalized to the $\Delta N = 0$ signal in each branch) are given in Table I. The calculated relative intensities for the $\Delta N = 0$ signals for the four branches are $R_{12} + Q_{22} = 1.000$, $R_{11} + Q_{21} = 0.5006$, $R_{22} = 0.1989$, and $R_{21} = 0.0682$. Comparison to the experimental results suggests that the most likely candidate among these branches is the mixed $R_{12} + Q_{22}(21.5)$ branch. It is also seen, that the $\Delta N = \pm 1$ signals, although present, are embedded in the strong $\Delta N = 0$ signal, and therefore not experimentally observable.

Agreement between the experimental and the calculated branching ratios is less satisfactory for perpendicular detection than for parallel detection. The experimentally observed strong $\Delta N = 0$ signal is only partly reproduced in the calculated branching ratios, with the best agreement once again for the mixed $R_{12} + Q_{22}(21.5)$ branch. This discrepancy could in part be caused by the finite width of the detector in combination with the forward peaked (around $\theta = 0^\circ$) angular distribution for the $\Delta N = 0$ peak. (See Fig. 6). Averaging the signal over a finite detector acceptance angle for a realistic width of 3° did not improve the agreement. The perpendicular signal is calculated to be about 50 times weaker than the parallel signal. Even a small experimental misalignment or less than 100% linearly polarized light could lead to a "contamination" of the perpendicular signal by the parallel signal. With this large difference in the signal

of the perpendicular signal by the parallel signal is sufficient to cause the measured "perpendicular" signal to have a substantially stronger $\Delta N = 0$ peak, as experimentally observed.⁷ We will, however, in the following assume the system to be aligned and the light source to be 100% linearly polarized. Another possible reason for this discrepancy between theory and experiment could be high intensity effects, arising from the higher laser intensity necessary to achieve a detectable signal in the perpendicular case.

To estimate the effects of saturation, we have calculated relative branching ratios at various laser intensities by directly solving the rate equations (2). The K_{0i} and K_{0j} are assumed equal, and their values are taken from Ref. 31. The rate equations are integrated numerically under the assumption of a constant laser bandwidth and detection function (FWHM = 6 meV). The resulting branching ratios, as a function of intensity, are shown in Fig. 4 for parallel detection and in Fig. 5 for the perpendicular detection. It is seen that the branching ratios for the R_{22} and the R_{21} branches, which were identical in the perturbative limit, do change with higher laser intensities, and that the $\Delta N = 0$ peak for the mixed branches becomes less dominant at higher intensities. The perpendicular signal shows the same trend which is opposite to that seen experimentally. The differences are hence probably due to effects not incorporated in the present study.

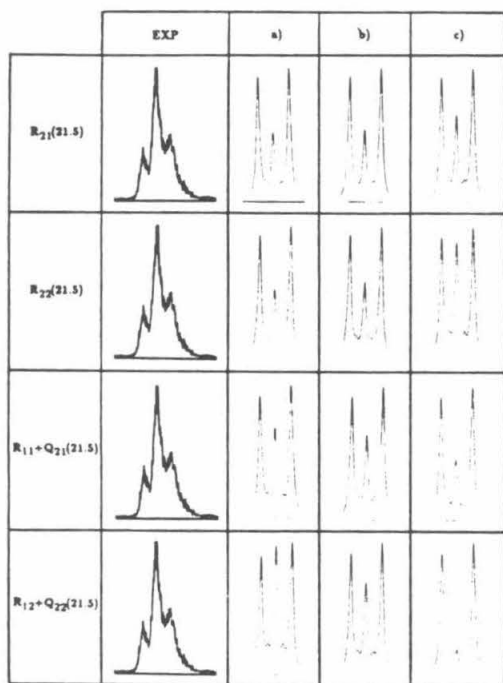


FIG. 4. Comparison of the experimental (left) and the calculated (right) branching ratios as a function of laser intensity, for detection along the direction of polarization. The total energy per unit area is (a) 1.0 J cm^{-2} , (b) 10 J cm^{-2} , and (c) 50 J cm^{-2} .

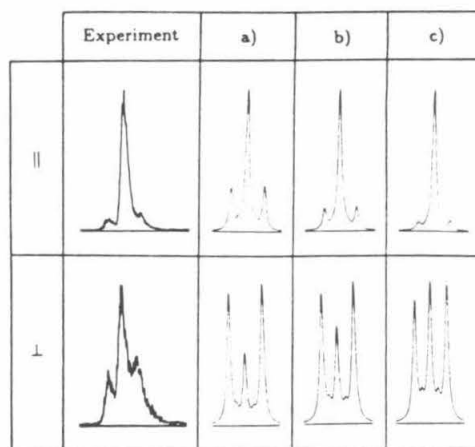


FIG. 5. Same as Fig. 4, but for detection perpendicular to the light polarization direction.

For higher laser intensities saturation effects will give rise to higher β values (higher than the perturbative limit of β_0).²⁴ The magnitude of the higher β values depend on the relative saturation rates for the different M_j channels. The photoionization cross sections are nearly constant for the different M_j sublevels, as found experimentally by Jacobs *et al.*³¹ and theoretically by us.²¹ Therefore, the terms beyond β_0 will have finite values for higher field intensities although their magnitudes are expected to be small. In fact, our calculations indicate that the only higher β value of significance is the β_2 value, and it never becomes larger than 5% of the β_0 value. The photoelectron angular distributions for the different rotational branches ($\Delta N = 0, \pm 1, \pm 2$) ionized via the $R_{12} + Q_{22}(21.5)$ branch are plotted in Fig. 6 as a function of intensity. It is seen that the photoelectron angular distribution for the $\Delta N = 0$ signal in the perturbative (low intensity) limit are strongly peaked around $\theta = 0^\circ$ and that the distributions for the different ΔN signals become similar for higher intensities.

CONCLUSIONS

We have discussed rotational branching ratios resulting from the $(1+1)$ REMPI of NO via the 0-0 transition of the $A-X$ band (γ band) for the four possible branches that can be assigned as $R(21.5)$. The calculations were done in the frozen-core approximation at the Hartree-Fock level. The four different branches, of which three are distinctly different in the perturbative limit, have rather different branching ratios. The mixed $R_{12} + Q_{22}(21.5)$ branch, which is most intense and has the lowest transition energy, seems to give the best agreement with the experimental branching ratios for parallel detection. For perpendicular detection the agreement is less satisfactory. Neither the effect of finite-acceptance angle of the photoelectron detector nor high intensities can explain the discrepancy.

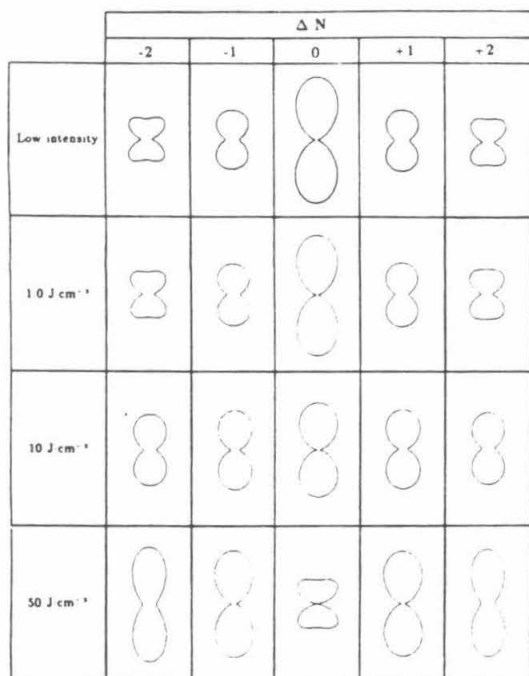


FIG. 6. Photoelectron angular distributions as a function of total laser intensity for the different rotational lines. $\beta_0 \equiv 1.00$ for all the rotational lines.

ACKNOWLEDGMENTS

This material is based on research supported by the National Science Foundation under Grant No. CHE-8521391, by AFOSR under Grant No. 87-0039, by the office of Health and Environmental Research of DOE (DE-FG03-87ER60513), and by NASA Cooperative Agreement NCC2-319. Work done by S. N. D. was performed under the auspices of the U. S. Department of Energy by Lawrence Livermore National Laboratory under Contract No. W-7405-Eng-48. H. R. gratefully acknowledges the support of the Danish Natural Science Research Council.

¹J. P. Booth, S. L. Bragg, and G. Hancock, *Chem. Phys. Lett.* **113**, 509 (1985).

²P. Chen, J. B. Ballix, W. A. Chupka, and S. D. Colson, *J. Chem. Phys.* **86**, 516 (1987).

- ³R. G. Evans and P. C. Thonemann, *Phys. Lett. A* **38**, 398 (1972).
- ⁴Y. Nagano, Y. Achiba, and K. Kimura, *J. Chem. Phys.* **84**, 1063 (1986).
- ⁵Y. Achiba, K. Sato, K. Shobatake, and K. Kimura, *J. Chem. Phys.* **79**, 5213 (1983).
- ⁶W. G. Wilson, K. S. Viswanathan, E. Sekreta, and J. P. Reilly, *J. Phys. Chem.* **88**, 672 (1984).
- ⁷K. S. Viswanathan, E. Sekreta, E. R. Davidson, and J. P. Reilly, *J. Phys. Chem.* **90**, 5078 (1986).
- ⁸K. S. Viswanathan, E. Sekreta, and J. P. Reilly, *J. Phys. Chem.* **90**, 5658 (1986).
- ⁹M. G. White, M. Seaver, W. A. Chupka, and S. D. Colson, *Phys. Rev. Lett.* **49**, 28 (1982).
- ¹⁰S. T. Pratt, P. M. Dehmer, and J. L. Dehmer, *J. Chem. Phys.* **78**, 4315 (1983).
- ¹¹S. T. Pratt, P. M. Dehmer, and J. L. Dehmer, *Chem. Phys. Lett.* **105**, 28 (1984).
- ¹²S. L. Anderson, G. D. Kubiak, and R. N. Zare, *Chem. Phys. Lett.* **105**, 22 (1984).
- ¹³J. C. Miller and R. N. Compton, *J. Chem. Phys.* **84**, 675 (1986).
- ¹⁴K. Müller-Dethlefs, M. Sander, and W. Schlag, *Chem. Phys. Lett.* **112**, 291 (1984).
- ¹⁵S. T. Pratt, E. D. Poliakoff, P. M. Dehmer, and J. L. Dehmer, *Chem. Phys.* **78**, 65 (1983).
- ¹⁶S. T. Pratt, P. M. Dehmer, and J. L. Dehmer, *J. Chem. Phys.* **79**, 3234 (1983).
- ¹⁷S. T. Pratt, P. M. Dehmer, and J. L. Dehmer, *J. Chem. Phys.* **81**, 3444 (1984).
- ¹⁸J. C. Miller and R. N. Compton, *J. Chem. Phys.* **75**, 2020 (1981).
- ¹⁹K. P. Huber and G. Herzberg, *Constants of Diatomic Molecules* (Van Nostrand Reinhold, New York, 1979).
- ²⁰R. Engleman, Jr., P. E. Rouse, H. M. Peek, and V. D. Baiaomonte, Los Alamos Report, LA-4364, UC-34 Physics, TID-4500 (Los Alamos, Laboratory Los Alamos, 1970).
- ²¹S. N. Dixit, D. L. Lynch, V. McKoy, and W. M. Huo, *Phys. Rev. A* **32**, 1267 (1984).
- ²²H. Rudolph, S. N. Dixit, V. McKoy, and W. M. Huo, *Chem. Phys. Lett.* **137**, 521 (1987).
- ²³H. Rudolph, S. N. Dixit, V. McKoy, and W. M. Huo, *J. Chem. Phys.* **88**, 1516 (1988).
- ²⁴S. N. Dixit and V. McKoy, *J. Chem. Phys.* **82**, 3546 (1985).
- ²⁵S. N. Dixit and V. McKoy, *Chem. Phys. Lett.* **128**, 49 (1986).
- ²⁶S. N. Dixit, D. L. Lynch, and V. McKoy, *Phys. Rev. A* **30**, 3332 (1984).
- ²⁷H. Rudolph, D. L. Lynch, S. N. Dixit, and V. McKoy, *J. Chem. Phys.* **84**, 6657 (1986).
- ²⁸H. Rottke and H. Zacharias, *J. Chem. Phys.* **83**, 4831 (1985).
- ²⁹V. S. Letokhov, V. I. Mishin, and A. A. Puzetzy, *Prog. Quantum Electr.* (Pergamon, London, 1977), Vol. 5, p. 139.
- ³⁰D. C. Jacobs and R. N. Zare, *J. Chem. Phys.* **85**, 5457 (1986).
- ³¹D. C. Jacobs, R. J. Madix, and R. N. Zare, *J. Chem. Phys.* **85**, 5469 (1986).
- ³²L. T. Earls, *Phys. Rev.* **48**, 423 (1935).
- ³³R. R. Lucchese, G. Raseev, and V. McKoy, *Phys. Rev. A* **25**, 2572 (1982).
- ³⁴K. Kaufmann, C. Nager, and M. Jungen, *Chem. Phys.* **95**, 385 (1985).
- ³⁵S. N. Dixit and P. Lambropoulos, *Phys. Rev. A* **27**, 861 (1983).
- ³⁶C. H. Green and R. N. Zare, *J. Chem. Phys.* **78**, 674 (1983).
- ³⁷G. Herzberg, *Spectra of Diatomic Molecules* (Van Nostrand Reinhold, New York, 1950).
- ³⁸B. R. Judd, *Angular Momentum Theory for Diatomic Molecules* (Academic, New York, 1975).